KAUNO TECHNOLOGIJOS UNIVERSITETAS

ARTIOM MAGOMEDOV

KARBAZOLO IR HIDRAZONO FRAGMENTUS TURINČIOS SKYLES TRANSPORTUOJANČIOS MEDŽIAGOS: SINTEZĖ, SAVYBĖS IR PRITAIKYMAS PEROVSKITINIUOSE SAULĖS ELEMENTUOSE

Daktaro disertacija
Gamtos mokslai, chemija (N 003)

2020, Kaunas

Disertacija rengta 2015–2019 metais Kauno technologijos universiteto Chemines technologijos fakultete, Organinės chemijos katedroje. Mokslinius tyrimus rėmė Lietuvos mokslo taryba; BALTECH; Vokietijos akademinių mainų tarnyba; Europos Sąjungos programa „Horizontas 2020“ (PERTPV).

Mokslinis vadovas:

Prof. dr. Vytautas GETAUTIS (Kauno technologijos universitetas, gamtos mokslai, chemija, N 003).

Redagavo: Armandas Rumšas ir Aurelija Gražina Rukšaitė (leidykla „Technologija“).

Chemijos mokslo krypties disertacijos gynimo taryba:

Prof. dr. Saulius GRIGALEVIČIUS (Kauno technologijos universitetas, gamtos mokslai, chemija, N 003) – **pirmininkas**;

Prof. habil. dr. Vidmantas GULBINAS (Fizinių ir technologijos mokslų centras, gamtos mokslai, fizika, N 002);

Prof. dr. Vytas MARTYNAITIS (Kauno technologijos universitetas, gamtos mokslai, chemija, N 003);

Prof. dr. Edvinas ORENTAS (Vilniaus universitetas, gamtos mokslai, chemija, N 003);

Dr. Wolfgang TRESS (Miuncheno Liudviko Maksimiliano universitetas, gamtos mokslai, fizika, N 002).

Disertacija bus ginama viešame chemijos mokslo krypties disertacijos gynimo tarybos posėdyje 2020 m. kovo 20 d. 11 val. Kauno technologijos universiteto Disertacijų gynimo salėje.

Adresas: K. Donelaičio g. 73-403, 44249 Kaunas, Lietuva.
Tel. (370) 37 300 042; faks. (370) 37 324 144; el. paštas doktorantura@ktu.lt.

Disertacija išsiųsta 2020 m. vasario 20 d.
Su disertacija galima susipažinti internetinėje svetainėje http://ktu.edu ir Kauno technologijos universiteto bibliotekoje (K. Donelaičio g. 20, 44239 Kaunas).

KAUNAS UNIVERSITY OF TECHNOLOGY

ARTIOM MAGOMEDOV

CARBAZOLE- AND HYDRAZONE-BASED HOLE TRANSPORTING MATERIALS: SYNTHESIS, PROPERTIES AND APPLICATION IN PEROVSKITE SOLAR CELLS

Doctoral dissertation
Natural Sciences, Chemistry (N 003)

2020, Kaunas

This doctoral dissertation was prepared at Kaunas University of Technology, Faculty of Chemical Technology, Department of Organic Chemistry during the period of 2015–2019. The studies were supported by the Research Council of Lithuania; BALTECH; German Academic Exchange Service; European Union's Horizon 2020 Research and Innovation Programme (PERTPV)

Scientific Supervisor:

Prof. dr. Vytautas GETAUTIS (Kaunas University of Technology, Natural Sciences, Chemistry, N 003).

Edited by: Armandas Rumšas and Aurelija Gražina Rukšaitė (Publishing Office "Technologija").

Dissertation Defence Board of Chemistry Science Field:

Prof. Dr. Saulius GRIGALEVIČIUS (Kaunas University of Technology, Natural Sciences, Chemistry, N 003) – **chairman**;

Prof. Dr. Habil. Vidmantas GULBINAS (Center for Physical Sciences and Technology, Natural Sciences, Physics , N 002);

Prof. Dr. Vytas MARTYNAITIS (Kaunas University of Technology, Natural Sciences, Chemistry, N 003);

Prof. Dr. Edvinas ORENTAS (Vilnius University, Natural Sciences, Chemistry, N 003);

Dr. Wolfgang TRESS (Ludwig Maximilian University of Munich, Natural Sciences, Physics, N 002).

The official defense of the dissertation will be held at 11 a.m. March 20, 2020 at the public meeting of Dissertation Defence Board of Chemistry Science Field in Dissertation Defence Hall at Kaunas University of Technology.

Address: Donelaičio 73-403, LT-44249 Kaunas, Lithuania.

Phone: (+370) 37 30 00 42; fax: (+370) 37 32 41 44; email: doktorantura@ktu.lt.

Doctoral dissertation was sent on February 20, 2020.

The doctoral dissertation is available on the internet at http://ktu.edu and at the library of Kaunas University of Technology (Donelaičio 20, LT-44239 Kaunas, Lithuania).

Table of Contents

List of Abbreviations

CIGS – copper indium gallium selenide (solar cell)

Da – dalton

DFT – density functional theory

DMF – dimethylformamide

DMSO – dimethyl sulfoxide

DSC – differential scanning calorimetry

DSSC – dye-sensitized solar cells

ETM – electron-transporting material

FA – formamidinium

FF – fill factor

FK209 – tris(2-(1*H*-pyrazol-1-yl)-4-*tert*-butylpyridine)cobalt(III) tri[bis(trifluoromethane)sulfonimide]

FTIR – fourier-transform infrared spectroscopy

FTO – fluorine-doped tin oxide

HOMO – highest occupied molecular orbital

HTM – hole-transporting material

ICTA – indene-C_{60}-trisadduct

I_p – ionization potential

ITO – indium tin oxide

J_{sc} – short-circuit current density

J/V – current density–voltage characteristic

LED – light-emitting diode

LUMO – lowest unoccupied molecular orbital

MA – methylammonium

MS – mass spectrometry

NMR – nuclear magnetic resonance

NREL – National Renewable Energy Laboratory

OLED – organic light-emitting diode

PCBM – phenyl-C_{61}-butyric acid methyl ester

PCE – power conversion efficiency

PESA – photoelectron spectroscopy in air

Ph – phenyl group

P_{max} – maximum power

PTAA – poly[bis(4-phenyl)(2,4,6-trimethylphenyl)amine]

PSC – perovskite solar cell

SAM – self-assembled monolayer

SEM – scanning electron microscopy

SFX – spiro[fuorene-9,9'-xanthene]

Spiro-OMeTAD – 2,2',7,7'-tetrakis[N,N-di(4-methoxyphenyl)amino]-9,9'-spirobifluorene

SQ – Shockley-Queiser (limit)

tBP – 4-*tert*-butylpyridine

TFSI – bis(trifluoromethane)sulfonimide

T_g – glass transition temperature

THF – tetrahydrofuran

T_m – melting temperature

UV/vis – ultraviolet/visible (light)

V_{oc} – open-circuit voltage

μ – hole drift mobility value at 6.4×10^5 V cm^{-1} field strength

μ_0 – hole drift mobility value at 0 V cm^{-1} field strength

1. INTRODUCTION

Organic materials, while traditionally used as insulators, in the second half of the 20th century were found to conduct charges under certain conditions [1]. With the development of the field, more and more examples of organic semiconductors have gradually appeared, including conjugated polymers [2], small-molecule semiconductors [3], fullerene-based materials [4], etc. Due to their properties, such as light weight, good mechanical characteristics, and the formation by solution processes, they have become central for several popular concepts, such as wearable and/or printable electronics. Several successful applications have already been demonstrated, such as xerographic devices [5] (laser printers) and organic light-emitting diodes [6] (OLEDs), however, there is still a large scope for the development of the applications.

In the last decade, the field of organic semiconductors has been undergoing a new rise with the emergence of the third generation of solar cells [7]. Due to the ever increasing awareness about global climate changes, direct transformation of solar light into electricity is often considered as the most attractive way of energy production. It is also one of the ways to reduce the CO_2 emission, which is commonly correlated to the rise of the average Earth temperature. Currently, the motivation behind the use of solar energy is mostly political, however, with the up-scaling of solar cell production, it is starting to become also economically attractive. Even though the Si-based technologies are currently dominating the market, new technologies could further expand the scope of the application of solar cells.

Among other options, perovskite solar cells (PSCs) is the fastest developing technology. Starting from the first application of the perovskite material as an absorber layer back in 2009 [8], and after achieving the first breakthrough in 2012 [9], it is now on the verge of transition from lab to fab. While the material itself contains organic cations, there are also other organic materials that are important for the progress of the field.

One of such components is the organic hole-transporting material (HTM), which is the main object of this work. In the scope of this dissertation, several issues related to HTMs are addressed, i.e., efficient synthesis, doping-induced degradation, and the alternative layer formation method. The experimental results have been presented in five publications, which are further discussed. The publications and the author's contributions to them are as follows:

1. A. Magomedov, S. Urnikaite, O. Paliulis, V. Jankauskas, V. Getautis. "Click-chemistry" inspired synthesis of hydrazone-based molecular glasses, *RSC Adv.*, **2016**, *6*, 8701–8704. JIF: 3.049; times cited: 5.
   Contributions:
   O.P. and V.G. developed the initial idea. A.M. conducted the synthesis of the compounds. V.G. and S.U. supervised the research. V.J. carried out the ionization potential and charge mobility measurements. A.M. and V.G. drafted the manuscript. All the authors contributed to the editing of the paper.

2. P. Gratia, A. Magomedov, T. Malinauskas, M. Daskeviciene, A. Abate, S. Ahmad, M. Grätzel, V. Getautis, M.K. Nazeeruddin. A Methoxydiphenylamine-Substituted Carbazole Twin Derivative: An Efficient Hole-Transporting Material for Perovskite Solar Cells, *Angew. Chemie – Int. Ed.*, **2015**, *54* (39), 11409–11413. JIF: 12.257; times cited: 142; the article was highlighted as frontispiece.
   P. Gratia, A. Magomedov, T. Malinauskas, M. Daskeviciene, A. Abate, S. Ahmad, M. Grätzel, V. Getautis, M.K. Nazeeruddin. Methoxydiphenylamin-substituiertes Carbazol-Zwillingsderivat: ein effizienter organischer Lochleiter für Perowskit-Solarzellen, *Angew. Chemie*, **2015**, *127*(39), 11571–11575.)
   Contributions:
   M.K.N., M.G. and V.G. conceived the initial idea and supervised the research. P.G. optimized and prepared perovskite solar cells. A.M. conducted the synthesis of **V886**. T.M. and A.M. performed characterization of the synthesized compounds. P.G. and A.A. characterized the prepared perovskite solar cells. M.D. contributed to the optimization of the synthetical procedures. P.G. and A.M. drafted the manuscript. A.A. and S.A. contributed to the interpretation of the data. All the authors contributed to the editing of the paper.
3. A. Magomedov, S. Paek, P. Gratia, E. Kasparavicius, M. Daskeviciene, E. Kamarauskas, A. Gruodis, V. Jankauskas, K. Kantminiene, K.T. Cho, K. Rakstys, T. Malinauskas, V. Getautis, M.K. Nazeeruddin. Diphenylamine-Substituted Carbazole-Based Hole Transporting Materials for Perovskite Solar Cells: Influence of Isomeric Derivatives, *Adv. Funct. Mater.*, **2018**, *28*, 1704351. JIF: 15.621; times cited: 29.
   Contributions:
   M.K.N and V.G. conceived the initial idea and supervised the research. S.P., P.G. and K.T.C. optimized and prepared perovskite solar cells. A.M. conducted the synthesis of the compounds. E. Kasparavicius carried out photoluminescence and UV/vis measurements. V.J. and E.Kamarauskas carried out the ionization potential and charge mobility measurements. A.G. carried out the quantum chemical simulations of hole-transporting materials. M.D. contributed to the optimization of the synthetical procedures. P.G. carried out conductivity measurements. S.P. characterized perovskite solar cells. A.M., K.R. and T.M. performed characterization of the synthesized compounds. A.M. and K.K. drafted the manuscript. All the authors contributed to the editing of the paper.
4. A. Magomedov, E. Kasparavičius, K. Rakstys, S. Paek, N. Gasilova, K. Genevičius, G. Juška, T. Malinauskas, M.K. Nazeeruddin, V. Getautis. Pyridination of hole transporting material in perovskite solar cells questions the long-term stability, *J. Mater. Chem. C*, **2018**, *6*, 8874–8878. JIF: 6.641; times cited: 21; the article was highlighted on the back cover page.

Contributions:
A.M. and T.M. conceived the initial idea. M.K.N. and V.G. participated in the development of the concept and supervised the research. A.M. optimized the synthesis of the pyridinated products and performed structural analysis of the isolated products. A.M. and V.G. analyzed NMR data, proposed the reaction pathway and suggested a mechanism. E.K. performed characterization of the materials. K.G. and G.J. measured the conductivities of the compounds. S.P. prepared and characterized perovskite solar cells. K.R. and N.G. performed MS analysis of the aged devices. A.M. drafted the manuscript. All the authors contributed to the editing of the paper.

5. A. Magomedov, A. Al-Ashouri, E. Kasparavičius, S. Strazdaite, G. Niaura, M. Jošt, T. Malinauskas, S. Albrecht, V. Getautis. Self-Assembled Hole Transporting Monolayer for Highly Efficient Perovskite Solar Cells, *Adv. Energy Mater.*, **2018**, 1801892. JIF: 24.884; times cited: 20; the article was highlighted on the front cover page.
   Contributions:
   A.M. and T.M. conceived the initial idea. A.M., A.A.A., T.M., S.A. and V.G. participated in the development of the concept. T.M., S.A. and V.G. supervised the research. E.K. developed the synthesis procedure, synthesized the compounds and performed characterization of the synthesized materials. M.J. optimized the inverted perovskite solar cells fabrication process. A.M. and A.A.A. fabricated and characterized the perovskite solar cells. A.A.A. conducted electrochemical impedance measurements and optical simulations. A.M. carried out the quantum chemical optimization of the material and the contact angle measurements. S.S. conducted vibrational sum frequency generation spectroscopy measurements. G.N. conducted the FTIR measurements. A.M. and A.A.A. drafted the manuscript. All the authors contributed to the editing of the paper.

The aim of the work is the development of simple and efficient hole-transporting materials for perovskite solar cells.

The tasks proposed for the achievement of the above-stated aim were as follows:

1. To develop a simple synthetical strategy for branched hydrazone-based hole-transporting materials with the aim of obtaining a stable amorphous phase;
2. To adapt the developed synthesis scheme to the synthesis of the carbazole-based hole-transporting materials suitable for the application in efficient perovskite solar cells;
3. To study the influence of the isomeric derivatives of carbazole-based hole-transporting materials on the performance of the final devices;

4. To study the degradation process of hole-transporting materials induced by dopants;
5. To develop a novel, dopant-free deposition technique for the formation of the hole-selective layer.

Scientific novelty and relationship between the publications:

At the beginning of the development of the field of PSCs, there was a very limited choice of HTMs. This issue can mainly be attributed to the lack of the understanding of the required structure to achieve the highest efficiency. The most popular small-molecule HTM used in PSCs is 2,2',7,7'-Tetrakis[N,N-di(4-methoxyphenyl)amino]-9,9'-spirobifluorene (Spiro-OMeTAD). However, its synthesis involves 6 steps and requires the use of sensitive and aggressive reagents. The first three publications by the author of the present thesis deal with the development of a simple synthetical pathway which leads to efficient HTMs with a branched structure and a stable amorphous phase. The initial work led to successful synthesis of a family of hydrazone-based HTMs. However, as these molecules did not show high efficiency in the PSCs, the synthesis scheme was adopted to the synthesis of carbazole-based HTMs. One of the synthesized compounds was commercialized under the name **V886** by *Tokyo Chemical Industry Co., Ltd.*

In the following paper, another parameter, long-term stability, which is important for successful commercial application, is discussed. Due to their low conductivity in the pristine state, HTMs are used in a combination with several dopants. Even though it is known that the doping procedure generates radical cations, so far, there have been no reports on the chemical stability of such materials. In the next publication, the pathway of chemical interaction between the constituents of the HTM layer was studied *in vitro*. It was shown that oxidized HTM species undergo a chemical reaction with 4-*tert*-butylpyridine (tBP), and novel species are formed. As further confirmation, pyridinated species were detected *in situ* in the aged devices.

In the final paper, seeking for a way to exclude dopants from the HTM composition, as well as looking for transparent selective contacts, a novel layer formation procedure was proposed. Instead of the traditional spin-coating, self-assembly of **V886**-inspired phosphonic acid was used to make an HTM layer on indium tin oxide (ITO) substrate. The devices made with such layers have shown a very promising efficiency of 17.8% thus making this alternative approach attractive for further development.

In the following sections, a review of the PSCs with an emphasis on the role of organic materials in the development of the devices is presented.

Statements to be defended:

- The reaction between bromomethyl-substituted benzene derivatives and hydrazones with unsubstituted hydrogen is useful to obtain fully amorphous small-molecule hole-transporting materials;

- By changing the chromophore from aromatic hydrazone to dimethoxydiphenylamine-substituted carbazole, an efficient hole-transporting material for perovskite solar cells is obtained;
- The charge transporting properties of the branched carbazole-based hole-transporting material can be altered by synthesizing isomeric derivatives, however, the strong change in hole drift mobilities only leads to a minor improvement in the performance of perovskite solar cells;
- The use of a common additive, 4-*tert*-butylpyridine, leads to the formation of pyridinated species, which over time reduces the effective doping of the hole-transporting layer;
- Hole-selective monolayers can serve as a dopant-free hole-transporting layer in efficient perovskite solar cells providing good selectivity and change transporting properties.

1.1. Developments in the field of perovskite solar cells

In this section, a brief history of perovskite materials and their uses in solar cells is presented. In particular, hybrid organic-inorganic perovskites are discussed in the context of deposition techniques and composition variations. In addition, other materials used for the fabrication of PSCs are overviewed so that to give a background for further discussion of organic HTMs. Finally, at the end of the section, a brief overview of the performance parameters is given.

First of all, it is important to mention that the term ‘perovskite’ is currently widely used in the scientific literature to describe a variety of different materials depending on the specific traditions of the field. All of them share the same crystal structure, and the most general formula can be written as ABX_3, where A and B are cations of different sizes, and X stands for an anion (Figure 1). The original perovskite mineral is calcium titanate ($CaTiO_3$), which for the first time was discovered in the Ural Mountains in 1839 and was named after Russian nobleman and mineral collector Lev Perovski [10]. In the context of solar energy harvesting, the most important material is the hybrid organic/inorganic material methylammonium lead iodide ($MAPbI_3$). In this work, as it is common in the scientific community, the term ‘perovskite’ would relate to $MAPbI_3$ and its derivatives (e.g., $MAPbBr_3$, $FAPbI_3$, $CsPbI_3$, $MASnI_3$, mixed perovskites, etc.).

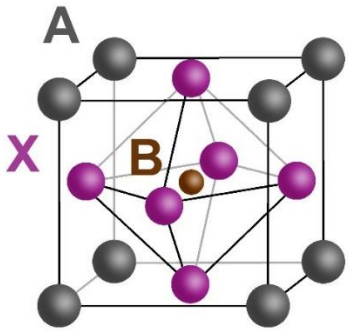

Figure 1. Graphical representation of the perovskite structure. The gray circle stands for the A cation, the brown circle is the B cation, the magenta circle is the X anion. Adapted from [11].

1.1.1. The emergence of hybrid perovskites

Synthesis of hybrid organic/inorganic tin- (i.e., $MASnBr_3$, $MASnBr_2I$, $MASnI_3$) and lead-based (e.g., $MAPbCl_3$, $MAPbBr_3$, $MAPbI_3$) perovskites for the first time was demonstrated by D. Weber back in 1978 [12,13]. However, at that time, these materials did not attract much attention, and only several publications followed, mainly focusing on the phase transitions of the material [14,15,16].

Pioneering works on the development of the deposition techniques and applications of perovskites in optoelectronic devices were performed by D. Mitzi at IBM [17,18]. The first work, published in 1994, was inspired by the success of the layered copper oxide perovskites demonstrating high-temperature superconductivity. Hybrid organic/inorganic perovskites were shown to have an advantage of low-temperature synthesis and high flexibility for the tunability of their properties (Figure 2) [19]. Following the first report, several deposition techniques were developed, i.e., single source thermal ablation [20], and two-step dipping technique, where vapor-deposited metal halide is dipped in the solution of an organic salt [21]. Films formed by these methods were tested in LEDs [22] and thin film transistors [23].

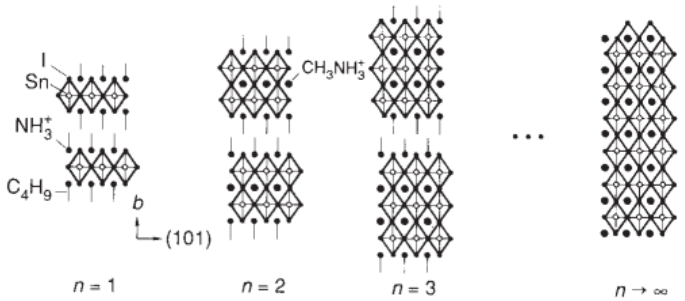

Figure 2. Schematic representation of n=1 (layered perovskite) to ∞ (cubic perovskite) compounds. Reprinted with permission from [19].

It took another decade till the first report on a solar cell employing perovskite ($MAPbI_3$ and $MAPbBr_3$) as an absorbing layer was published by the group led by T. Miyasaka in 2009 [8]. The authors employed the dye-sensitized solar cell (DSSC) architecture, in which, the organic dye was replaced by perovskite quantum dots (Figure 3). The highest power conversion efficiency (PCE) of 3.8% was achieved for such devices. Despite being denoted by good light absorption and relatively high V_{oc} values, the devices suffered from a very short lifetime due to the decomposition of perovskite by liquid iodide/triiodide electrolyte.

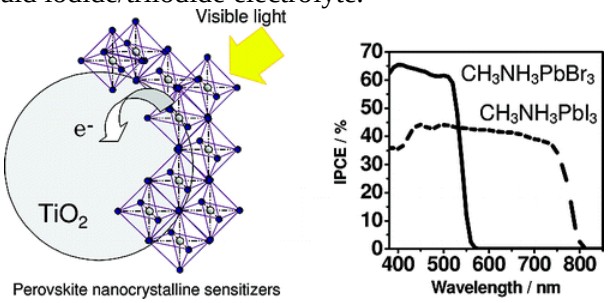

Figure 3. The first published results of the solar cell utilizing a perovskite material as the absorber layer. Reprinted with permission from [8].

The real breakthrough was achieved in 2012 when a liquid electrolyte was changed by solid-state organic HTM Spiro-OMeTAD (Figure 4). It was reported almost at the same time in two separate publications by H.J. Snaith *et al.* [9] and N.G. Park *et al.* [24] who shared the same idea. Moreover, in one of the publications, the semiconducting TiO_2 scaffold was replaced by insulating Al_2O_3, which resulted in 10.9% PCE with a remarkably high V_{oc} value of 1.1 V [9]. Starting from these works, a lot of optimization work of perovskite deposition, composition, and device architecture has been done when trying to maximize PCE.

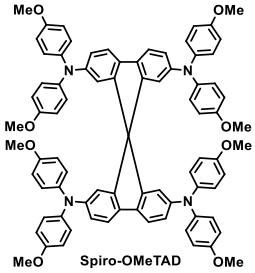

Figure 4. Structure of solid-state small-molecule organic HTM Spiro-OMeTAD [25].

1.1.2. Deposition techniques

The easiness of the formation of perovskite materials is one of the main competitive advantages against the traditional Si-based solar cells. In order to obtain high-quality monocrystalline Si which is required to achieve top-notch performance, Si is grown at 1425 °C while following the Czochralski process. On the other hand, crystallization of perovskite starts at temperatures below 100 °C. In addition,

perovskite is formed from inexpensive starting materials (e.g., PbI_2 and methylammonium iodide (MAI) for $MAPbI_3$). However, the performance of perovskite-based devices strongly correlates with the film morphology [26] and the size of the grains [27], which, in turn, is very sensitive to the formation conditions. Therefore, precise control over this process is important thus ensuring an opportunity to tune the film thickness and the size of the grains as well as to minimize the number of trap states.

Deposition techniques can be divided into two major groups: solution processes, and solvent-free techniques (Figure 5). The first group is attractive due to the simplicity of the film formation process and because of the compatibility with scalable printing technologies. The methods from the second group are expected to provide better reproducibility due to the better control over the deposition parameters. Below, a short review of the developments in this field is provided.

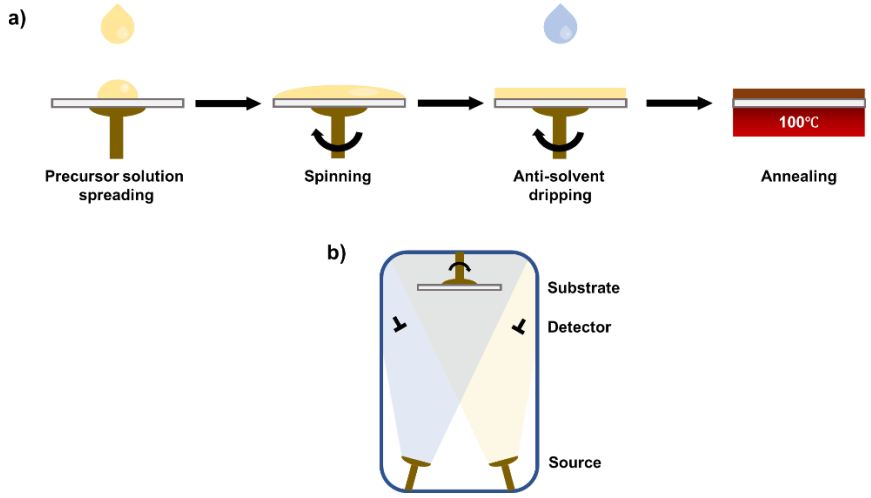

Figure 5. Schematic representation of a) spin-coating deposition from the single precursor solution with anti-solvent dripping; b) co-evaporation from two sources. Adapted with permission from [28] and [29].

The first method applied for perovskite synthesis from solution was spin-coating. Despite many disadvantages, such as high waste of materials and inhomogeneous coverage of the larger substrates, this method is very popular in academia due to the very simple equipment and processing. In its simplest form, the reagents are dissolved in an organic solvent so that to make a precursor solution, which is followed by spin-coating and annealing. However, as the crystallization of perovskite is a fast process, it often results in non-even films [26]. To solve this problem, several ways to retard crystallization have been developed. The process is slowed down by the use of intermediate phases by adding some reagents to the precursor solution. Currently, there are two most popular additives: methylammonium chloride (MACl), and dimethyl sulfoxide (DMSO). In both cases, intermediate phases, which are more stable and less sensitive to the environment, are formed, and the target perovskite is obtained during the slow annealing process.

Recently, the crystal structure of the intermediate crystalline phase formed from the solution of $PbCl_2 + 3$ MAI was determined experimentally thus showing that, during annealing, MACl evaporates from the film [30]. In the case of DMSO, due to its slow evaporation from the film, the so-called 'antisolvent dripping' method is used [28] in order to promote the formation of the intermediate phase [31]. By carefully choosing the antisolvent and the dripping time, highly reproducible results can be achieved [32]. The one-step deposition method with antisolvent dripping was used for the highest reported efficiencies by the groups from Korea Research Institute of Chemical Technology [33] and Swiss Federal Institute of Technology in Lausanne [34].

An interesting variation to the one-step spin-coating method was developed by the group of D. Prochowicz *et al*. when, initially, perovskite is synthesized mechanochemically, and, afterwards, dissolving in an organic solvent is used for spin-coating [35,36]. It can be useful for the incorporation of insoluble reagents into the perovskite composition [37] and for the reduction of batch-to-batch variations associated with the suboptimal stoichiometry [38]. However, solvent-free depositions would provide more advantages to this method.

Another approach towards perovskite formation is the so-called two-step deposition when, at first, PbI_2 is deposited (either by vacuum deposition or by spin-coating), and then it is transformed into perovskite by immersing into (or spin-coating on top) the MAI solution [39]. Initially, it was developed as an alternative to the one-step method thus providing a simpler way towards uniformly covered films while utilizing the advantage of good film formation on different substrates of PbI_2. Even though the one-step method is more popular due to its simplicity, the two-step method was used in 2019 for the fabrication of the record-breaking tandem Si/perovskite solar cell. In the work by F. Sahli *et al*., a textured Si solar cell was used to increase the performance by improved light management. Therefore, the usual one-step spin-coating was not applicable for perovskite deposition. To overcome this limitation, co-evaporation of the PbI_2 and CsBr was used in order to achieve conformal and uniform coverage. Further, on top of the vapor-deposited film, a solution of FAI and FABr was spin-coated. After annealing, perovskite was formed. The authors were able to achieve a record ratio of 25.2% [40].

Among the solvent-free methods, the largest group is the vapor deposition techniques [29,41,42,43]. Their use is related to the possibility to obtain more reproducible coatings on a large area, and to the compatibility with large-scale fabrication. However, due to the more complex optimization process and the difficulty in fabrication of mixed perovskite, such devices are still behind in terms of efficiency. In the work by L. Gil-Escrig *et al*. [43], fully vapor-deposited PSC with mixed cation/anion perovskite showed a PCE of 16%.

An interesting approach towards the perovskite film formation was created by the team of A. Tarasov [44]. They showed that MAI (also MABr and FAI) react with iodine thus forming dark liquids, the so-called reactive polyiodide melts. Metallic lead films treated with such a liquid are readily transformed into high-quality perovskite layers. Following the great interest in the community due to the

possibility of the up-scaling of the process, it was further developed to the transformation of the lead/organic salt bilayers (formed by vapor deposition) into perovskite by treating them with iodine vapor [45]. Promising PCEs of ~17% were demonstrated for various perovskite compositions.

1.1.3. Chemical compositions

In the early works, $MAPbI_3$ was used as the absorbing layer [8]. However, it suffers from a suboptimal bandgap (~1.55–1.60 eV [46]) and offers bad stability due to the presence of the volatile methylammonium cation. One of the advantages of the hybrid perovskite systems is the possibility to use mixtures of different cations and anions. This could potentially lead to the tunability of the properties over a wide range of values as it was demonstrated in the case of perovskite quantum dots (Figure 6) [47].

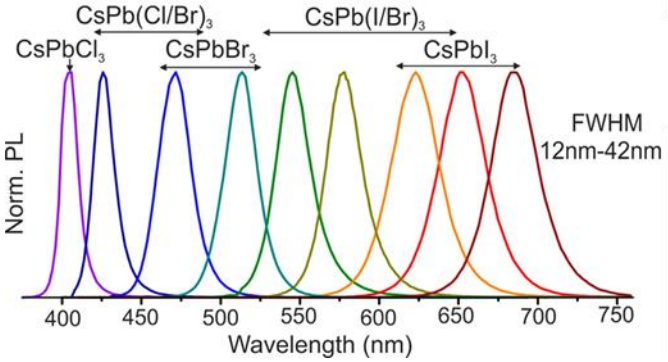

Figure 6. Photoluminescence spectra of colloidal perovskite nanocrystals demonstrating the tunability of photophysical properties by means of compositional changes. Reprinted with permission from [47].

In the case of perovskite thin-films used in PSCs, for the first time, the possibility of band-gap tuning was demonstrated by preparing mixtures of $MAPbI_3$ and $MAPbBr_3$. By increasing the relative amount of bromide, an increase in V_{oc} is observed. However, it should be noted that the change is not linear due to the beginning of the phase segregation for some mixtures. The highest PCE of 12.3% was achieved for the composition of $MAPb(I_{0.8}Br_{0.2})_3$ [48]. On the cation side, methylammonium can be replaced with another organic cation – formamidinium (FA). $FAPbI_3$ is known to feature a more suitable bandgap for solar energy conversion (1.43 eV) [49]. However, at room temperature, it crystallizes in an inactive yellow crystalline phase [50]. To overcome this limitation, mixtures of methylammonium and formamidinium can be prepared. By optimizing the ratio between these two cations, improved performance was obtained thus reaching $MA_{0.4}FA_{0.6}PbI_3$ 14.9% PCE [51]. By combining anion and cation mixtures, after optimization of the possible variations, improved efficiencies were achieved ($(FAPbI_3)_{0.85}(MAPbBr_3)_{0.15}$ – 18.4% [52]; $MA_{2/6}FA_{4/6}Pb(Br_{1/6}I_{5/6})_3$ – 20.7% [53]).

As a part of further explorations of the possibility to tune/change properties of the perovskite absorber material, cesium cation was used as an additive. It is of

interest that, as in the case with FA, pure $CsPbI_3$ does not form a stable black phase at room temperatures. However, as in the previous case, its combination with MA results in the formation of the right phase. Even more, the so-called 'triple-cation' composition, combining Cs, MA, and FA, was shown to offer better reproducibility of the performance results and improved stability [34]. Further studies attributed the effect of improved reproducibility to the difference in perovskite crystallization pathways while avoiding environmentally-sensitive intermediate phases [54]. Due to this reason, it rapidly became the baseline for many researchers.

Apart from the change of the cations and anions in the crystalline structure, there is also a vast amount of passivating additives. Several researches show improved performance parameters of PSCs with alkaline metals additives, such as sodium [55], potassium [56], and rubidium [57]. Recent reports have been suggesting that these additives are not incorporated into the crystalline structure of perovskite, but rather act as passivating agents [58,59,60,61]. A further example is the divalent cation of strontium, which increased V_{oc} [62].

Another fundamentally important issue of perovskite chemical composition is the use of toxic lead. While in terms of small-scale production it is not a big problem due to the very low amount of the perovskite absorber (its typical thickness is around 300–500 nm) and the limited solubility of lead iodide in water [63], with the upscaling of the production this might become a limiting factor [64]. One way to avoid this limitation is the implementation of the strict recycling process after the end of the solar cells lifetime. So far, the initial assessment of recycling has been shown on laboratory-scale devices [65,66]. Some researchers are trying to implement lead-free perovskite absorbers, mainly based on tin [67,68,69]. However, tin perovskite is very unstable due to oxidation; therefore, its successful incorporation into devices is very difficult.

1.1.4. Other materials used for PSCs and the architectures of devices

Apart from the perovskite absorber material, other constituents of PSC are also playing a major part in the development of devices. The materials that are used with perovskite should fulfill strict requirements in terms of a variety of aspects. First, they must be denoted by suitable energetic and electronic properties. Next, the deposition processes should be compatible. Third, the interfaces between the materials should not introduce additional trap states. Finally, the materials and their combinations should be stable under the operational conditions of solar cells. Below, a brief overview of the most popular materials is presented.

The materials required for the fabrication of PSC can be divided into five categories:

i) A substrate based on a transparent conductive oxide
ii) An electron-selective layer
iii) A perovskite absorber layer
iv) A hole-selective layer
v) A top electrode.

Such a sequence describes the so-called n-i-p (often referred to as ‘regular’) configuration. If the electron-selective and hole-selective layers are interchanged, then it is called the p-i-n (or ‘inverted’) configuration (Figure 7). In addition, some optional layers can be added in order to reduce recombination or improve stability (e.g., polystyrene [70], reduced graphene oxide [71], etc.). Also, ready-to-market devices should have encapsulation layers [72,73,74], however, at the research stage, they are usually omitted for the sake of simplicity.

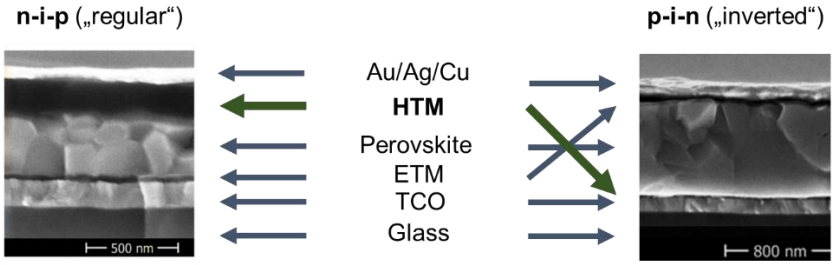

Figure 7. Scanning electron microscope cross-section images demonstrating two possible configurations of PSCs. Adapted with permission from [75,76].

In this work, only devices based on i) transparent conductive oxide (TCO), such as ITO or FTO on the glass, and v) metal electrode (Au or Ag for n-i-p; Cu or Ag for p-i-n) are overviewed. For plastic substrates [77] and carbon-based top electrodes [78], the readers are referred to the relevant literature.

As an electron-transporting material (ETM), both organic and inorganic materials are used depending on the architecture of the specific device. For the n-i-p devices, it is usual to employ inorganic materials as an ETM. At the beginning, TiO_2 layers were used, however, high-temperature sintering makes this process less attractive. On the other hand, SnO_2 can be deposited at relatively lower temperatures. In the work by E.H. Anaraki, several deposition methods were compared, including atomic layer deposition, spin-coating, and spin-coating with chemical bath deposition post-treatment. For the latter case, the highest PCE of 20.7% (with V_{oc} of 1.21 eV) was achieved [79]. In the work by L. Kegelmann, the use of two ETMs is proposed, and, in particular, the best result was obtained for a combination of TiO_2/PCBM materials [75]. For p-i-n devices, the usual choice is a combination of C_{60}/BCP [80], where C_{60} is responsible for the charge transport, and BCP acts as an interfacial layer enhancing the overall performance [81,82]. Also, C_{60} derivatives (PCBM, ICTA) were shown to offer satisfactory performance [83]. There have been not many non-fullerene small molecule organic ETMs tested in PSCs so far, with the promising exception of the simple naphthalene diimide-based molecule NDI-ID [84]. This molecule may serve as a model compound for the further development of new ETMs. The structures of the above mentioned organic materials are presented in Figure 8.

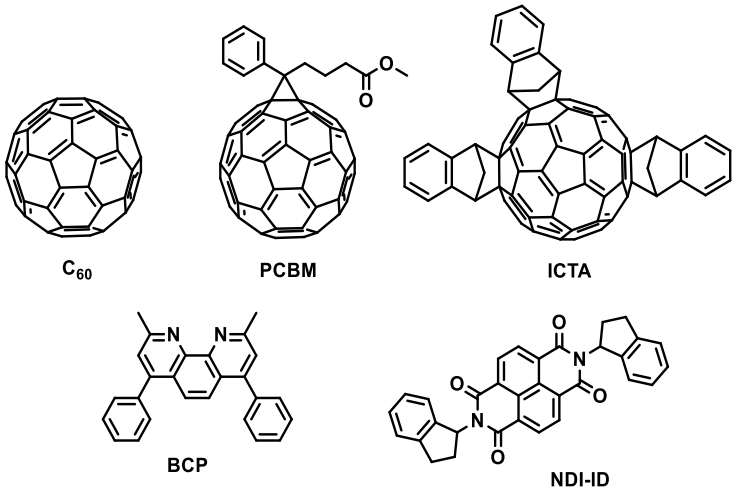

Figure 8. Structures of organic ETMs used in PSCs [81,82,83,84]

As HTMs are usually deposited by solution methods, it is important for them to have orthogonal solubility with the perovskite absorber. In the n-i-p devices, HTM is deposited on top of perovskite. The most commonly used solvent is chlorobenzene even though it is considered to be a problematic substance for the use in production lines based on its environmental impact [85]. For the p-i-n devices, there are no limitations for the HTM solvent, however, the deposited layer should withstand polar solution of perovskite dissolved in DMF/DMSO mixture. A broader review of HTMs is provided in Section 1.2.

At the current state, higher PCE values are usually obtained for the n-i-p devices (>23% [33]), however, there are no fundamental differences between the two configurations. For the p-i-n devices, already >21% [86] PCE values have been demonstrated, making it a close competition. The main difference between the two configurations lies in the fabrication methods and may become decisive at the up-scaling and market application stage.

1.1.5. Performance parameters

While discussing and comparing different solar cells, it is important to understand several main parameters used for the description of devices. In this section, a brief introduction into the field is provided.

The most commonly used number that represents a solar cell is its power conversion efficiency (PCE, [%]). In brief, it shows the ratio between the light power that is illuminating the surface of the solar cell and the maximum power output (P_{max} in Figure 9) that can be generated by the device. To make it fixed to some illumination, usually, it is measured for the standardized AM1.5 solar spectrum [87] (Figure 9). It corresponds to the extraterrestrial solar spectrum filtrated through 1.5 atmosphere thickness with the integrated power of 100 mW/cm^2.

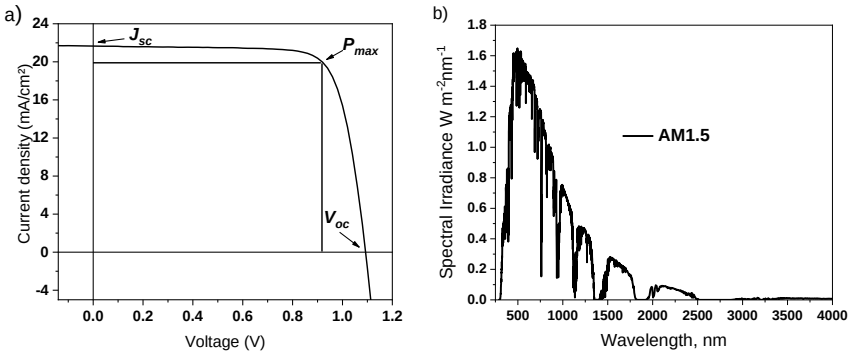

Figure 9. a) Representative current density-voltage (J/V) curve of the solar cell; b) Solar spectrum from the international standard ISO 9845-1, 1992 [87]

There are several limitations strongly reducing the maximum value of PCE. In the band theory representation, a semiconductor can absorb only photons whose energy is lower than the band gap, thus there are unavoidable losses in the infrared region. Another issue that does not allow to infinitely narrow the bandgap is the thermalization of hot electrons. When a photon with the energy higher than the bandgap is absorbed, it quickly loses the excess of the energy. Theoretically, the maximum theoretical PCE for the single-junction solar cells is described by the Shockley-Queiser (SQ) limit (Figure 10). It was calculated based on the detailed balance while accounting for the (unavoidable) radiative losses and ignoring other losses (i.e., non-radiative recombination and absorption losses) [88]. For a semiconductor with the optimal bandgap of 1.34 eV (or 928 nm), the calculated maximum PCE is ~33.2% [89]. For $MAPbI_3$, the bandgap is ~1.55–1.60 eV, therefore, the maximum efficiency is a bit lower, at around ~31% [46]. In the real-life devices, there are additional losses observed, however, the SQ limit serves as a good guideline for device optimization.

Currently, the highest PCE for perovskite, tandem, and best Si-based solar cells, including the results from National Renewable Energy Laboratory (NREL) Best Research-Cell Efficiency Chart [90], are:

- Unpublished from NREL – 25.2%
- Published n-i-p – 23.2% (certified 22.6%) [33]
- Published p-i-n – 21.5% (certified 20.9%) [86]
- 1 cm^2 – published n-i-p 21.7% (certified 20.9%) [33]
- 1 cm^2 – published p-i-n 20.0% (certified 19.8%) [91]
- Unpublished Si/Perovskite tandem from NREL – 29.1%
- Published Si/Perovskite tandem – 26.0% [92]
- The record for Si-based solar cells from NREL – 26.6%.

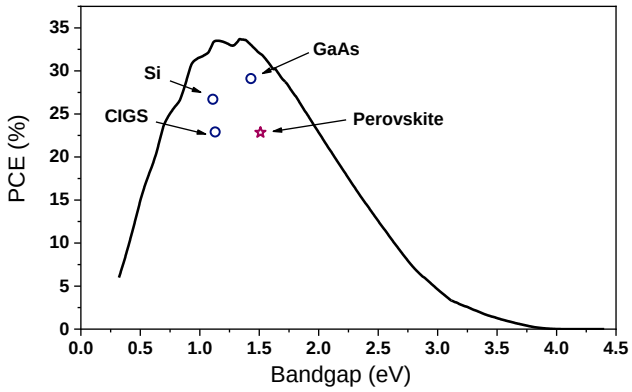

Figure 10. Shockley-Queisser limit: maximum power-conversion efficiency as a function of bandgap [93], and the record values for some solar cell materials [94]

While obtaining the highest PCE is the main goal of device optimization, there are several more performance parameters that can be useful for the comparison of different devices, namely, short-circuit current density (J_{sc}), open-circuit voltage (V_{oc}), and the fill factor (*FF*). They are extracted from J/V measurements and can provide additional information regarding the performance of the devices.

The first one, J_{sc}, shows how many electrons are generated by the solar cell when no bias is applied. The highest possible value would be in the case when every absorbed photon would generate one electron. It depends on the light absorption ability of the photoactive layer and on the charge extraction properties of the selective layers. In real-life devices, it is reduced by the parasitic absorption from the other layers and by reflections from interfaces. Practically achievable J_{sc} values for the MAPI perovskite usually are in a range of 22–23 mA/cm^2 (e.g., 23.4 mA/cm^2 was achieved by S.S. Shin *et al.* [95]). For perovskite compositions with a higher formamidinium ratio, it can be higher (24.9 mA/cm^2 for $(FAPbI_3)_{0.95}(MAPbBr_3)_{0.05}$ perovskite) due to the broader absorption.

The second, V_{oc}, represents the maximum potential difference between the electrodes when there is no flow of the current. The maximum V_{oc} depends on the bandgap of the material and is reduced by the recombination processes. For MAPI, with the bandgap being close to 1.6 eV, the radiative limit (accounting only for unavoidable radiative recombination) is ~1.32 V. In devices, it is further reduced by the bulk and interface recombination. In the work by M. Stolterfoht *et al.*, it was shown that the interfaces play a crucial role in the device performance [91], and the use of interlayers can increase the V_{oc} value. In the work of Z. Liu *et al.*, devices featuring optimized deposition processes based on MAPI demonstrated over 1.26 V V_{oc}, which is currently one of the highest-achieved published values [96].

Finally, *FF* is the parameter showing the ratio between the maximum power point and the maximum power which could be extracted in case of no resistive losses. It is mostly limited by the transport properties of the selective contacts as well as by the charge-collecting electrodes. Usually, over 80% *FF* is considered to

be very high [97]. For more extensive information, readers are referred to the relevant literature [98].

1.2. Hole-transporting materials and their synthesis

The advantage of organic HTMs over inorganic analogues lies in the high variety of the materials, the possibility to fine-tune the properties by means of molecular engineering, and in exceptional mechanical properties. In particular, the use of amorphous materials offers the possibility to form a good contact on top of crystalline materials by means of simple solution-based processes. However, it is more difficult to achieve good charge transport ability in a disordered solid.

In this section, a short overview of HTMs and their role in PSCs is presented. First, the most popular HTM Spiro-OMeTAD is discussed. Then, the selected examples of small-molecule organic HTMs are presented, and their performance and synthesis are discussed. In the third part, new trends, such as HTMs for inverted PSCs, inorganic HTMs, and dopant-free HTMs shall be overviewed. At the end of the section, a brief overview of the key parameters of HTMs is given.

1.2.1. Tradition – Spiro-OMeTAD

Since the very first application in efficient PSCs, Spiro-OMeTAD (Figure 11) is still the most popular HTM in the field. For the first time, the structure of Spiro-OMeTAD was published in 1997, when it was used for blue OLEDs [25]. In this material, the spiro-core is utilized in order to improve the morphological properties of the popular hole-transporting molecules, such as TAD. The use of spiro carbon provides a perpendicular arrangement of the two interconnecting electroactive fragments. It prevents π–π stacking, and doubles the molecular weight [99], which in turn leads to the more stable amorphous phase.

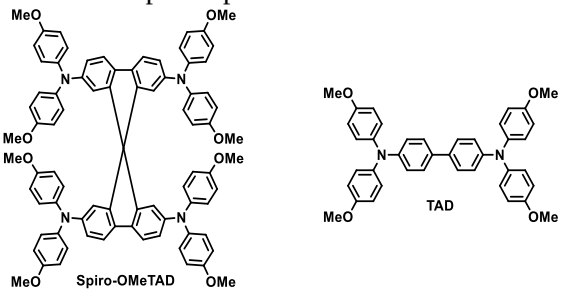

Figure 11. Structure of Spiro-OMeTAD and TAD [25]

In solar cells, for the first time, Spiro-OMeTAD was used in 1998 as an alternative to the liquid iodide/triiodide electrolyte in DSSC [100]. Despite having lower efficiencies, solid-state devices are much more attractive to market applications. The deposition methods and additives have been extensively optimized to maximize the performance of solid-state DSSCs [101]. With the emergence of PSCs, the main strategies were adopted after additional optimization.

Despite being the most popular HTM, there are several critical issues associated with Spiro-OMeTAD, namely:

a) The high price of Spiro-OMeTAD [65];
b) The morphological instability of the amorphous film [102];
c) Gold diffusion at elevated temperatures [103,104];
d) Complicated doping procedure (and the related instability).

The cause of the high price lies in the complicated synthesis of the spirobifluorene core. For the first time, the synthesis of the 9,9'-spirobifluorene was reported in 1930 by R.G. Clarkson and M. Gomberg [105], starting from 2-aminobiphenyl. The main reaction scheme has remained unchanged since then (an example of the synthetic route is presented in Scheme 1). It is one of the reasons why the prices are at the level of 350–500 €/g. The cost of materials required for the synthesis of 1 g of Spiro-OMeTAD was evaluated in the work by M.L. Petrus *et al.* [106] who utilized the method described by T.P. Osedach *et al.* [107] thus giving the final price of 92 $/g.

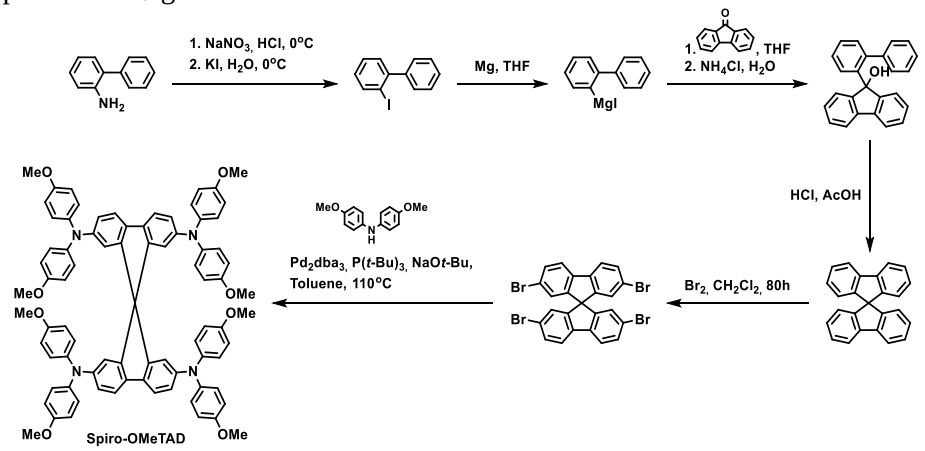

Scheme 1. One of the possible synthetic pathways towards Spiro-OMeTAD [99]

Morphological instability originates from the fact that Spiro-OMeTAD has a meta-stable amorphous phase which spontaneously transforms into the crystalline state over time. In the work by T. Malinauskas *et al.* [102], the crystallization of Spiro-OMeTAD was shown under operational conditions in solid-state DSSCs. Solar cells are expected to work for over 25 years, and, under direct sun, the temperature of the surface can rise significantly (>80°C), thus it is required that HTM does not feature a detectable crystalline state.

Another problem is introduced by the metal top contact. For the first time, gold migration through the Spiro-OMeTAD layer was shown by K. Domanski *et al.* [103] by means of the time-of-flight secondary ion mass spectrometry ToF-SIMS spectrometry. In this work, it was proposed to use a chromium interlayer as a means to surpass gold migration, however, at the cost of significant reduction of PCE (from 20.6% for Au-based devices down to 13% for a device with a 10 nm Cr interlayer). The detailed mechanism was described by S. Cacovich *et al.* [104] showing that the

process is light-activated and accelerated with an increase of the temperature. Research suggests that polymeric HTMs could be more resistive to this process [108], however, detailed comparison needs to be performed for the confirmation.

Doping is important for higher performance, however, it is commonly associated with the instability of the HTM layer. It is supported by the observation of the higher stability of dopant-free HTMs [109,110]. The doping procedure is discussed more thoroughly in Section 1.3.

All these issues serve as the driving force in the search of new HTMs.

1.2.2. Selected examples of small-molecule organic HTMs

During the last several years, a vast number of alternatives to Spiro-OMeTAD have been synthesized and studied regarding their performance in PSCs. Below, several representative approaches to the synthesis of new HTMs are discussed.

a) Spiro-OMeTAD modifications:

One of the strategies is to modify the structure of Spiro-OMeTAD (Figure 12). The first publication on the investigation of the isomers of Spiro-OMeTAD was written by N.J. Jeon *et al*. [111] in 2014. In their paper, the authors investigated the influence of the position of the methoxy-substituent. The highest PCE of 16.7% was achieved for the material *po*-spiro-OMeTAD.

An interesting change to the structure of Spiro-OMeTAD was described in the publication by M. Saliba *et al*. In the new HTM called FDT, one of the TAD fragments was substituted by bithiophene [112]. Solar cells with this material demonstrated 20.2% PCE, which was higher than that of Spiro-OMeTAD (19.7%). It was attributed by the authors to the additional interaction between thiophenes and perovskite, which might have reduced interface recombination and improve charge extraction thus improving the overall performance of the devices.

In the most recent publication by N.J. Jeon *et al*., the highest 23.2% PCE was achieved for the device with spiro-based HTM DM [33]. It is denoted by lower symmetry due to the change of a half of *p*-methoxy benzene fragments by dimethylfluorene. As a consequence, a slight shift in the energy levels is observed as well as improved morphological stability with a higher glass transition temperature. Surprisingly, such a small change in the structure was sufficient to improve not only the efficiency but also the stability of the devices.

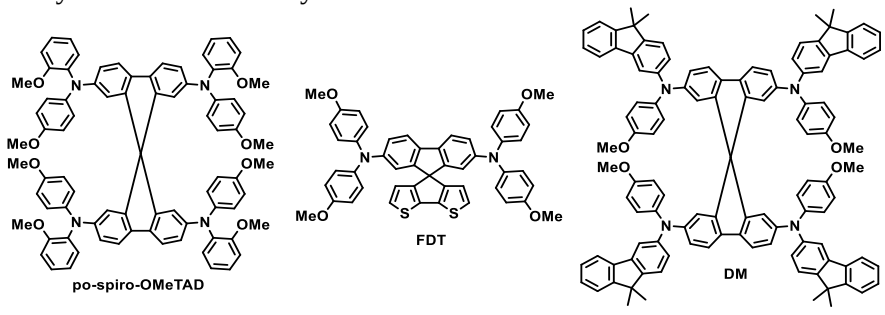

Figure 12. Structures of Spiro-OMeTAD-inspired HTMs [33,111,112]

b) Low-cost alternatives to the synthesis of the spiro-core:

The synthesis of the previously mentioned HTMs requires complicated synthetical procedures to obtain the spiro core. In several works seeking to solve this problem, spiro[fuorene-9,9'-xanthene] (SFX) was used instead (Figure 13). Contrary to 9,9′-spirobifluorene, SFX can be easily obtained starting from inexpensive fluorenone and phenol [113] (Scheme 2). The first study of various SFX-based compounds was reported by M. Maciejczyk *et al.* [114] who demonstrated the versatility of the approach while obtaining the target compounds in a three-step synthetic procedure. The best-performing material SFX-MeOTAD demonstrated 12.4% PCE, which was close to that of the device featuring Spiro-OMeTAD (13.0%). Almost at the same time, another paper with the same material (named X60) was published by B. Xu *et al.* [115], and an impressive PCE of 19.8% was achieved. In this case, 4-bromophenol and 2,7-dibromo-9-fluorenone were used as the starting materials, therefore, the overall reaction scheme was reduced to only two steps. Several more SFX-based HTMs have been developed later on, including X59 [116] (19.8% PCE) and X55 (20.8% PCE).

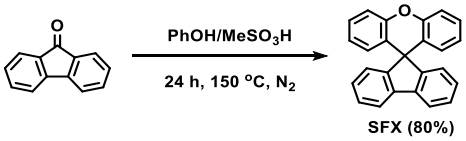

Scheme 2. Synthesis of SFX compound. Adapted with permission from [113]

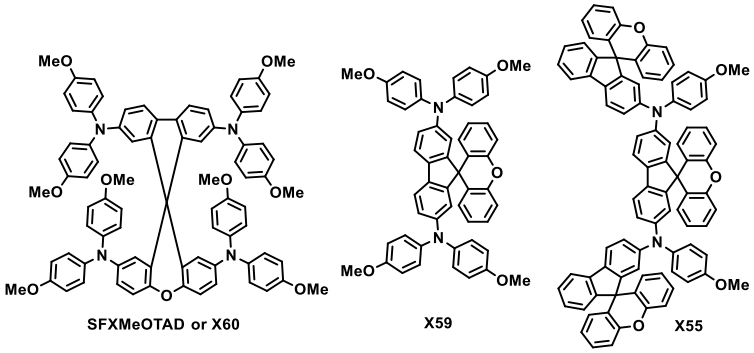

Figure 13. Structures of the SFX-based HTMs [115,116]

c) Another aromatics/heteroaromatics approaches:

Another approach is to completely avoid the synthesis of the spiro core by using heteroaromatic compounds as the core fragments which are further functionalized with several dimethoxy-triphenylamine or dimethoxy-diphenylamine fragments (Figure 14). This functionalization is easily performed by means of Pd-catalyzed reactions, and a large amount of aromatic and heteroaromatic compounds makes it a viable synthetical strategy.

One of the first successful HTMs based on the aromatic core was pyrene-based compound Py-C [117]. In 2013, 12.4% PCE was achieved, which at that time was close to the best results. As a drawback, the broad absorption range of Py-C can be

mentioned, with the λ_{max} of 492 nm. Another example was reported by H. Li *et al*. in 2014. They tested 3,4-ethylenedioxythiophene-based HTM H101 in PSCs [118]. Due to the relatively high efficiency of 13.8%, it was commercialized and became an alternative to Spiro-OMeTAD.

In this thesis, an important role is played by the carbazole heterocycle; therefore, it is important to mention the first successful application of this fragment in efficient HTMs. The first published HTM with a carbazole fragment for PSC was prepared by a team from Uppsala University [119]. Two 3,6-dimethoxydiphenylamine bissubstituted carbazoles were connected with biphenyl. At the moment of publication, it demonstrated an efficiency of 9.8%, which was comparable to that of the Spiro-OMeTAD reference (10.2%).

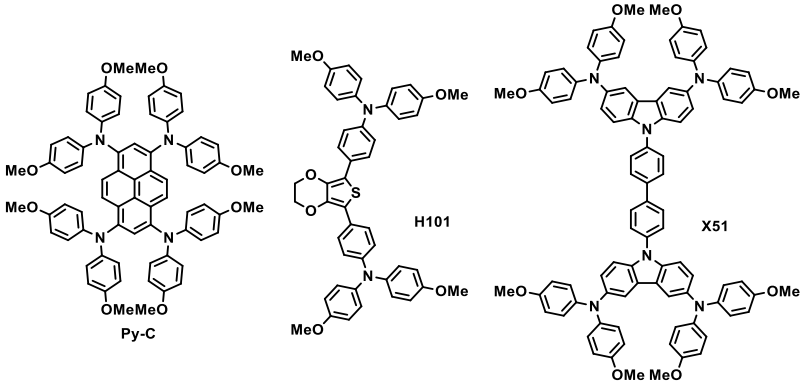

Figure 14. Structures of aromatics/heteroaromatics-based HTMs [117,118,119]

d) New promise – condensation chemistry:

The so far mentioned HTMs in their last step were functionalized by means of Pd-catalyzed reactions with dimethoxy-diphenylamine fragments. While these reactions are synthetically robust, the problem arises from the use of the metal catalyzer. A comparison of laboratory-synthesized Spiro-OMeTAD with the commercial one reported by K. Rakstys *et al*. [120] reveals that high-purity sublimed HTM offers higher conductivity, and, as a consequence, better performance. Palladium traces were shown to exert negative influence on the device performance in bulk heterojunction solar cells [121], which is relevant for PSCs. These findings explain the motivation behind the search for metal-free synthesis routes. To achieve this goal, it is important to utilize alternative ways to expand conjugation, for example, by using condensation chemistry (Figure 15).

The first example, which utilized the metal-free synthesis route, was published in 2015. In the paper, the authors presented new azomethine HTM EDOT-OMeTPA [106]. To extend conjugation, instead of Pd-catalyzed reactions, condensation between aromatic aldehyde and aromatic amine was used. The performance was similar to that of the other thiophene-based HTM H101, and it reached 11% PCE. Another example of the use of the reaction between aromatic amine and aldehyde was published by M. Daskeviciene *et al*. In this case, enamine-based compound V950 [122] was obtained with a promising PCE of 17.8%. One of the highest results

for the compounds synthesized starting from aromatic amines was achieved by D. Vaitukaityte *et al.* A new HTM V1091 was synthesized starting from a simple building block – aniline – and an impressive PCE of 20.2% was achieved [123].

The synthetical approach that was used for the synthesis of the EDOT-OMeTPA was further extended to the other classes of materials which can be obtained by means of condensational chemistry. In particular, hydrazone-based HTM EDOT-MPH was obtained by employing the reaction between aromatic aldehyde and hydrazine. Devices based on these materials showed a decent performance of 15.8% PCE [124]. Another material of interest is EDOT-Amide-TPA. In this case, the authors suggest that the hydrogen-bond network is formed thus increasing the order of the film and therefore promoting charge transport across the HTM layer. A very high PCE of 20.3% was achieved thus even outperforming Spiro-OMeTAD (19.7% PCE) [125]. A systematic comparison of different classes of materials is of top interest.

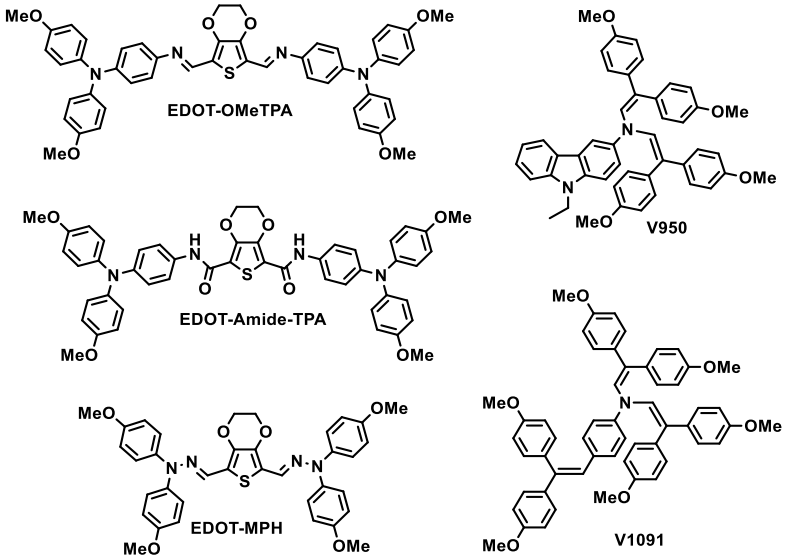

Figure 15. Structures of HTMs obtained by condensation chemistry [106,122,123,124,125]

1.2.3. Other challenges

So far, all HTMs mentioned in Section 1.2 have been developed for the use in the most efficient n-i-p architecture. However, with the development of the field, new promising concepts are appearing with the high demand for new materials. In particular, a short overview of HTMs used in p-i-n and tandem devices shall be presented. In addition, competitors to the traditional small-molecule HTMs, such as dopant-free HTMs and inorganic HTMs, shall be discussed.

a) HTMs for p-i-n

‘Inverted’ PSCs are becoming more popular due to some advantages in the deposition methods and their promise for tandem application. Due to the difference in construction, there are slightly different requirements for the HTMs used in the p-i-n configuration. As already mentioned in Section 1.1.4., HTMs should sustain deposition of the perovskite solution which usually consists of polar DMF and DMSO as solvents. This requirement strongly reduces the possible candidates, and, as a result, only several organic materials are known to exhibit high performance in the p-i-n configuration (Figure 16).

In the earlier works, the most commonly used material was conductive polymer PEDOT:PSS [126]. It can be deposited from aqueous colloidal solutions, which, after annealing, forms stable and non-soluble films. However, there are some fundamental limitations at the PEDOT:PSS/perovskite interface, e.g., due to the lower selectivity of the conductive polymer [127,128]. As a consequence, devices based on PEDOT:PSS systematically demonstrate lower V_{oc} values. The V_{oc} losses can be reduced by using some additional interlayer. Some works are focusing on improving the properties of PEDOT:PSS by means of post-treatment [129,130].

Currently, state-of-the-art devices are using PTAA polymeric HTM with the record PCE values of 21.5% [86] for doped and 20.4% [97] for dopant-free films. The key disadvantage of PTAA is the prohibitively high price due to the complicated purification process of the polymers from the traces of the metals and the issues with the reproducibility of the weight distribution. In addition, PTAA is denoted by a low glass transition temperature which depends on the molecular weight and is close to 100°C [131]. It might exert negative influence on the thermal stability of the devices.

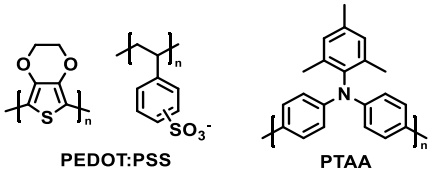

Figure 16. Structures of polymeric HTMs PEDOT:PSS and PTAA [86,126]

b) Tandem application

The PSC technology is currently undergoing a transition from laboratories to market application. However, it is difficult to compete with the existing mature Si-based technologies. To make its entrance into the market simpler, some researchers and companies are trying to benefit from the already existing products. In particular, the Si/perovskite tandem solar cell can provide a higher efficiency while only adding several deposition steps. There are several tandem configurations, with the most promising being the so-called *two-terminal tandem*, where two cells are electrically interconnected.

The first works in this field revealed stricter requirements to the HTM. In the work by S. Albrecht *et al*., it was shown that Spiro-OMeTAD significantly reduces the J_{sc} of the PSC by 2.2 mA cm^{-1} due to the parasitic absorption in the tandem cell

with 18.1% PCE. In addition, a MoO_3 interlayer was used to protect the organic HTM from sputtering damage [132].

In the work by K. Bush *et al*., p-i-n PSC was utilized for the fabrication of a 23.6% PCE tandem solar cell with a NiO_x HTM. As the light in such a configuration first passes through the perovskite absorber layer, the HTM has a significantly lower impact on J_{sc} reduction [133]. A tandem solar cell with a PTAA HTM was developed by M. Jošt *et al*., and it offered low parasitic absorption and yielded the final PCE of 25.5% [134].

Further advancement in this field is associated with the utilization of textured Si solar cells for efficient light management. For that, HTMs should be conformally covered on the rough surface of ~5 μm-height pyramids. For this purpose, F. Sahly *et al*. utilized vapor deposition of the spiro-TTB, which is denoted by a high T_g value (Figure 17). The final PCE of 25.2% was achieved [40].

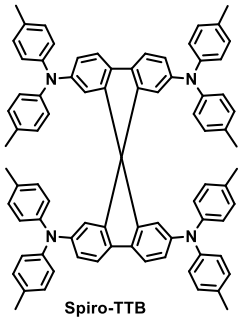

Figure 17. Structure of the Spiro-TTB HTM [40]

c) Inorganic HTMs

Commercialization of perovskites is impossible without achieving excellent long-term stability [135]. To achieve this goal, the stability of every component is crucial. In the literature, there is a prevailing opinion that inorganic materials are intrinsically more stable than organic analogues. Therefore, some researchers are focusing on the development of inorganic HTMs. In this section, two most popular inorganic HTMs, CuSCN, and NiO_x, are reviewed. For a more detailed overview, the readers are referred to the relevant literature [136].

One of the candidates to replace Spiro-OMeTAD is CuSCN HTM. It features a suitable energy level value and is highly transparent in the visible range. One of the main drawbacks of CuSCN is its very limited solubility in common organic solvents. Only organic sulfides are known to dissolve substantial amounts of CuSCN suitable for the deposition by spin-coating. The best PCE of 20.4% for CuSCN-based devices was reported by N. Arora *et al*. in 2017. CuSCN was dynamically spin-coated from diethyl sulfide on perovskite. Coupled with the reduced graphene oxide interlayer, the devices showed excellent stability. However, many researchers experience issues with the adaptation of the described deposition method. In the work by N Wijeyasinghe *et al*., it was shown that the deposition of CuSCN from diethyl sulfide under the same experimental conditions can result in significant

morphology variations [137] thus making the device fabrication optimization process excessively complicated.

Another inorganic material, NiO_x, is widely used in p-i-n PSCs. It is attractive due to many available deposition techniques. S. Seo *et al*. in their work utilized the atomic layer deposition (ALD) method to form an ultra-thin (7.5 nm) NiO_x layer, which yielded 16.4% PCE [138]. In the work by I.J. Park *et al*., electrochemical deposition of NiO_x from aqueous solutions of $Ni(NO_3)_2$ was utilized. A high PCE of 17% was demonstrated for 1 cm^2 devices [139]. Both of these methods required annealing at 300°C, which reduces the possible substrates. The low-temperature solution processing of NiO_x was developed by X. Yin *et al*. As high as 16.5% PCE was demonstrated. The films are annealed at 130°C, making this process compatible with most substrates [140].

d) Dopant-free HTMs

Another strategy to improve the stability of the HTM layer is to avoid the use of dopants. Several synthetical strategies have been successfully adopted to achieve this goal over the last several years thus obtaining dopant-free devices closer to the standard patterns (Figure 18).

In one of the initial works with efficient dopant-free HTM-based PSCs by Z. Li *et al*., this goal was achieved by synthesizing a molecule with a strong dipole moment while utilizing a strong donor and a strong acceptor. It was shown that the molecule BTPA-TCNE in the ground state exhibits features of the zwitterionic structure, and in the solid-state it features beneficial packing for charge transport. The highest PCE of 16.9% was achieved for PSCs containing this material [141].

A slightly different approach was demonstrated in the work by M. Cheng *et al*. Similarly, the acceptor-donor-acceptor type of molecule was used as an HTM, however, in addition, a pyridine fragment was ionized to form ionic compounds. Materials with two counterions were tested, with the superior performance being offered by the compound with the $TFSI^-$ ion. HTM M7-TFSI demonstrated sufficiently high conductivity and mobility to yield the final performance of 17.4% [142].

In the work by S. Paek *et al*., two star-shaped D-π-A molecules were studied as HTMs in PSCs. The highest PCE of 18.9% was achieved for FA-CN material with the quinolizino acridine central donor fragment [143]. The FA-CN molecule can adopt the flat configuration, which might promote advantageous packing of HTM molecules in the film. The use of the preferential orientation of the material in the bulk was further exploited by L. Zhang *et al*. It was shown that the polymeric HTM DTB adopts edge-on orientation with π–π stacking in the parallel direction to the surface of perovskite. It was further speculated that such an arrangement facilitates more intensive exposure of the aromatic rings to the perovskite layer and therefore improves the extraction of the holes. Due to the strongly increased J_{sc}, a high PCE of 19.7% was achieved [144].

One of the most notable results achieved in p-i-n PSCs was reported in a paper by M. Stolterfoht *et al*. The authors used the well-known polymer organic HTM

PTAA and optimized the film thickness in order to maximize *FF*. As thin as 8 nm film of HTM offered the best performance in the device. The best PCE of 20.4% is one of the highest for such solar cells, thereby making this approach highly attractive for further studies [97].

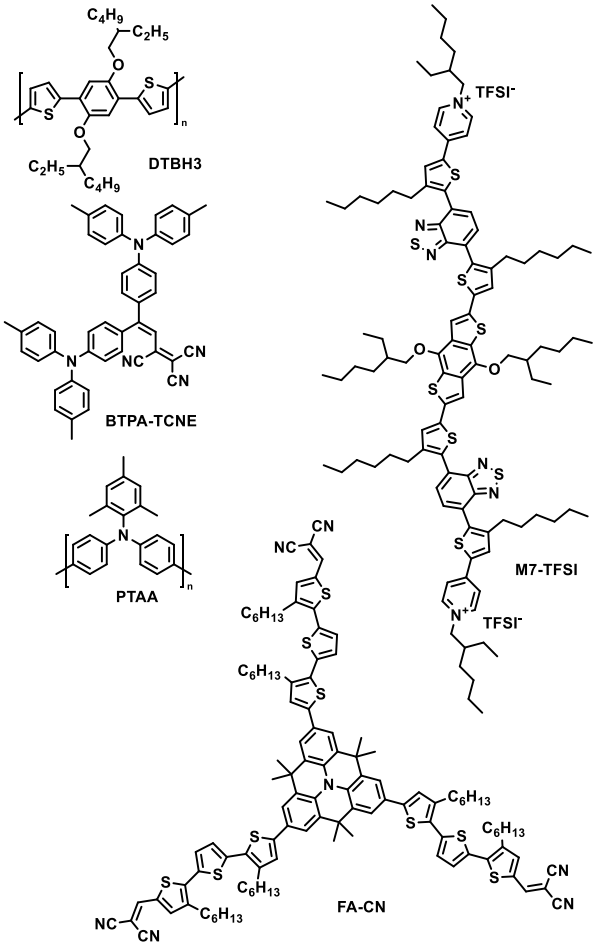

Figure 18. Structures of the selected dopant-free HTMs [97,141,142,143,144]

If comparing the thicknesses of the best-performing HTMs, it can be noticed that, for dopant-free materials, the thickness is usually several times smaller (Table 1). This can be attributed to the shorter length needed for the charge to travel from the perovskite absorbing layer to the charge collecting electrode. Therefore, resistive losses are minimized. It is evident that achieving good coverage with thinner films in a combination with good charge transport ability in the same materials is a challenging task.

Table 1. Comparison of the selected HTMs

HTM	Thickness, nm	PCE, %	Year, source
Doped HTMs			
n-i-p (‘regular’) device architecture			
Spiro-OMeTAD	160–200[a]	21.2	2016, M. Saliba *et al.* [34]
V885	150	18.9	2018, A. Magomedov *et al.* [145]
FDT	140–200[a]	20.2	2016, M Saliba *et al.* [112]
DM	150–180[a]	23.2	2018, N.G. Jeon *et al.* [33]
X59	220–300[a]	19.8	2016, D. Bi *et al.* [116]
p-i-n (‘inverted’) device architecture			
PTAA[c]	30	19.4	2017, C.M. Wolff *et al.* [146]
Dopant-free HTMs			
n-i-p (‘regular’) device architecture			
BTPA-TCNE	50[a]	16.9	2016, Z. Li *et al.* [141]
M7-TFSI	50	17.4	2016, M. Cheng *et al.* [142]
FA-CN	40	18.9	2017, S. Paek *et al.* [143]
DTB	150[b] (50–80[a])	19.7	2018, L. Zhang *et al.* [144]
p-i-n (‘inverted’) device architecture			
PTAA[c]	8	20.4	2017, M. Stolterfoht *et al.* [97]

[a] extracted from a scanning electron microscopy (SEM) image

[b] value given by the authors is larger than that extracted from a SEM image

[c] device of inverted architecture.

1.2.4. Performance parameters and characterization techniques

There are several metrics that are important for the discussion of amorphous organic HTMs. Some of them are related to the phase properties of the materials, whereas others are related to the electronic characteristics.

The use of organic materials for electronics is related to their advantageous mechanical properties. In order to achieve it, HTMs need to possess a stable amorphous phase, which gives the advantage of good mechanical stability, homogeneity, etc. For the characterization of the phase state of the material, differential scanning calorimetry (DSC) can be used. In brief, the difference in the amount of heat required to maintain the same heating speed (usually 10 °C min^{-1}) of the sample and the reference is registered. As a consequence, exothermic (i.e., crystallization, polymerization, etc.) and endothermic (i.e., melting, etc.) processes produce a specific signal on the DSC curve. For amorphous materials, the glass transition temperature is observed, which is a far less determined temperature, and a change in the heat capacity is detected.

Small-molecule organic HTMs after purification procedures are usually obtained in the crystalline state. However, after melting and fast cooling, the crystallization process is retarded, and materials solidify in the amorphous phase. A similar process takes place when the HTM is deposited by spin-coating with fast evaporation of the solvent [102]. Such materials are called molecular glasses. During the first DSC scan, the melting process is observed, however, when repeating the heating cycle after fast cooling, only T_g is observed (Figure 19). As the amorphous state is a non-equilibrium state, such films tend to crystallize over time, especially when the temperatures are rising closer to T_g. Therefore, the higher T_g values are commonly attributed to the more stable amorphous phase.

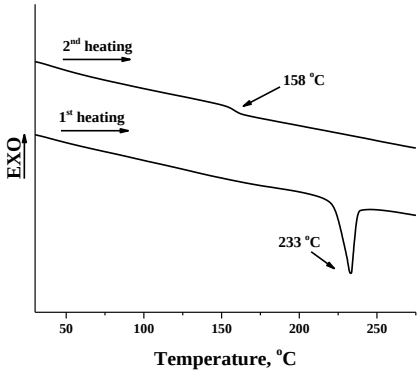

Figure 19. Representative DSC curves of molecular glass. Reprinted with permission from [145].

Another important parameter is the value of the energy levels. To provide efficient charge separation, favorable alignment of the energy levels is required. For organic HTMs, several ways of determining the energy levels are available. The value that is characteristic for the molecule of the HTM is the position of the highest occupied molecular orbital (HOMO) level, however, it is only accessible by theoretical calculations. From electrochemical measurements, the oxidation potential in solutions can be measured. Solid-state ionization potential measurements are useful for the description of the bulk material. A more detailed comparison can be found in a publication by J.-L. Bredas [147]. In this work, the ionization potential (I_p) value determined by the photoelectron spectroscopy in air (PESA) technique is used for the characterization of materials.

The issue of the correlation between the I_p of the HTM and the V_{oc} of the final device is still unresolved. While in many studies some correlation has been revealed [33], specifically designed experiments so far have not revealed the origins of such correlations [148,149]. In any case, the usual I_p value of efficient HTMs is in the range of 5.0–5.4 eV, which can serve as a guideline for the search of new materials.

For the evaluation of the charge transport ability of HTMs, the values are usually obtained by one of the two most common techniques, namely, the xerographic time-of-flight method, and by fabrication of field-effect transistors. It

must be kept in mind that different measurement stations could yield different values of the transporting ability, therefore, it is always advisable to use a reference material for the measurements.

These are the routinely studied characteristics of organic HTMs. Additional information can be obtained by studying perovskite-HTM bilayers by means of photoluminescence measurements, however, it gives a superposition of passivation (increase in the lifetime) and charge extraction (reduction of the lifetime), and thus the results can sometimes be misleading.

1.3. Doping of HTMs and associated degradation

In the previous sections, we have already mentioned the importance of the doping of HTMs when seeking to achieve the highest PCE. Most organic HTMs are used in PSCs in a combination with several dopants. Over the years, the 'standard' recipe was established and serves as the starting point for further developments.

The most popular composition of the hole-selective layer is as follows (Figure 20):

1 eq. of HTM
0.5 eq. of LiTFSI
0.03 eq of FK209
3.3 eq of tBP,

where LiTFSI stands for lithium bis(trifluoromethane)sulfonimide, FK209 for tris(2-(1*H*-pyrazol-1-yl)-4-*tert*-butylpyridine)cobalt(III) tri[bis(trifluoromethane) sulfonimide], and tBP for *tert*-butylpyridine.

The additives serve several purposes, namely, they improve the charge transporting properties, act as interfacial passivation, and contribute to the control of the film morphology. Here, an overview of the most popular dopants and their effect on HTMs is presented.

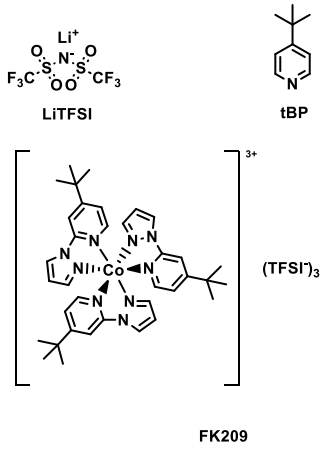

Figure 20. Structures of LiTFSI, tBP, and FK209 [150]

1.3.1. Oxidative additives

The largest group of additives is used for partial oxidation of HTM molecules. The motivation behind the use of such dopants lies in the very low conductivity of organic semiconductors in their pristine state, e.g., for Spiro-OMeTAD, it was measured to be ~10^{-8} S/cm [151]. Limited transport leads to the strongly reduced *FF* of the solar cells due to the high series resistance. From the conductivity equation, it can be seen that conductivity depends on

$$\sigma = pe\mu_h$$

where σ is the electrical conductivity; p stands for concentration of the holes; e denotes elementary charge; μ_h refers to the mobility of the holes.

The mobility of the holes is a property of the material, and, in general, is quite low for organic semiconductors (~10^{-7}–10^{-4} at low electrical fields). On the other hand, the concentration of the holes can be controlled by means of chemical doping.

The most commonly used additive LiTFSI for the first time was introduced to Spiro-OMeTAD by U. Bach [101] while searching for an efficient dopant to increase the conductivity of the organic HTM. At the beginning, it was thought to serve as a source of Li^+ ions which change the energy levels of TiO_2 [100]. However, this version contradicts the idea of the addition of LiTFSI to the HTM solution.

A more detailed description of the action mechanism was published in 2013. It was shown by A. Abate *et al*. that Spiro-OMeTAD with the LiTFSI additive oxidizes in the presence of air thereby forming a radical-cation species [152]. A strong increase in the conductivity of Spiro-OMeTAD was observed, starting from $3 \cdot 10^{-8}$ S cm^{-1} and rising up to $3 \cdot 10^{-5}$ S cm^{-1}. Following this insight, devices prepared with LiTFSI-doped HTM are routinely kept in dry air (<1% relative humidity) over the course of several days [153]. However, it must be considered that oxygen can exert a negative impact on perovskite, and on the overall device performance [154]. In addition, highly hygroscopic unreacted LiTFSI salt can provide pathways for moisture penetration through the HTM layer [155].

In literature, there is still lack of study on the effect of the $TFSI^-$ counterion on the final performance of the devices. One of the reasons for this choice is the possibility to use a relatively high amount of the dopant in the organic solvent [156]. Another reason could be attributed to the low nucleophilicity and the noncoordinating property of $TFSI^-$ [157], and, as a consequence, to the stabilization of the generated HTM radical-cation due to the strong delocalization of the negative charge over the whole molecule.

Another group of oxidative additives was introduced by J. Burschka *et al*. for the application in solid-state DSSDs [158]. Organic cobalt complexes, in particular, FK209 [159,160], do not require oxygen for the oxidation of Spiro-OMeTAD thus making the doping process faster and more robust. However, the amount of the added FK209 is usually limited to 0.03–0.05 eq. as a larger amount reduces the final performance of the devices.

An interesting development of the idea of the oxidation of HTM was proposed by W.H. Nguyen *et al*. In their work, the authors synthesized pre-oxidized Spiro-OMeTAD by treating it with the AgTFSI salt. The isolated spiro(TFSI)$_2$ compound was used instead of the LiTFSI additive thereby giving the competitive performance of ~10% (also, ~10% PCE was achieved with the LiTFSI standard) [151]. In a later work by T. Leijtens *et al*., this concept was further adapted to HTM EH44 with a hydrophobic long aliphatic group in order to increase stability against moisture [161]. This material was further used in the work by J.A. Christians *et al*. for the fabrication of PSCs with one of the best reported levels of stability [162].

1.3.2. 4-*tert*-butylpyridine – interfacial and/or morphological modifier

Apart from oxidative additives, there is one more compound, tBP, routinely used in the HTM solution composition. Despite being one of the most popular additives, the exact role of tBP is not entirely clear yet. Its use originates from the early works on DSSCs, where sensitized TiO_2 films were dipped into tBP before the final assembly of the solar cell [163]. Later on, tBP was used as an additive to HTM in the solid-state DSSCs [100]. In all the devices, the use of tBP resulted in a significantly increased performance level.

In the literature, several possible mechanisms of the positive effect of tBP in PSCs can be found. In the work by N. Noel *et al.*, the pyridine base was shown to act as a passivating material of the surface trap states [164]. This process might lead to the reduced recombination at the HTM/perovskite interface, and, therefore, to higher PCE values. These findings are further supported by the work of S. Habisreutinger *et al*., where indications of the direct chemical interaction between tBP and perovskite materials were demonstrated [165].

An alternative view regarding the problem was shown by S. Wang *et al*. In their work, it was demonstrated that tBP acts as a co-solvent improving the solubility of LiTFSI salt in the HTM solution. As a consequence, a better distribution of LiTFSI is achieved, and the quality of the spin-coated layer is greatly increased [166]. Based on these findings, in a more recent work, the formation of the complexes between tBP and LiTFSI was studied. Experimental data supports the idea of the solubilization of the inorganic salt with the tBP additive. In addition, the importance of the ratio optimization between these two components was demonstrated as it leads to superior device stability [167].

Despite the general positive effect on the device performance, in the work by Y. Yue *et al*., it was shown that pyridine derivatives can lead to the degradation of perovskite. As an alternative, the authors proposed to use less reactive 2-amylpyridine which had a positive effect on the overall device stability [168].

2. Review of Articles

2.1. 'Click-Chemistry' Inspired Synthesis of Hydrazone-Based Molecular Glasses

This chapter is based on published work: *A. Magomedov, S. Urnikaite, O. Paliulis, V. Jankauskas, V. Getautis, RSC Adv., 2016,* ***6****, 8701–8704. JIF: 3.049; times cited: 5.*

As it was discussed in the previous sections, efficient synthesis of amorphous functional materials is an important challenge for further advances in the field of molecular electronics. In the first work, hydrazone-based semiconductors, which are known to have good charge transporting properties [169], however, usually in a combination with a strong tendency to crystallize, were used for the investigations. In the scholarly literature, there are several examples of the ways how to circumvent this problem, e.g., by the use of a polymeric binder [169], or by the synthesis of polymers with hydrazones as side chains [170]. Unfortunately, the use of insulating fragments significantly reduces the ability of the materials to transport charges. Thus new strategies need to be developed to achieve hydrazones with a stable amorphous state.

At the beginning of the 21st century, a novel view regarding applied synthetical chemistry was proposed by K.B. Sharpless [171]. The idea lies in the use of simple and versatile synthesis schemes to achieve complex structures. This should lead to a faster transfer of materials from the laboratory to large-scale manufacturing, and thus reduce costs of the functional materials. To reflect the ideas behind the concept, it was called 'click-chemistry'. In this work, some of the principles of 'click-chemistry' were adopted to the synthesis of branched hole-transporting materials.

The hydrazone functional group (>C=N–N<) can be obtained by the condensation reaction between aromatic aldehyde and hydrazine (Scheme 3). In this work, triphenylamine [172] and N,N-diethylaniline aldehydes [173] were used. After the reaction with phenylhydrazine, intermediate products were obtained with an unsubstituted active hydrogen atom which can be used for further functionalization.

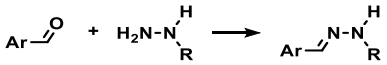

Scheme 3. Synthesis of hydrazones

In this paper, a stable amorphous phase in hydrazones was achieved by the synthesis of the branched structures. The target compounds were obtained by means of the reaction between the bromomethyl group of benzene derivatives and the intermediate reactive hydrazones. Overall, six molecules with two, three, and four branches were synthesized and subjected to further analysis (Scheme 4).

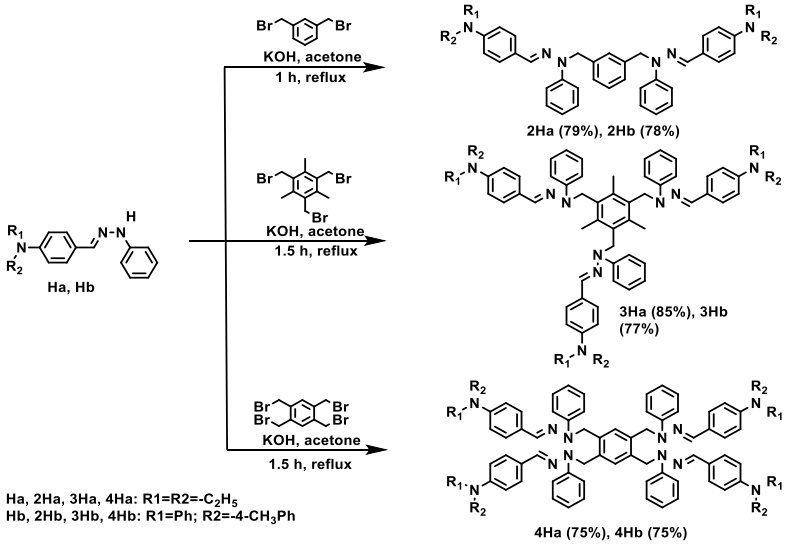

Scheme 4. Synthesis of branched hydrazone-based HTMs

To study phase transitions of the synthesized hydrazones, DSC analysis was performed. Molecules with two and four branches were isolated as crystalline materials. On the other hand, molecules with three branches already during the first scan do not show the melting phase transition, and they show only glass transition, which is a characteristic of amorphous materials.

To characterize the semiconducting properties of the synthesized compounds, two important parameters were measured, namely, the solid-state ionization potential (I_p) and the hole drift mobility (μ). The results are presented in Table 2. I_p was found to be independent from the number of branches in a molecule, being 5.0–5.02 eV for **2Ha**, **3Ha** and **4Ha** with triphenylamine chromophore and 5.33–5.35 eV for **2Hb**, **3Hb**, and **4Hb** with N,N-diethylaniline chromophore. This result was expected due to the non-conjugated nature of the central linking fragment. The values of the hole drift mobilities in a series of **2H**, **3H**, and **4H** were found to be the highest for the molecules with two branches.

Table 2. I_p and hole mobility data for (**2–4**)**H**(**a**,**b**)

Compound	I_p[a], (eV)	μ_0[b], ($cm^2\ V^{-1}\ s$)	μ[c], ($cm^2\ V^{-1}\ s$)
2Ha	5.02	3×10^{-7}	8×10^{-5}
2Hb	5.35	7.4×10^{-5}	1.3×10^{-3}
3Ha	5.00	3.5×10^{-8}	2.2×10^{-5}
3Hb	5.33	4.6×10^{-6}	2.0×10^{-4}
4Ha[d]	5.00	-	$\sim 1 \times 10^{-5}$
4Hb[d]	5.35	-	$\sim 6.7 \times 10^{-4}$

[a] Ionization potential was measured by the PESA method.

[b] Mobility value at zero field strength.

[c] Mobility value at 6.4×10^5 V cm^{-1} field strength.

[d] Due to the high dispersity, the mobilities were measured only at strong electrical fields.

Overall, the proposed synthesis scheme proved to be useful for the synthesis of molecular glasses with a high T_g and for the synthesis of fully amorphous compounds. High μ values were obtained, and they reached the 10^{-3} $cm^2\ V^{-1}\ s$ order of magnitude for **2Ha** at strong electrical fields.

Upon noting these promising results, several hydrazone-based HTMs were tested in PSCs, however, the devices showed only minor performance of <1% PCE. It can be speculated that such a performance could be attributed to the incompatibility of the synthesized hydrazones with the established doping process.

Author's contribution: Synthesis and characterization of the compounds, preparation of the draft of the manuscript.

2.2. A Methoxydiphenylamine-Substituted Carbazole Twin Derivative: An Efficient Hole-Transporting Material for Perovskite Solar Cells

This chapter is based on published work: *P. Gratia, A. Magomedov, T. Malinauskas, M. Daskeviciene, A. Abate, S. Ahmad, M. Grätzel, V. Getautis and M.K. Nazeeruddin, Angew. Chemie – Int. Ed., 2015, 54, 11409–11413. JIF: 12.257; times cited: 142; the article was highlighted as frontispiece.*

The synthetical strategy applied to the synthesis of branched hydrazone derivatives proved to be efficient to achieve an amorphous state in a combination with good charge transport properties. To avoid arising problems associated with the doping process, it was decided to develop a material with a structure resembling that of the Spiro-OMeTAD compound. In particular, the chromophoric system should consist of two donoric dimethoxydihenylamine fragments interconnected with a π-conjugated bridge. A material which can be used as the starting material to achieve such a goal is 3,6-dibromocarbazole.

The modified synthesis scheme consists of two steps (Scheme 5). In the first stage, two equivalents of 3,6-dibromocarbazole react with *o*-

bisbromomethylbenzene. As early as after 10 min of refluxing the reaction mixture in THF, with the addition of KOH, the product precipitated in the form of white crystals. The purification procedure consisted of filtration and washing of the product with H_2O. During the second stage, the intermediate product was functionalized with dimethoxydiphenylamine moieties by means of palladium-catalyzed Bushwald-Hartwig C-N cross-coupling reaction.

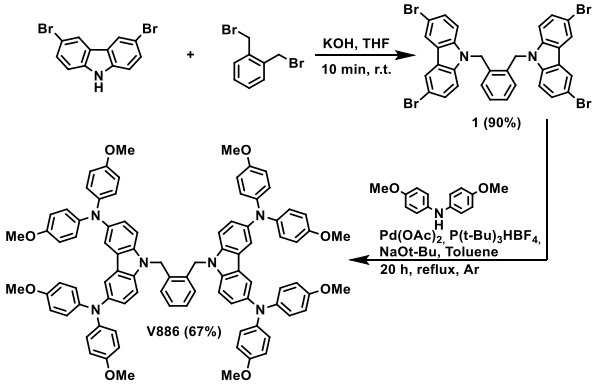

Scheme 5. Synthesis of **V886**

The simple first stage offers a significant advantage to **V886** in comparison to Spiro-OMeTAD. Such a synthetical strategy avoids the use of sensitive and aggressive reagents (such as BuLi; Br_2, etc.) that are required for the synthesis of Spiro-OMeTAD and delivers an intermediate compound in high yield via a simple and fast procedure. The overall yield of the scheme is 60%, which makes this material suitable for large-scale synthesis.

A comparison of the properties of **V886** with those of Spiro-OMeTAD is given in Table 3. In brief, **V886** is denoted by comparable hole drift mobility at low electrical fields and a comparable I_p value. While for Spiro-OMeTAD, during the first DSC cycle, the melting process is detected, **V886** exhibits only T_g, which means that it is fully amorphous. Additionally, the conductivity of the doped materials with 10 mol% of FK209 was measured showing that chemical doping gives reasonable conductivity.

Table 3. Properties of **V886** and Spiro-OMeTAD

Material	T_m, (°C)	T_g, (°C)	I_p, (eV)	μ_0, ($cm^2\ V^{-1}\ s$)[a]	μ, ($cm^2\ V^{-1}\ s$)[b]	S, ($S\ cm^{-1}$)[c]
V886	-	141	5.04	2×10^{-5}	6×10^{-4}	4.2×10^{-5}
Spiro-OMeTAD	248 [174]	125 [174]	5.00	4×10^{-5}	5×10^{-4}	4.7×10^{-4}

[a] Mobility value at zero field strength.

[b] Mobility value at $6.4 \times 10^5 V\ cm^{-1}$ field strength.

[c] Lateral conductivity was measured for doped films (10 mol% FK209).

Finally, to test the performance of **V886** in devices, an $MAPbI_3$-based device was constructed (a more detailed description of the devices is given in the publication). A very high PCE of 16.9% was achieved for the device prepared with **V886** HTM. Devices with Spiro-OMeTAD showed a superior performance of 18.4%, however, the much simpler synthesis of **V886** makes this material extremely competitive. At the time of the publication, it was the second-best result achieved for small-molecule organic HTM-based PSCs.

Due to the comparable performance with Spiro-OMeTAD in a combination with the simple synthesis, **V886** was patented under European patent. Eventually, the license for the distribution of **V886** was acquired by *Tokyo Chemical Industry Co., Ltd.* (TCI).

Author's contribution: Synthesis and characterization of the **V886** material.

2.3. Diphenylamine-Substituted Carbazole-Based Hole Transporting Materials for Perovskite Solar Cells: Influence of Isomeric Derivatives

This chapter is based on published work: *A. Magomedov, S. Paek, P. Gratia, E. Kasparavicius, M. Daskeviciene, E. Kamarauskas, A. Gruodis, V. Jankauskas, K. Kantminiene, K.T. Cho, K. Rakstys, T. Malinauskas, V. Getautis and M.K. Nazeeruddin, Adv. Funct. Mater., 2018, 28, 1704351. JIF: 15.621; Times cited: 29.*

Following the initial success with **V886**, more derivatives were synthesized by utilizing the same synthetical scheme when trying to make a systematic study of the influence of the structure on the performance of the final device. Overall, 11 materials were tested, including 9 new carbazole-based HTMs as well as **V886** and Spiro-OMeTAD for comparison. Owing to the fact that there is usually a large spread in the achieved PCE values even while working at the same lab [153], there is lack of broad studies of the larger families of the relevant materials.

The same two-step synthetical strategy was used as described previously for the synthesis of **V886**-like structures, namely, structural isomers **V885** and **V911**, three methyl-substituted analogues (**V931**, **V928**, and **V908**) (Figure 21), a series of branched materials with one, three, and four photoactive fragments (**V990**, **V1039**, and **V957**) (Figure 22), a carbazole-substitution isomer of **V886** with 2,7-substitution (**V946**) (Figure 23).

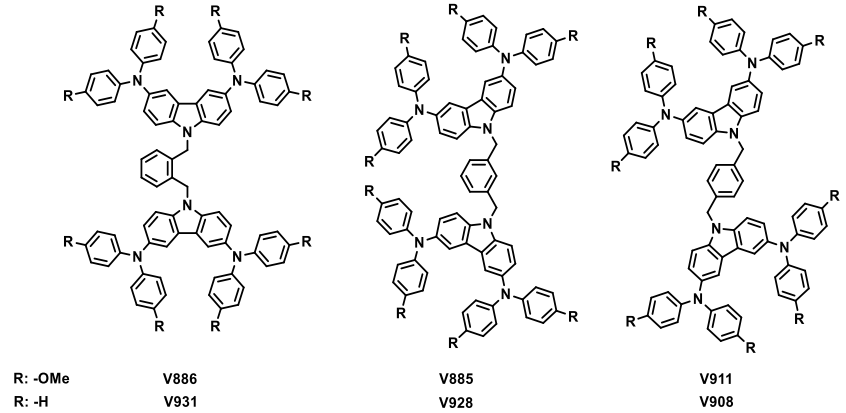

Figure 21. Structures of structural isomers **V886**, **V885**, **V911**, and their methyl-substituted analogues **V931**, **V928**, **V908**

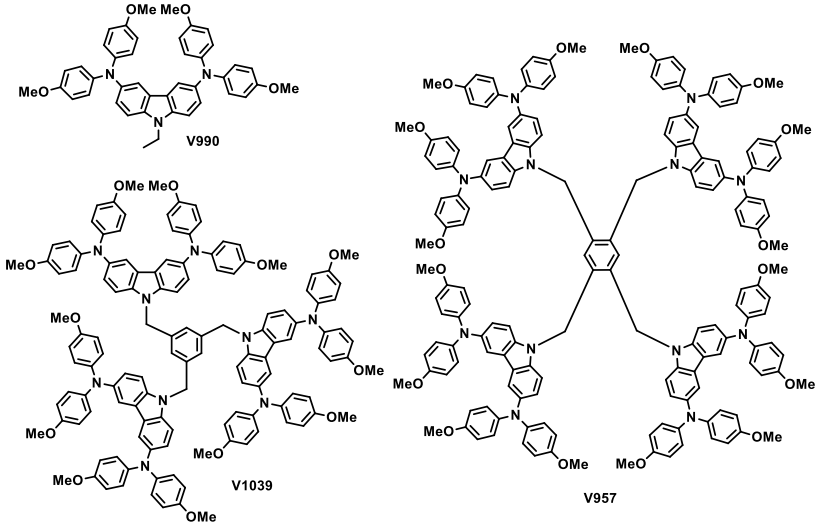

Figure 22. Structures of the branched **V886** analogues with one (**V990**), three (**V1039**), and four photoactive fragments (**V957**)

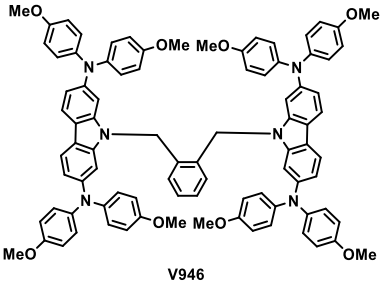

Figure 23. Structure of **V886** carbazole-substitution isomer with 2,7-substitution (**V946**)

DSC analysis revealed that most of the new materials after purification procedures are obtained in the amorphous state with no melting process detected during the first heating cycle. Only for two materials, *ortho*- (**V931**) and *para*- (**V908**) derivatives with dimethyldiphenyl fragments, melting processes were detected. In particular, interesting behavior was observed for **V908** material, where, during the first heating cycle, three transitions occurred: glass transition, recrystallization (219 °C), and melting (337 °C). Both of these materials during the second heating cycle showed only glass transition. High T_g values of the investigated materials suggest good morphological stability of the deposited films. In addition, all the materials showed good thermal stability as determined by thermogravimetric analysis.

The I_p of the new HTMs is mostly determined by the substitution of the chromophoric part of the molecule, which suggests that there are no strong π–π interactions (both intra- and intermolecular) between separate chromophores. The absence of the π–π intramolecular interaction is also confirmed by UV/vis spectroscopy. In particular, in a series of structural isomers (methoxy-substituted: **V886**, **V885**, **V911** and methyl-substituted: **V931**, **V928**, **V908**), the UV/vis absorption spectra follow exactly the same line.

An interesting observation can be done while comparing hole drift mobilities. For the structural isomers with methyl substituents (**V931**, **V928**, **V908**), the values are of the same order of magnitude (μ: 7.8×10^{-4}, 3.7×10^{-4}, 4×10^{-4} $cm^2\ V^{-1}\ s$, respectively). However, for the methoxy-analogues, a significant increase of the μ value was measured going from **V886** (6×10^{-4} $cm^2\ V^{-1}\ s$) through **V885** (4.6×10^{-3} $cm^2\ V^{-1}\ s$) and to **V911** (1×10^{-2} $cm^2\ V^{-1}\ s$). Such a behavior suggests the formation of intermolecular hydrogen bonding in the bulk of the materials thus promoting charge transfer. This result indicates the significance of the molecular structure to the charge transporting ability of organic HTMs.

Finally, the performance of the synthesized compounds was tested in PSCs of mesoporous architecture with triple-cation perovskite composition. Devices prepared with the standard material Spiro-OMeTAD showed a performance score of 18.8%. Two new compounds (**V885** and **V911**) showed performance that was almost the same level as that of the Spiro-OMeTAD. The highest PCE of 18.92% was obtained for *m*-isomer **V885**.

The simplest compound **V990** showed a very low performance score of only 5%, which can be attributed to the poor charge transporting properties of this material. More complicated branched compounds showed a moderate performance level of 17.1% for **V1039** and 16.9% for **V957** thus showing that a more complicated structure not necessarily leads to better performance.

Materials with methyl groups showed a slightly lower performance of ~16%. Such a behavior can be attributed to the increased I_p, and, as a consequence, the efficiency of the doping process was reduced.

Compound **V946** also showed reduced performance (15.7%) in comparison to that of **V886**. A possible cause is the more disordered packing of the molecules due to the higher steric strain.

Author's contribution: Synthesis and characterization of the new materials. Preparation of the draft of the manuscript.

2.4. Pyridination of the Hole Transporting Material in Perovskite Solar Cells Questions the Long-Term Stability

This chapter is based on published work: *A. Magomedov, E. Kasparavičius, K. Rakstys, S. Paek, N. Gasilova, K. Genevičius, G. Juška, T. Malinauskas, M.K. Nazeeruddin, and V. Getautis, J. Mater. Chem. C, 2018, 6, 8874–8878. JIF: 6.641; Times cited: 21; the article was highlighted on the back cover page.*

As it was discussed in Section 1.3, HTMs need doping to achieve high performance. As a consequence, the search for new HTMs is strongly complicated due to the empirically optimized doping procedure of Spiro-OMeTAD. What is even more important, there is lack of understanding of the effects of the dopants on the final performance of devices.

In this work, one of the previously omitted factors, namely, the intrinsic stability of the HTM layer composition with the dopants, was studied. It might exert a significant impact on the final device stability and/or performance.

The basis for the work became an empirical observation, of the evolution of the HTM solution. Directly after doping with oxidative additives, the color of the solution changes to the intensively colored (e.g., brick red for Spiro-OMeTAD and green/blue for **V886**, Figure 24). However, after the addition of tBP, the solution tends to lose its color in the course of several days. Such transformations suggest some chemical interaction between the components of the mixture.

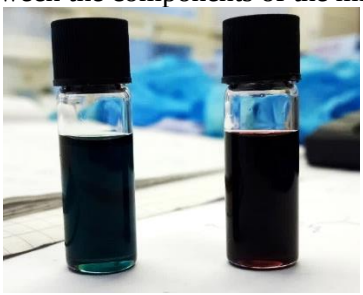

Figure 24. Solutions of oxidized **V886** (left) and Spiro-OMeTAD (right)

In order to study the underlying process, model compound **V990** was used, which is close in structure to the best-performing carbazole-based HTMs but is much simpler in the analysis. Pre-oxidized **V990** was synthesized following the procedure published by W.H. Nguyen *et al*. [151]. In brief, **V990** was oxidized by AgTFSI salt in dichloromethane, with the formation of elemental Ag. The precipitated particles were removed by means of filtration, and the product was concentrated to give a dark-blue-green solid of **V990^{+}TFSI^{-}**.

Next, the interaction between **V990^{+}TFSI^{-}** and tBP was studied. To keep the process as simple as possible, and to exclude the influence of the solvent, **V990^{+}TFSI^{-}** was dissolved in pure tBP. While stirring the reaction mixture at 60°C,

already after 10 min, the color of the solution completely changed from intense green to orange. TLC analysis revealed that two products were formed, which were further isolated by means of column chromatography in 38.5% and 33% yields (total yeld 71.5%) (Scheme 6).

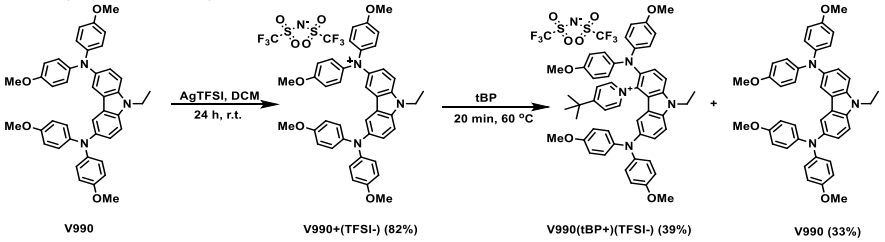

Scheme 6. Oxidation and C–H pyridination of the dimethoxydiphenylamine-substituted carbazole fragment in **V990**

NMR analysis revealed that the first compound is starting material **V990**, while in the other material, a pyridinium moiety is attached to the carbazole fragment. To determine the most probable position of the substitution, DFT calculations were used while following the previously published procedure [175]. In brief, nucleophilic substitution occurs at the position where the LUMO density is the highest in the cation-radical species. For the unsubstituted aromatic positions, the highest LUMO density is at the 4th position of the carbazole fragment (Figure 25). Such a substitution was further confirmed by ^{1}H NMR spectra where five characteristic signals with integrals corresponding to one proton were observed in a range of 7.96–6.16 ppm, with the spin-spin coupling consistent with the substitution at the 4th position. Finally, the structure can be confirmed by comparison of the calculated and measured ^{13}C NMR spectra, where the characteristic signal of the carbon at the 4th position of the *tert*-butylpyridinium ring was calculated to be at 174.34 ppm and was observed at 172.46 ppm from DMSO-*d6* and at 174.36 ppm from acetone-*d6*. Knowing the structures of the final products and the relationship between the yields, the reaction mechanism was suggested (Scheme 7).

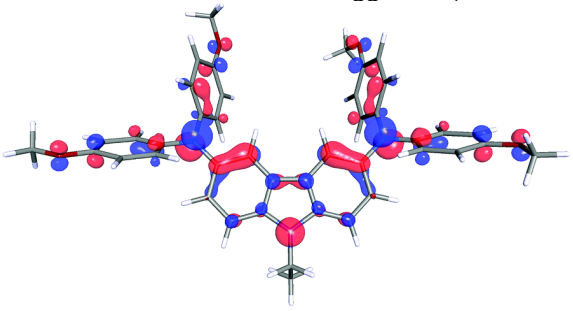

Figure 25. The lowest unoccupied molecular orbitals of **V990**$^{+}$ obtained by DFT calculations

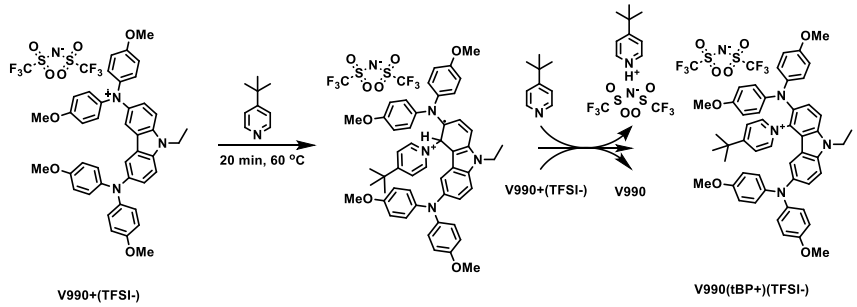

Scheme 7. Suggested mechanism of the C–H pyridination

The same reaction was performed with pre-oxidized **V886**, and, in this case, three products, namely, initial compound **V886**, monosubstituted **V886(tBP$^+$)(TFSI$^-$)**, and bissubstituted **V886(tBP$^+$)$_2$(TFSI$^-$)$_2$** materials were isolated in 20.5%, 37.9%, and 17.1% yields (total yield 75.5%), respectively (Figure 26).

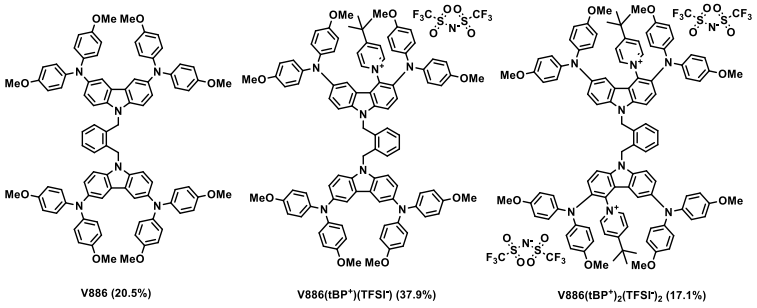

Figure 26. Structures of pyridinated **V886** species

The photophysical properties of the isolated new materials were studied indicating unfavorable energy level alignment and charge transporting properties.

In order to study if the process takes place in the actual devices, aged PSCs with **V886** HTM were analyzed. The devices were stored in air at 80 °C 340 h. After that time, the HTM layer was washed from the aged device with THF, and the solution was subjected to MS analysis. A weak signal at 1478.856 *m/z* was detected, which can be attributed to **V886(tBP$^+$)** cation (1478.6694 Da). This assignment was further confirmed by means of MS/MS analysis.

These results for the first time revealed the mechanism of the intrinsic instability of doped HTMs used in PSCs. The effect of doping effectively reduces over time due to the pyridination process, as a consequence leading to reduced long-term stability. In addition, this could potentially be used in the synthetical chemistry for the synthesis of C-N bonds.

Indirect proof can be found in the works of other scientists regarding formation of the ‘voids’ [176]. In a paper by J.P. Bastos *et al*., it is emphasized that tBP is linked to the degradation of devices, and, in particular, one of the suggestions being “*Light Degrades tBP and the Degraded Species are Positively Charged*” [177]. More recently, a further confirmation of the proposed mechanism was published by F. Lamberti *et al*. [178].

Author's contribution: The initial idea. Synthesis of the pyridinated products and structural analysis of the isolated products. Analysis of the NMR data, proposal of the reaction pathway and suggestion of the mechanism. Draft of the manuscript.

2.5. Self-Assembled Hole Transporting Monolayer for Highly Efficient Perovskite Solar Cells

This chapter is based on published work: *A. Magomedov, A. Al-Ashouri, E. Kasparavičius, S. Strazdaite, G. Niaura, M. Jošt, T. Malinauskas, S. Albrecht and V. Getautis, Adv. Energy Mater., 2018, 1801892. JIF: 24.884; Times cited: 20; the article was highlighted on the front cover page.*

As the doping of HTM, in particular, generation of cation-radicals by oxidation, leads to the reduction of long-term stability, it is very important to create a dopant-free alternative. Based on the literature overview, it can be seen that conventional dopant-free HTMs prepared by spin-coating are usually much thinner than the doped analogues. However, for such a thin film, it is very important to obtain uniform coverage of the underlying material. In particular, in the work by M. Stolterfoht *et al*. [97], it was shown that, by reducing the thickness of PTAA, significant reduction in V_{oc} is observed.

A very powerful tool to achieve uniform coverage of the substrate is the self-assembly of organic molecules with the anchoring group. It is known that phosphonic acids strongly bind to the surface of ITO. Therefore, novel HTM **V1036** was synthesized by E. Kasparavicius, in which, a hole-selective carbazole-based fragment was functionalized with a phosphonic acid anchoring group (Figure 27.).

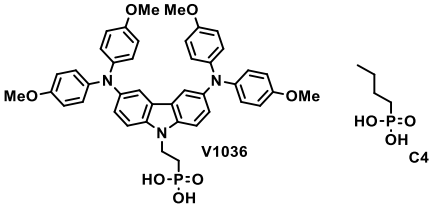

Figure 27. Structure of carbazole-based phosphonic acid **V1036** and butylphosphonic acid **C4**

The process of monolayer formation consists of several steps: a) cleaning of the substrate; b) immersion of the substrate into a solution of phosphonic acid; c) annealing; d) washing and drying. In this work, O_3 cleaning was used for the cleaning of the substrates. This step is important so that to get rid of the physically adsorbed organic molecules, which helps to get uniform coverage. For the immersion, 1 mM solutions were used. Another important step is annealing. Annealing promotes chemical binding of the molecules, however, the exact mechanism is not yet clear. Finally, the substrates are intensively washed with chlorobenzene and 2-propanol in order to remove any physically adsorbed material, and dried.

The formation of a monolayer can be easily monitored by means of contact angle measurements. The perovskite solution showed better wetting on monolayer-functionalized substrates, which can be advantageous for larger-scale production. It was demonstrated that the contact angle can be varied over a wide range of values by means of mixing with butylphosphonic acid (**C4**) (Figure 28). This feature can be used for the optimization of the inject-printing deposition process.

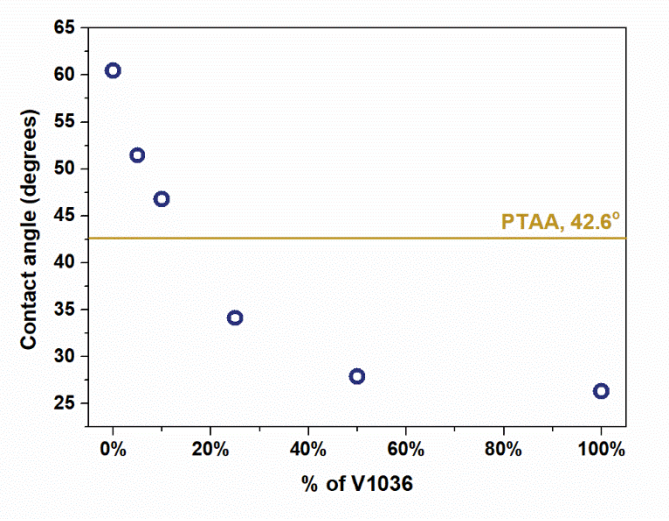

Figure 28. Contact angle dependence on the percentage of the **V1036** in the SAM composition

To prove that **V1036** was bound to the surface of ITO, FTIR measurements were performed. The FTIR spectra of the monolayer recorded from the functionalized ITO substrate are very close to that of **V1036** dispersed in KBr tablet (Figure 29). This result serves as proof of the successful binding of **V1036** to the surface of ITO.

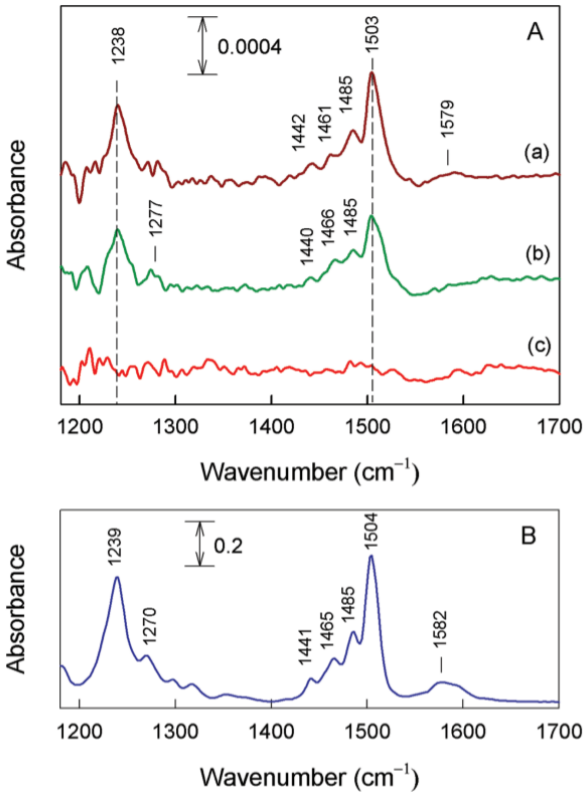

Figure 29. A) FTIR absorbance spectra of monolayers on ITO substrates prepared from (A-(a)) 1×10^{-3} m solution of V1036, (A-(b)) 1×10^{-3} m of mixed solution **V1036**:**C4** (1:9), and (A-(c)) 1×10^{-3} m solution of **C4**. B) FTIR spectrum of bulk **V1036** in KBr tablet

Finally, devices of the p-i-n configuration with the monolayer hole-selective layer were constructed and tested. Devices with the pure **V1036** monolayer showed reduced V_{oc} values in comparison to that of the PTAA standard. This problem was partially resolved by using the mixed-SAMs approach with the butylphosphonic (**C4**) small molecule used as a 'filler'. By optimizing the ratio between **C4** and **V1036**, an increase in V_{oc} was achieved thus leading to a highly promising PCE of 17.8%.

The use of monolayers as a hole-selective contact promises several important advantages for future applications. First, as it is a dopant-free technique, better stability of the devices is expected. Second, the deposition method is suitable for the conformal coverage of uneven surfaces, which is important for successful fabrication of tandem devices. In addition, a monolayer does not introduce additional parasitic absorption (Figure 30). Finally, due to the very thin nature of the film (<2 nm), the consumption of materials is minimized.

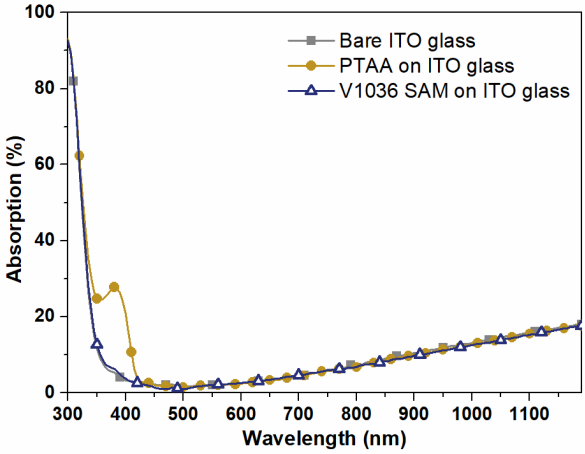

Figure 30. UV/vis absorption spectra of bare ITO substrate, ITO with PTAA, and ITO with 100% **V1036** SAM

Starting with this work, more hole-selective molecules with a phosphonic acid fragment were synthesized and tested for the performance on PSCs. With one of them, close to 21% PCE was achieved, which is considerably higher than the state-of-the-art HTM PTAA.

Author's contribution: The initial idea. Fabrication of solar cells. DFT calculations. Draft of the manuscript.

3. Conclusions

In conclusion, this work presents a significant improvement in the field of hole transporting materials for perovskite solar cells by setting a new pathway for the development of functional materials. In particular:

1. A series of hydrazone-based branched hole-transporting materials utilizing a simple reaction between hydrazone and bromomethyl benzene derivatives were synthesized and investigated. It was determined that:
    a. the fully amorphous state of materials can be achieved in the case of less-symmetrical molecules with three side-arm branches;
    b. the best charge transporting ability was demonstrated for the smaller compounds with two branches;
    c. the photoelectrical properties and the morphological state can be easily variated by changing the central linking fragment.
2. The simple synthetical strategy was adopted for the synthesis of an efficient hole-transporting material for perovskite solar cells. It was shown that:
    a. The spiro-core can be changed by a synthetically more robust non-conjugated bridge;
    b. dimethoxydiphenilamine-substituted carbazole is an efficient hole-transporting fragment ensuring high performance (16.9%) of the devices close to that obtained with the standard material Spiro-OMeTAD (18.4%).
3. The influence of the material's molecular structure on the device performance was studied by synthesizing a series of carbazole-based hole-transporting materials. The study showed that:
    a. an increase in the number of branches does not lead to the improvement in the performance;
    b. while isomeric changes of the molecular topology can lead to a significant difference in the hole mobility, this has only a minor implication on the final performance of the devices;
    c. the highest achieved efficiency with carbazole-based compounds (18.9%) is on par with that of the standard material Spiro-OMeTAD (18.8%).
4. Chemical interaction between the components of the hole-transporting layer was studied, and it was determined that:
    a. 4-*tert*-butylpyridine reacts with the cation-radicals of the hole-transporting materials that are generated during the doping procedure;
    b. reaction products are denoted by electrical properties that are disadvantageous for the device's performance;
    c. the pyridination process leads to the reduction of the effective doping of the hole-transporting material eventually leading to reduced long-term stability.

5. A novel approach towards the hole-selective layer's formation was proposed, and proof of the developed concept was shown. It was demonstrated that:
    a. the use of the monolayer-thick carbazole-based phosphonic acids provides sufficient selectivity to get efficient perovskite solar cells (the highest achieved efficiency was 17.8%).
    b. by means of the formation of mixed monolayers, it is possible to fine-tune the properties of the selective layer thus maximizing the performance.

4. SANTRAUKA

Organinės medžiagos tradiciškai naudojamos elektronikoje dėl jų izoliuojančių savybių. Tačiau praėjusio amžiaus antroje pusėje buvo pastebėta, kad kai kurios iš jų, esant tam tikroms sąlygoms, gali transportuoti krūvininkus [1]. Šis atradimas sukėlė spartų organinių puslaidininkių srities augimą. Buvo išsamiai išnagrinėtos įvairios medžiagų klasės, tokios kaip: konjuguoti polimerai [2], molekuliniai stiklai [3], fulereno dariniai [4] ir pan. Organinės medžiagos dėl mažo svorio, mechaninio atsparumo, galimybės formuoti iš tirpalų ir kitų savybių yra svarbios keleto ateities koncepcijų (integruojama į drabužius, spausdinama elektronika) įgyvendinimui. Sėkmingiausi organinių puslaidininkių pritaikymo pavyzdžiai yra kserografiniai prietaisai [5] (lazeriniai spausdintuvai) ir organiniai šviestukai (OLED) [6], tačiau artimoje ateityje tikimasi dar platesnio tokių medžiagų panaudojimo.

Pastarąjį dešimtmetį viena iš populiariausių tyrimų krypčių yra susijusi su trečiosios kartos saulės elementais [7]. Kylant žmonių susirūpinimui dėl globalių klimato pokyčių, vis daugiau dėmesio sulaukia tiesioginis saulės šviesos konvertavimas į elektrą, kas neretai yra traktuojama kaip patraukliausias energijos gamybos būdas. Taip pat tai leistų sumažinti CO_2 emisiją, taip siekiant sumažinti žmonijos įtaką vidutinės Žemės temperatūros kilimui. Nepaisant privalumų, šiuo metu saulės elementų įrengimas yra daugiausiai remiamas politiniais sprendimais. Vis dėlto, didėjant gamybos apimtims, mažėja saulės elementų gamybos kaštai, taip padidėja jų konkurencingumas. Šiuo metu rinkoje dominuoja Si-pagrindu kuriami saulės elementai, tačiau naujosios technologijos galėtų praplėsti saulės energijos panaudojimo galimybes.

Tarp naujųjų saulės elementų technologijų išsiskiria sparčiausiai besivystantys perovskitiniai saulės elementai (PSE). Pradedant pirmąja publikacija 2009 metais [8] ir pasiekus technologinį proveržį 2012 [9], šiuo metu PSE technologija yra perkeliama iš laboratorijų į masinę gamybą.

Šios technologijos progresas yra glaudžiai susijęs su naudojamomis organinėmis medžiagomis. Vienos jų – organinės skyles transportuojančios medžiagos (STM). Šioje disertacijoje yra paliestos kelios su STM susijusios problemos, tokios kaip efektyvi sintezė, su legiravimu susijęs degradavimas bei sluoksnio formavimo alternatyva. Tyrimų rezultatai publikuoti penkiose publikacijose.

Darbo tikslas – paprastų ir efektyvių skyles transportuojančių medžiagų, skirtų perovskitiniams saulės elementams, vystymas.

Šiam tikslui pasiekti buvo išsikelti uždaviniai:

- Sukurti paprastą sintezės strategiją, skirtą gauti stabilios amorfinės būsenos šakotos struktūros skyles transportuojančias medžiagas su hidrazono chromoforu;
- Adaptuoti sukurtą sintezės schemą karbazolo chromoforą turinčioms skyles transportuojančioms medžiagoms, tinkamoms pritaikyti efektyviuose perovskitiniuose saulės elementuose;

- Ištirti karbazolo chromoforą turinčių skyles transportuojančių medžiagų izomerinių darinių įtaką galutiniam prietaiso efektyvumui;
- Ištirti legiruojančių priedų sukeliamo degradavimo proceso mechanizmą;
- Sukurti naują, nereikalaujantį legiruojančių priedų skyles transportuojančio sluoksnio formavimo metodą.

Naujumas ir sąryšis tarp publikacijų:

PSE tyrimų pradžioje buvo labai ribotas STM pasirinkimas, kurį nulėmė ryšio tarp struktūros ir efektyvumo supratimo trūkumas ir komplikuotos legiravimo procedūros. Iki šių dienų populiariausia išlieka mažamolekulinė STM 2,2',7,7'-tetrakis[N,N-di(4-metoksifenil)amino]-9,9'-spirobifluorenas (Spiro-OMeTAD). Tačiau šios medžiagos sintezė susideda iš 6 pakopų, reikalaujančių jautrių ir agresyvių reagentų. Šiame darbe, pirmose trijose publikacijose, yra pristatomos sintezės paieškos, siekiant gauti efektyvias šakotos struktūros amorfines STM. Pirmiausia buvo susintetinta serija šakotos struktūros junginių su hidrazono chromoforu, tačiau šios klasės junginiai nepasižymėjo dideliu efektyvumu PSE. Tuomet, siekiant gauti didelio našumo PSC, sintezės schema buvo pritaikyta karbazolo chromoforui. Viena iš susintetintų medžiagų, pavadinimu **V886**, buvo komercializuota kompanijos *Tokyo Chemical Industry Co., Ltd.*

Tęsiant tyrimus, dėmesys buvo sutelktas į kitą sėkmingam komercializavimui svarbų parametrą – ilgalaikį stabilumą. Dėl mažo laidumo STM yra naudojamos kartu su legiruojančiais priedais. Nors yra žinoma, kad legiravimo metu susidaro katijon-radikalai, iki šiol nebuvo atlikti susidariusių oksiduotų medžiagų stabilumo tyrimai. Ketvirtoje publikacijoje yra pristatomi cheminės sąveikos mechanizmo tyrimai tarp naudojamų priedų ir STM *in vitro*. Buvo nustatyta, kad oksiduota STM reaguoja su *tret*-butilpiridinu, susidarant naujiems junginiams, vykstant piridininimo reakcijai. Reakcijos produktai taip pat buvo aptikti *in situ* sendintuose prietaisuose.

Paskutinėje publikacijoje pristatytas naujas STM sluoksnio formavimo metodas, padedantis išvengti priedų naudojimo. Vietoje tradiciškai naudojamo liejimo išsukant buvo pasiūlyta panaudoti savitvarkius monosluoksnius ant indžio alavo oksido (ITO) pagrindo. Prietaisų, pagamintų su tokiu sluoksniu, efektyvumas buvo 17,8%, tai parodė dideles pasiūlyto metodo galimybes.

4.1. „Klik-chemijos“ įkvėpta hidrazono fragmentą turinčių molekulinių stiklų sintezė

Šis skyrius parašytas remiantis publikuotu straipsniu: *A. Magomedov, S. Urnikaite, O. Paliulis, V. Jankauskas, V. Getautis, RSC Adv., 2016, **6**, 8701–8704. JIF: 3.049; Cituota 5 kartus.*

Siekiant tolimesnio progreso molekulinės elektronikos srityje, viena iš svarbių užduočių yra amorfinių medžiagų sintezė. Pirmiausia, šiame darbe buvo siekiama gauti hidrazono chromoforą turinčias amorfines medžiagas. Hidrazonai yra plačiai tyrinėjami dėl jų puslaidininkinių savybių [169], tačiau dažniausiai aromatinių aldehidų hidrazonai yra kristalinės medžiagos. Populiariausi metodai šiam trūkumui

pašalinti yra polimerinio rišiklio naudojimas [169] arba polimero su hidrazono šoninėmis grandinėmis sintezė [170]. Tačiau izoliuojančių fragmentų panaudojimas smarkiai pablogina tokių medžiagų transportines savybes. Tai nulemia poreikį kurti naujas sintezės strategijas, siekiant gauti stabilios amorfinės būsenos hidrazonus.

21-ojo amžiaus pradžioje išpopuliarėjo naujas požiūris į taikomąją sintetinę chemiją, kurį pasiūlė K. B. Sharpless [171]. Idėjos esmė – paprastų ir universalių sintezės schemų panaudojimas sudėtingoms struktūroms gauti. Tai turėtų paspartinti laboratorijoje gautų medžiagų pritaikymą masinei gamybai, taip sumažinant galutinę produkto kainą. Norint atspindėti idėjos principus, koncepcijai buvo suteiktas „klik-chemijos“ (angl. *click-chemistry*) pavadinimas. Mūsų darbe kai kurie „klik-chemijos“ principai buvo pritaikyti šakotų STM sintezei.

Vykstant reakcijai tarp aromatinio aldehido ir hidrazino, susidaro hidrazono funkcinė grupė (>C=N–N<) (11 schema). Šiam tyrimui atlikti buvo panaudoti trifenilamino [172] ir N,N-dietilanilino [173] aldehidai. Jiems kondensuojantis su fenilhidrazinu, buvo gauti tarpiniai produktai su nepakeistu aktyviu vandenilio atomu, kuris gali būti naudojamas tolimesniam funkcionalizavimui.

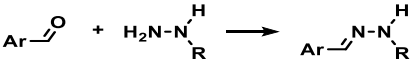

1 schema. Hidrazonų sintezė

Amorfinė būsena hidrazonuose buvo pasiekta sintetinant šakotas struktūras. Tiksliniai produktai gauti reakcijos tarp bromometilinės grupės benzeno darinių ir tarpinių reaktingų hidrazonų metu. Buvo susintetintos, išskirtos ir ištirtos šešios naujos medžiagos su dviem, trimis ir keturiomis šakomis (2 schema.).

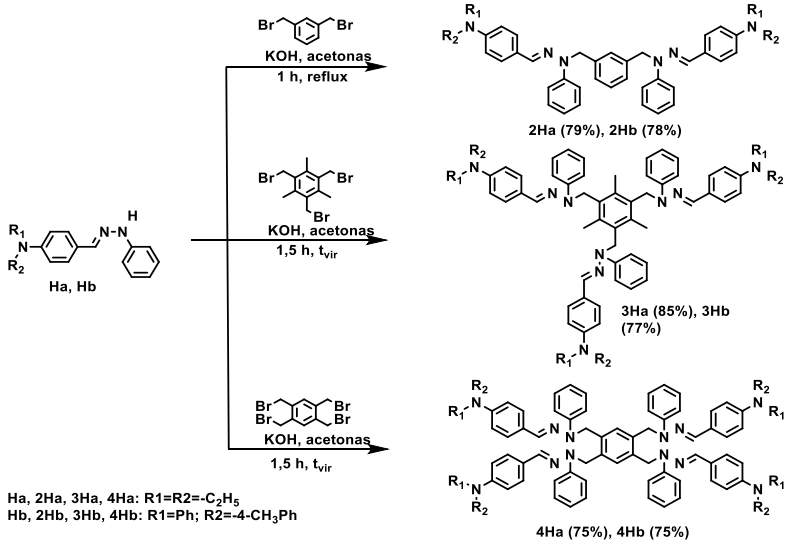

2 schema. Šakotos struktūros hidrazono fragmentą turinčių STM sintezė

Siekiant išsiaiškinti susintetintų hidrazonų fazinę būseną, buvo atlikta DSK analizė. Molekulės su dviem ir keturiomis atšakomis po išskyrimo gautos kaip

kristalinės medžiagos. O medžiagos su trimis šakomis jau pirmojo kaitinimo metu buvo užfiksuota stiklėjimo temperatūra, kas yra būdinga amorfinėms medžiagoms.

NorintNorint įvertinti naujų medžiagų puslaidininkines savybes, buvo išmatuoti du svarbūs parametrai: kietos būsenos jonizacijos potencialas (I_p) ir skylių dreifinis judris (μ). Rezultatai yra pristatyti 1 lentelėje. Kaip matoma iš rezultatų, I_p vertės yra 5,0–5,02 eV junginių **2Ha**, **3Ha** ir **4Ha** su trifenilamino chromofotu bei 5,33–5,35 eV junginių **2Hb**, **3Hb** ir **4Hb** su N,N-dietilanilino chromoforu ir praktiškai nepriklauso nuo šakų skaičiaus molekulėje. Toks rezultatas yra tikėtinas dėl konjugacijos nutrūkimo tarp atskirų fragmentų. Aukščiausios skylių dreifinio judrio vertės serijoje **2H**, **3H**, **4H** buvo nustatytos molekulėms su dviem šakomis.

1 lentelė. Medžiagų (**2–4**)**H**(**a**,**b**) I_p ir skylių dreifinis judris

Medžiaga	I_p[a], (eV)	μ_0[b], ($cm^2\ V^{-1}\ s$)	μ[c], ($cm^2\ V^{-1}\ s$)
2Ha	5,02	3×10^{-7}	8×10^{-5}
2Hb	5,35	$7{,}4 \times 10^{-5}$	$1{,}3 \times 10^{-3}$
3Ha	5,00	$3{,}5 \times 10^{-8}$	$2{,}2 \times 10^{-5}$
3Hb	5,33	$4{,}6 \times 10^{-6}$	$2{,}0 \times 10^{-4}$
4Ha[d]	5,00	-	$\sim 1 \times 10^{-5}$
4Hb[d]	5,35	-	$\sim 6{,}7 \times 10^{-4}$

[a] I_p išmatuotas fotoelektronų spektroskopijos ore metodu,
[b] judrio vertė esant nuliniam lauko stipriui,
[c] judrio vertė esant $6{,}4 \times 10^5\ V\ cm^{-1}$ lauko stipriui.
[d] Dėl didelio dispersiškumo judriai išmatuoti tik esant dideliam lauko stipriui.

Taigi buvo pademonstruota sintezės schema, kuri įgalina pasiekti stabilią amorfinę būseną organiniuose puslaidininkiuose su aukštomis T_g vertėmis. Kartu užtikrinamos aukštos skylių dreifinio judrio vertės, **2Ha** medžiagos jos siekė $10^{-3}\ cm^2\ V^{-1}\ s$, esant stipriems elektros laukams.

Remiantis šiais rezultatais, keletas hidrazono fragmentą turinčių STM buvo išbandyti PSE, tačiau prietaisų efektyvumas buvo labai mažas. Manome, kad tokį rezultatą nulėmė hidrazonų nesuderinamumas su egzistuojančia legiravimo procedūra.

Autoriaus indėlis: medžiagų sintezė ir charakterizavimas, straipsnio juodraščio parengimas.

4.2. Metoksidifenilaminu substituotas karbazolo darinys: efektyvi skyles transportuojanti medžiaga, skirta perovskitiniams saulės elementams

Šis skyrius parašytas remiantis publikuotu straipsniu: *P. Gratia, A. Magomedov, T. Malinauskas, M. Daskeviciene, A. Abate, S. Ahmad, M. Grätzel, V. Getautis and M. K. M. K. Nazeeruddin, Angew. Chemie - Int. Ed., 2015, 54, 11409–11413. JIF: 12.257; Cituota 142 kartų; Straipsnio iliustracija išspausdinta ant skyriaus viršelio*.

Ankstesniame straipsnyje buvo pademonstruotas efektyvus medžiagų, pasižyminčių stabilia amorfine būsena ir geromis krūvininkų pernašos savybėmis,

sintezės būdas. Norint išvengti problemų, susijusių su legiravimo procedūra, buvo siekiama susintetinti struktūriškai Spiro-OMeTAD artimesnę medžiagą. Šiam tikslui pasiekti chromoforinė sistema turi susidėti iš dviejų donorinių dimetoksidifenilamino fragmentų, sujungtų per π-konjuguotą tiltelį. Medžiaga, galinti suteikti tokias savybes, yra 3,6-dibromkarbazolas.

Modifikuota sintezės schema susideda iš dviejų stadijų (3 schema). Pirmoje stadijoje du ekvivalentai 3,6-dibromokarbazolo reaguoja su *o*-bisbromometilbenzenu. Jau po 10 min. reakciją laikant virimo temperatūroje THF, į reakcijos mišinį pridėjus KOH, susidarė produktas baltų kristalų pavidalu. Medžiagos išskyrimas buvo vykdomas filtruojant ir perplaunant gautus kristalus H_2O. Antros stadijos metu tarpinis produktas buvo funkcionalizuojamas dimetoksidifenilamino fragmentais, naudojantis klasikinėmis *Buchwald-Hartwig* reakcijos sąlygomis.

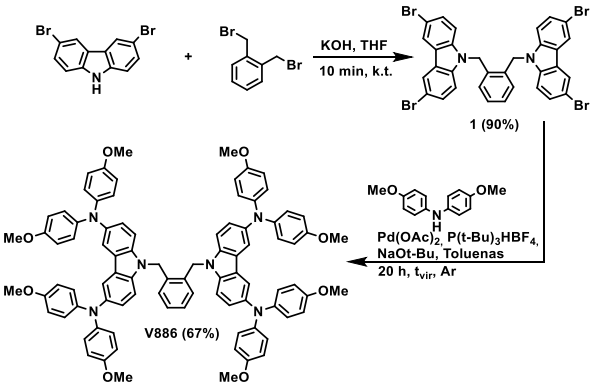

3 schema. Medžiagos **V886** sintezė

Pirmos stadijos paprastumas suteikia privalumų naujajai medžiagai **V886**, palyginti su Spiro-OMeTAD. Centrinio fragmento sintezės metu yra išvengiama jautrių ir agresyvių reagentų (tokių kaip BuLi, Br_2 ir kt.), kurie yra naudojami Spiro-OMeTAD sintezei ir leidžia gauti tarpinį junginį labai greitai ir didelėmis išeigomis. Bendra sintezės išeiga siekia 60%, tai padaro šią medžiagą tinkamą didesnio masto sintezei.

V886 savybių palyginimas su Spiro-OMeTAD yra pateikiamas 2 lentelėje. **V886** ir Spiro-OMeTAD pasižymi panašiu skylių dreifiniu judriu silpnuose elektros laukuose bei I_p verte. Tačiau **V886** atveju DSK analizės metu nebuvo užfiksuota lydymosi temperatūra, tai reiškia, kad medžiaga yra visiškai amorfinė. Papildomai buvo išmatuotas legiruotos V886 medžiagos laidumas, parodant, kad medžiaga pasižymi pakankamu elektriniu laidumu.

2 lentelė. **V886** ir Spiro-OMeTAD savybės

Medžiaga	T_m (°C)	T_g (°C)	I_p (eV)	μ_0 ($cm^2\ V^{-1}\ s$)[a]	μ ($cm^2\ V^{-1}\ s$)[b]	S ($S\ cm^{-1}$)[c]
V886	-	141	5,04	2×10^{-5}	6×10^{-4}	$4{,}2 \times 10^{-5}$
Spiro-OMeTAD	248 [174]	125 [174]	5,00	4×10^{-5}	5×10^{-4}	$4{,}7 \times 10^{-4}$

[a] judrio vertė esant nuliniam lauko stipriui,
[b] judrio vertė esant $6.4 \times 10^5 V\ cm^{-1}$ lauko stipriui,
[c] išilginis laidumas, išmatuotas legiruotoms plėvelėms (10 mol% FK209).

Norint ištirti **V886** veikimą prietaisuose, buvo sukonstruoti PSE su $MAPbI_3$ šviesą sugeriančiu sluoksniu. Labai didelis 16,9% efektyvumas buvo pasiektas naudojant **V886** STM. Prietaisų su Spiro-OMeTAD rezultatas buvo geresnis – 18,4%, tačiau daug paprastesnė sintezė suteikia **V886** konkurencinį pranašumą. Publikacijos paskelbimo metu tai buvo antras geriausias rezultatas, pasiektas su mažamolekuline STM.

Dėl sąlyginai gero veikimo bei paprastos sintezės **V886** medžiaga buvo užpatentuota, o patento licencija buvo įsigyta *Tokyo Chemical Industry Co., Ltd.* kompanijos.

Autoriaus indėlis: **V886** medžiagos sintezė ir charakterizavimas.

4.3. Difenilaminu substituoti karbazolo dariniai perovskitiniams saulės elementams: izomerinių pakaitų įtaka

Šis skyrius parašytas remiantis publikuotu straipsniu: *A. Magomedov, S. Paek, P. Gratia, E. Kasparavicius, M. Daskeviciene, E. Kamarauskas, A. Gruodis, V. Jankauskas, K. Kantminiene, K. T. Cho, K. Rakstys, T. Malinauskas, V. Getautis and M. K. Nazeeruddin, Adv. Funct. Mater., 2018, 28, 1704351. JIF: 15.621; Cituota 29 kartus.*

Remiantis **V886** medžiagos sėkme, buvo susintetinta serija junginių, siekiant išnagrinėti struktūros įtaką galutiniam veikimui, pasinaudojant ta pačia sintezės schema. Bendrai tyrimo metu 11 medžiagų buvo ištirtos ir išbandytos PSE, įskaitant 9 naujas karbazolo fragmentą turinčias STM ir palyginamąsias medžiagas **V886** ir Spiro-OMeTAD.

Anksčiau pristatyta sintezės strategija buvo pritaikyta **V886** analogų sintezei, t.y.: struktūriniams izomerams (**V885** ir **V911**); trims metilo pakaitus turintiems analogams (**V931**, **V928**, **V908**) (1 pav.); serijai šakotų junginių su vienu, trimis ir keturiais fotoaktyviais fragmentais (**V931**, **V928**, **V908**) (2 pav.); karbazolo pakeitimo izomerui (**V946**) (3 pav.).

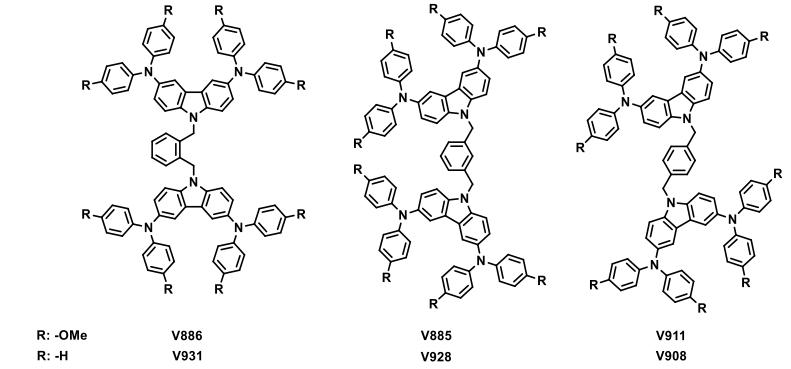

1 pav. Struktūrinių izomerų **V886**, **V885**, **V911** ir jų metil-pakeistų analogų **V931**, **V928**, **V908** struktūrinės formulės

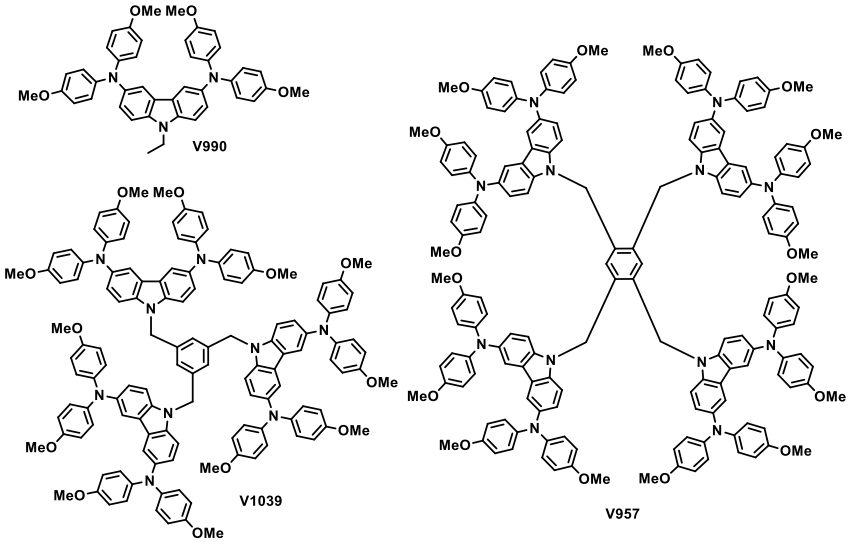

2 pav. Šakotų **V886** analogų su vienu (**V990**), trimis (**V1039**) bei keturiais fotoaktyviais fragmentais (**V957**) struktūrinės formulės

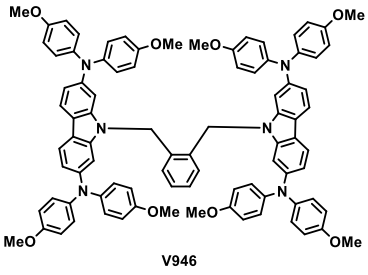

3 pav. **V886** karbazolo pakeitimo izomero su dimetoksidifenilamino fragmentais 2 ir 7 padėtyse (**V946**) struktūrinė formulė

DSK analizė parodė, kad dauguma naujų medžiagų po gryninimo yra išskirtos amorfinės būsenos, kadangi jų lydymosi temperatūra nebuvo užfiksuota pirmojo kaitinimo ciklo metu. Tik dviejų medžiagų, **V931** ir **V908**, lydymosi procesas buvo būdingas kristalinėms medžiagoms . Įdomus elgesys buvo nustatytas **V908** medžiagos, jos pirmojo kaitinimo metu buvo užfiksuoti trys faziniai virsmai: stiklėjimas, rekristalizacija (219°C), lydimasis (337°C). Abiejų medžiagų antrojo kaitinimo metu buvo užfiksuota tik stiklėjimo temperatūra. Aukštos T_g vertės parodo gerą suformuotų plėvelių morfologinį stabilumą. Papildomai termogravimetrinės analizės metodu buvo nustatytas geras visų medžiagų terminis stabilumas.

Naujų medžiagų I_p vertės yra nulemtos naudojamo chromoforo, kas parodo, kad nėra stiprių π-π sąveikų tarp atskirų fragmentų. Sąveikų nebuvimą taip pat patvirtina UV/vis spektroskopijos duomenys.

Įdomus pastebėjimas gali būti atliktas lyginant skylių dereifinius judrius. Struktūrinių izomerų su metilo pakaitais (**V931**, **V928**, **V908**) μ vertės yra tos pačios eilės (atitinkamai 7,8 × 10^{-4}, 3,7 × 10^{-4}, 4 × 10^{-4} cm^2 V^{-1} s). O metoksipakaitus turinčių analogų, keičiantis fragmentų tarpusavio išsidėstymui, vertės smarkiai padidėja ir yra: **V886** – 6 × 10^{-4} cm^2 V^{-1} s, **V885** – 4,6 × 10^{-3} cm^2 V^{-1} s **V911** – 1 × 10^{-2} cm^2 V^{-1} s. Tokios savybės leidžia išsikelti prielaidą, kad plėvelėje formuojasi vandeniliniai ryšiai tarp molekulių, skatinantys krūvininkų pernašą. Šis rezultatas parodo molekulinės struktūros svarbą krūvininkų pernašai organinėse STM.

Siekiant ištirti STM efektyvumą PSE, buvo sukonstruoti mezoporėtos architektūros prietaisai su trigubo katijono perovskitu. Prietaisų, pagamintų naudojant Spiro-OMeTAD standartą, efektyvumas buvo 18,8%. Dviejų iš naujų medžiagų buvo beveik identiškas efektyvumas kaip su Spiro-OMeTAD. Aukščiausias PCE 18,92% užfiksuotas *m*-izomero **V885**.

Paprasčiausios struktūros junginio **V990** efektyvumas buvo labai mažas – 5%. Toks veikimas gali būti siejamas su blogomis krūvininkų pernašos savybėmis. Sudėtingesnių struktūrų efektyvumas buvo vidutiniškai geras – 17,1% **V1039** junginio ir 16,9% – **V957**. Tai rodo, kad sudėtingesnės struktūros nebūtinai veda prie geresnio efektyvumo.

Medžiagų su metilo pakaitais našumas šiek tiek mažesnis ~16%. Toks efektyvumas gali būti siejamas su aukštesne I_p verte, dėl kurios sumažėja suderinamumas su naudojamais legiravimo priedais.

Medžiagos **V946** efektyvumas taip pat buvo mažesnis – (15,7%), palyginti su **V886** analogu. Galimas paaiškinimas yra didesnis molekulių išsidėstymo netvarkingumas dėl molekulinės netvarkos.

Autoriaus indėlis: naujų medžiagų sintezė ir charakterizavimas. Straipsnio juodraščio parengimas.

4.4. Skyles transportuojančios medžiagos piridininimo perovskitiniuose saulės elementouse įtaka ilgalaikiam stabilumui

Šis skyrius parašytas remiantis publikuotu straipsniu: *A. Magomedov, E. Kasparavičius, K. Rakstys, S. Paek, N. Gasilova, K. Genevičius, G. Juška, T.*

Malinauskas, M. K. Nazeeruddin, and V. Getautis, J. Mater. Chem. C, 2018, 6, 8874–8878. JIF: 6.641; Cituota 21 kartų; Straipsnio iliustracija išspausdinta ant galinio viršelio.

Anksčiau pristatytos STM yra naudojamos kartu su legiruojančiais priedais, tačiau jų naudojimas turi neigiamos įtakos ilgalaikiam prietaisų stabilumui. Tęsiant tyrimus, buvo ištirtas vienas iš anksčiau ignoruojamų faktorių – savaiminis legiruotų STM nestabilumas, kuris gali turėti didelį poveikį galutinio prietaiso stabilumui ir / arba efektyvumui.

Darbo pagrindu tapo empirinis pastebėjimas, kaip keičiasi legiruotų STM tirpalų spalva. Pridėjus oksiduojančius priedus, tirpalas įgauna intensyvią spalvą (pvz., tamsiai plytinę spalvą Spiro-OMeTAD atveju ir tamsiai žalią **V886** atveju, 4 pav.). Tačiau, pridėjus tBP, tirpalas iš lėto praranda spalvą. Tokie pokyčiai gali reikšti vykstančius cheminius transformavimus reaguojant mišinio komponentams.

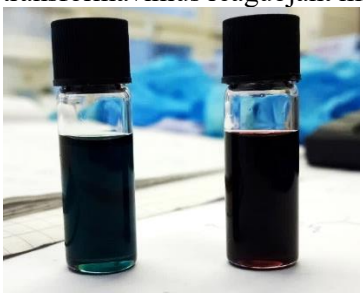

4 pav. Oksiduotų **V886** (kairėje) ir Spiro-OMeTAD (dešinėje) tirpalai

Norėdami ištirti vykstančius procesus, mes pasinaudojome modeliniu junginiu **V990**, kuris turi tokį pat chromoforą, kaip ir mūsų geriausiai veikiančios medžiagos, ir dėl paprastesnės struktūros supaprastina rezultatų analizę. Pirmiausia, remiantis W. H. Nguyen ir kt. publikuota procedūra [151], buvo susintetinta oksiduota **V990** forma. Tam tikslui **V990** buvo veikiamas AgTFSI druska dichlormetane, susidarant elementiniam sidabrui. Išsėdusios dalelės buvo pašalintos filtravimo būdu ir galutinis produktas sukoncentruotas. Buvo gauta tamsiai žalios spalvos derva.

Toliau buvo tiriama sąveika tarp **V990^{+}TFSI^{-}** ir tBP. Norint išlaikyti sąlygas kuo paprastesnes ir pašalinti tirpiklio įtaką vykstančiam procesui, **V990^{+}TFSI^{-}** medžiaga buvo ištirpinta gryname tBP. Gautą tirpalą maišant esant 60°C temperatūrai, jau po 10 min. spalva pasikeitė į oranžinę. Plonasluoksnė chromatograma parodė, kad susidarė du produktai, kuriuos atskyrus su skystine chromatografija, buvo nustatytos 38,5% ir 33% išeigos (bendra išeiga 71,5%) (4 schema).

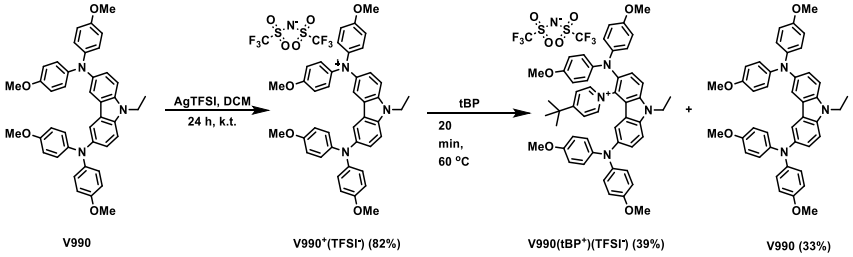

4 schema. Dimetoksidifenilaminu-substituoto karbazolo fragmento oksidacija ir C-H piridininimas **V990** medžiagoje

Atlikus BMR analizę paaiškėjo, kad pirmoji išskirta medžiaga yra neoksiduota **V990**, o antroje medžiagoje piridinio fragmentas yra prisijungęs prie karbazolo fragmento. Tikėtiniausia prisijungimo vieta buvo nustatyta pasinaudojus DFT skaičiavimais, pagal anksčiau aprašytą procedūrą [175]. Trumpai, nukleofilinė pakaitų reakcija vyksta į padėtį, kurioje žemiausios laisvos molekulės orbitalės (LUMO) tankis yra didžiausias katijon-radikale. Tarp padėčių, kur gali vykti pakaitų reakcija, didžiausias LUMO tankis yra 4-oje karbazolo fragmento padėtyje (5 pav.). Tai, kad reakcija vyksta šioje padėtyje, yra toliau patvirtinama analizuojant ^{1}H BMR spektrą, kuriame pastebimi penki signalai su 1H integralu nuo 7,96 iki 6,16 m.d., spin-spin sąveikomis, atitinkančiomis pakaito prisijungimą 4-oje padėtyje. Papildomas įrodymas yra palyginimas tarp apskaičiuoto ir išmatuoto ^{13}C BMR spektrų, kur charakteringas signalas *tret*-butilpiridinio žiedo 4-os padėties apskaičiuotas ties 174,34 m.d., o išmatuotas ties 172,46 m.d. iš dmso-*d6* ir ties 174,36 m.d. iš acetono-*d6*. Žinant galutinių produktų struktūras bei santykį tarp išeigų, buvo pasiūlytas reakcijos mechanizmas (5 schema).

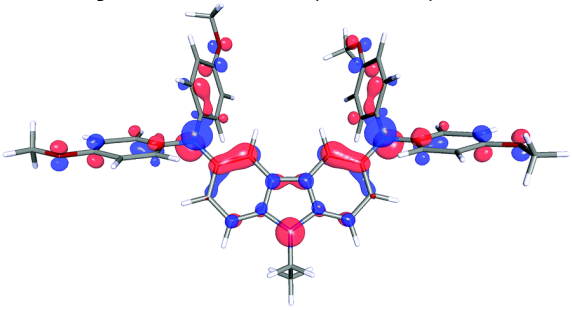

5 pav. **V990**$^{+}$ žemiausia laisva molekulės orbitalė (LUMO), pagal DFT skaičiavimus

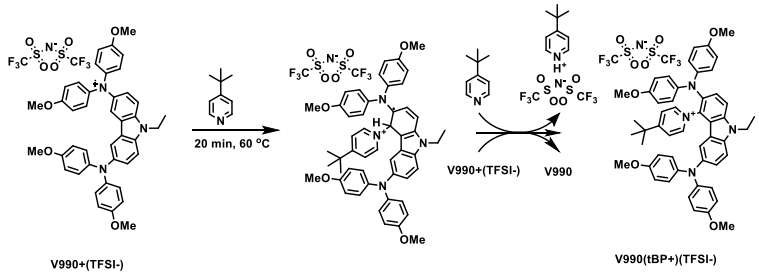

5 schema. Pasiūlytas C-H piridininimo mechanizmas

Tokia pati analizė buvo atlikta su oksiduota **V886** medžiaga. Tokiu atveju buvo išskirti trys produktai: neoksiduota medžiaga **V886**; monopakeistas junginys **V886(tBP$^+$)(TFSI$^-$)**, dipakeistas junginys **V886(tBP$^+$)$_2$(TFSI$^-$)$_2$**. Medžiagos išskirtos atitinkamomis 20,5%, 37,9% ir 17,1% išeigomis (bendra išeiga 75,5%) (6 pav.).

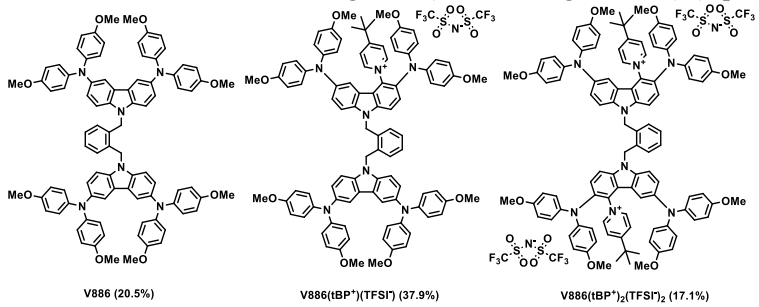

6 pav. Piridinintų **V886** darinių struktūros

Išanalizavus išskirtų naujų medžiagų fotofizikines savybes buvo nustatyta, kad energijos lygmenys bei krūvininkų pernaša yra nepalankūs efektyviam PSE darbui.

Norint ištirti, ar procesas prietaisuose vyksta, buvo išanalizuoti sendinti PSE su **V886** STM. Sendinimas buvo atliktas prietaisą 340 val. laikant ore, esant 80°C temperatūrai. Praėjus šiam laikui, STM sluoksnis buvo nuplautas THF ir gautas tirpalas analizuojamas MS analizės būdu. Buvo aptiktas silpnas signalas ties 1478,856 m/z, kuris atitinka **V886(tBP$^+$)** katijoną (1478,6694 Da). Šis priskyrimas toliau buvo patvirtintas atliekant MS/MS analizę.

Šie rezultatai pirmą kartą pademonstravo savaiminį oksiduotų STM, naudojamų PSE, nestabilumą. Legiravimo efektyvumas einant laikui mažėja vykstant piridininimo reakcijai, dėl to mažėja ilgalaikis prietaiso stabilumas. Papildomai ši reakcija gali būti naudinga tyrinėjant C-N ryšių formavimą.

Netiesioginiai šio proceso vyksmo įrodymai gali būti aptinkami kituose darbuose, pvz., aprašytas „ertmių“ formavimasis HTM sluoksnyje [176]. J. P. Bastos ir kt. straipsnyje yra pabrėžiama, kad tBP naudojimas yra susijęs su prietaisų degradavimu: *Veikiant šviesai tBP degraduoja, ir degradavimo produktai turi teigiamą krūvį* [177]. Neseniai šio proceso patvirtinimas publikuotas F. Lamberti ir kt. darbe [178].

Autoriaus indėlis: Pirminė idėja. Piridininių produktų sintezė bei struktūrinė analizė. BMR duomenų analizė ir reakcijos mechanizmo pasiūlymas. Straipsnio juodraščio parengimas.

4.5. Savitvarkis skyles transportuojantis monosluoksnis, skirtas efektyviems perovskitiniams saulės elementams

Šis skyrius parašytas remiantis publikuotu straipsniu: *A. Magomedov, A. Al-Ashouri, E. Kasparavičius, S. Strazdaite, G. Niaura, M. Jošt, T. Malinauskas, S. Albrecht and V. Getautis, Adv. Energy Mater., 2018, 1801892. JIF: 24.884; Cituota 20 kartų; Straipsnio iliustracija išspausdinta ant priekinio viršelio.*

Kadangi STM legiravimo procesas, ir ypač katijon-radikalų susidarymas, nulemia sumažėjusį ilgalaikį stabilumą, yra svarbu sukurti priedų nereikalaujančią alternatyvą. Dažniausiai iš STM, veikiančių be priedų, yra formuojamos daug plonesnės plevelės, palyginti su standartinėmis STM. Tačiau, esant mažesniam plėvelių storiui, yra svarbu užtikrinti tolygų žemiau esančio sluoksnio padengimą. Pavyzdžiui, M. Stolterfoht ir kt. darbe buvo parodyta, kad, mažinant PTAA sluoksnio storį, smarkiai sumažėja prietaiso V_{oc} [97].

Vienas iš būdų, siekiant užtikrinti tolygų sluoksnio susidarymą, yra organinių medžiagų, turinčių inkarines grupes, savitvarka. Iš literatūros duomenų yra žinoma, kad fosfono rūgštys sudaro stiprius kovalentinius ryšius su ITO paviršiumi. Taigi, buvo sukurtas naujas STM **V1036**, kuriame skylėms selektyvus karbazolo fragmentas yra funkcionalizuotas su fosfono rūgšties inkarine grupe (7 pav.).

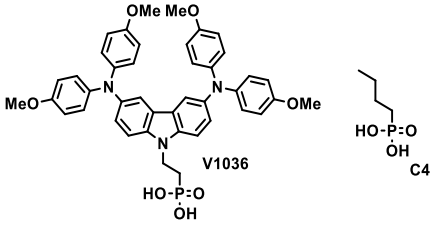

7 pav. Karbazolo chromoforą turinčios fosfono rūgšties **V1036** ir butilfosfono rūgšties **C4** struktūrinės formulės

Monosluoksnio formavimas ant ITO pagrindo susideda iš kelių stadijų, tai: a) pagrindo valymas; b) pagrindo mirkymas į fosfono rūgšties tirpalą; c) atkaitinimas; d) perplovimas ir džiovinimas. Mūsų darbe O_3 buvo naudojamas substratams valyti. Šis žingsnis yra svarbus norint atsikratyti fiziškai adsorbuotų organinių molekulių ir kitų nešvarumų. Mirkymui buvo naudojami 1 mM koncentracijos tirpalai 2-propanolyje. Atkaitinimas yra svarbus cheminių ryšių susidarymui, nors detalus mechanizmas vis dar nėra aiškus. Perplaunant funkcionalizuotus pagrindus yra pašalinamos fiziškai adsorbuotos molekulės.

Monosluoksnio susidarymą yra lengva aptikti, atliekant vilgymo kampo matavimus. Palyginti su PTAA, perovskito tirpalo drėkinimas ant **V1036** monosluoksnio buvo geresnis, kas gali būti naudinga formuojant didelio ploto SE. Papildomai buvo parodyta, kad vilgymo kampas gali būti keičiamas plačiu intervalu,

formuojant mišrius monosluoksnius su butilfosfono rūgštimi (**C4**) (8 pav.). Tai gali būti panaudojama optimizuojant perovskito spausdinimo procesą.

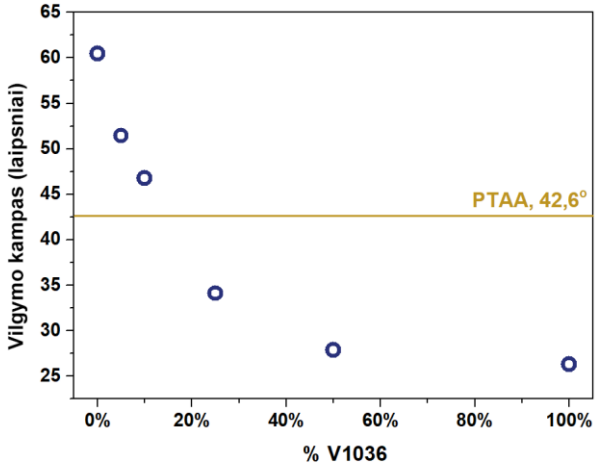

8 pav. Vilgymo kampo priklausomybė nuo **V1036** kiekio mišinyje

Siekiant įrodyti, kad **V1036** yra prisijungęs prie ITO paviršiaus, buvo atlikti FTIR matavimai. Monosluoksnio spektras yra labai artimas KBr disperguotos medžiagos **V1036** spektrui. Šis rezultatas patvirtina **V1036** prisijungimą prie ITO paviršiaus.

Koncepcijai įrodyti buvo sukonstruoti p-i-n architektūros PSE. Prietaisų su grynos **V1036** medžiagos monosluoksniu V_{oc} vertės buvo žemesnės, palyginti su PTAA standartu. Siekiant išvengti šios problemos, buvo panaudoti mišrūs monosluoksniai, kuriuose maža **C4** molekulė buvo panaudota kaip „užpildas“. Optimizavus santykį tarp **V1036** ir **C4,** buvo pasiektas daug žadantis 17,8% efektyvumas.

Monosluoksnių panaudojimas selektyvaus sluoksnio formavimui turi keletą privalumų, kurie yra svarbūs ateities pritaikymams. Pirmiausia, tai yra legiruojančių priedų naudojimo nereikalaujantis metodas, kurį taikant tikimasi gauti geresnį ilgalaikį stabilumą. Taip pat toks formavimo metodas yra tinkamas šiurkštiems arba tekstūruotiems paviršiams padengti. Papildomai monosluoksnis dėl nedidelės sugerties nekonkuruoja su šviesą sugeriančiomis medžiagomis (9 pav.). Galiausiai dėl labai plonos plėvelės suformavimo medžiagos sąnaudos yra minimalios.

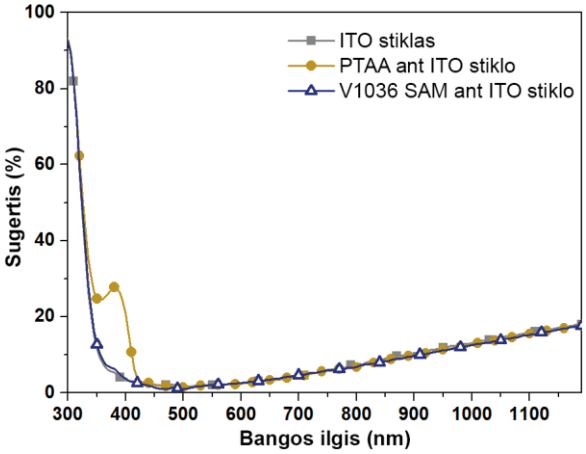

9 pav. ITO substrato, ITO su PTAA bei ITO su 100% **V1036** SAM, UV–vis sugerties spektrai

Tęsiant tyrimus buvo susintetintos naujos selektyvios medžiagos, gebančios sudaryti monosluoksnius ant ITO. Vienos iš jų buvo pasiektas 21% efektyvumas t. y. geresnis už PTAA standartą.

Autoriaus indėlis: Pirminė idėja. Saulės elementų gamyba. DFT skaičiavimai. Straipsnio juodraščio parengimas.

5. IŠVADOS

Šiuose darbuose pasiektas ryškus proveržis, nurodantis tolimesnius vystymosi kelius skyles transportuojančių medžiagų, skirtų perovskitiniams saulės elementams, srityje. Apibendrinimas:

1. Vykdant reakcijas tarp hidrazonų ir brommetilbenzeno darinių, susintetinta hidrazono chromoforą turinčių šakotos struktūros skyles transportuojančių medžiagų serija. Atlikus tyrimus nustatyta, kad:
    a. visiškai amorfinė būsena yra mažiau simetrinių junginių su trimis hidrazonų atšakomis;
    b. geriausios krūvininkų pernašos savybės nustatytos mažesnių junginių su dviem atšakomis;
    c. fotoekeltrinės ir morfologinės savybės gali būti lengvai keičiamos, pakeičiant centrinį jungiamąjį fragmentą.
2. Paprasta sintetinė strategija buvo adaptuota efektyvių skyles transportuojančių medžiagų, skirtų perovskitiniams saulės elementams, sintezei. Buvo parodyta, kad:
    a. spiro-centras gali būti pakeistas paprasčiau gaunamu nekonjuguotu tilteliu;
    b. dimetoksidifenilaminu pakeistas karbazolas yra efektyvus skyles transportuojantis fragmentas, užtikrinantis didelį prietaisų efektyvumą (16,9%), artimą rezultatui, gautam su standartine medžiaga Spiro-OMeTAD (18,4%).
3. Susintetinus seriją karbazolo chromoforą turinčių skyles transportuojančių medžiagų, atliktas molekulinės struktūros įtakos prietaiso efektyvumui tyrimas. Nustatyta, kad:
    a. atšakų skaičiaus didinimas neduoda didesnio efektyvumo;
    b. nors izomerai gali turėti stiprią įtaką krūvininkų transportui, tai tik nedaug atsiliepia galutiniam prietaiso efektyvumui;
    c. didžiausias efektyvumas, pasiektas su karbazolo fragmentą turinčiais junginiais (18,9%), yra lygiavertis rezultatui, gautam su standartine medžiaga Spiro-OMeTAD (18,8%).
4. Ištirta cheminė sąveika tarp komponentų, sudarančių skyles transportuojantį sluoksnį. Nustatyta, kad:
    a. *tret*-butilpiridinas reaguoja su skyles transportuojančios medžiagos katijon-radikalais, susiformavusiais dėl priedų poveikio;
    b. reakcijos produktai pasižymi elektrinėmis savybėmis, kurios neigiamai atsiliepia prietaiso efektyvumui;
    c. piridininimas mažina efektyvų skyles transportuojančios medžiagos legiravimą, taip mažindamas ilgalaikį prietaiso stabilumą.
5. Pasiūlytas ir išbandytas prietaisuose naujas selektyvaus skylėms sluoksnio formavimo metodas. Gauti rezultatai parodo, kad:

a. karbazolo chromoforą turinčios fosfono rūgšties monosluoksnis suteikia pakankamą selektyvumą, reikalingą dideliam efektyvumui užtikrinti (pasiektas 17,8% efektyvumas);
b. formuojant mišrius monosluoksnius, galimas savybių optimizavimas, maksimaliai padidinant prietaiso efektyvumą.

6. References

1. KALLMANN, H. and POPE, M. Bulk Conductivity in Organic Crystals. *Nature*. 1960, 186(4718), 31–33. DOI: 10.1038/186031a0

2. MOLITON, A. and HIORNS, R.C. Review of electronic and optical properties of semiconducting π-conjugated polymers: applications in optoelectronics. *Polymer International*. 2004, 53(10), 1397–1412. DOI: 10.1002/pi.1587

3. LIN, Y. *et al*. Small molecule semiconductors for high-efficiency organic photovoltaics. *Chemical Society Reviews*. 2012, 41(11), 4245. DOI: 10.1039/C2CS15313K

4. GATTI, T. *et al*. The Renaissance of fullerenes with perovskite solar cells. *Nano Energy*. 2017, 41, 84–100. DOI: 10.1016/j.nanoen.2017.09.016

5. GRAZULEVICIUS, J.V. *et al*. Carbazole-containing polymers: synthesis, properties and applications. *Progress in Polymer Science*. 2003, 28(9), 1297–1353. DOI: 10.1016/S0079-6700(03)00036-4

6. THEJO KALYANI, N., and DHOBLE, S.J. Organic light emitting diodes: Energy saving lighting technology – A review. *Renewable and Sustainable Energy Reviews*. 2012, 16(5), 2696–2723. DOI: 10.1016/j.rser.2012.02.021

7. YAN, J. and SAUNDERS, B.R. Third-generation solar cells: a review and comparison of polymer:fullerene, hybrid polymer and perovskite solar cells. *RSC Advances.* 2014, 4(82), 43286–43314. DOI: 10.1039/C4RA07064J

8. KOJIMA, A. *et al*. Organometal Halide Perovskites as Visible-Light Sensitizers for Photovoltaic Cells. *Journal of the American Chemical Society*. 2009, 131(17), 6050–6051. DOI: 10.1021/ja809598r

9. LEE, M.M. *et al*. Efficient Hybrid Solar Cells Based on Meso-Superstructured Organometal Halide Perovskites. *Science*. 2012, 338(6107), 643-647 DOI: 10.1126/science.1228604

10. Perovskite mineral data. [seen on 29th January, 2020]. Available at: http://webmineral.com/data/Perovskite.shtml

11. Perovskite ABO3 structure. [seen on 29th January, 2020]. Available at: https://commons.wikimedia.org/wiki/File:Perovskite_ABO3.jpg

12. WEBER, D. $CH_3NH_3PbX_3$, ein Pb(II)-System mit kubischer Perowskitstruktur. *Zeitschrift fur Naturforschung B*. 1978, 33(12), 1443–1445. DOI: 10.1515/znb-1978-1214

13. WEBER, D. $CH_3NH_3SnBr_xI_{3-x}$ (x = 0-3), ein Sn(II)-System mit kubischer Perowskitstruktur / $CH_3NH_3SnBr_xI_{3-x}$ (x = 0-3), a Sn(II)-System with Cubic Perovskite Structure. *Zeitschrift für Naturforschung B*. 1978, 33(8), 862–865. DOI: 10.1515/znb-1978-0809

14. POGLITSCH, A. and WEBER, D. Dynamic disorder in methylammoniumtrihalogenoplumbates (II) observed by millimeter-wave spectroscopy. *The Journal of Chemical Physics*. 1987, 87(11), 6373–6378. DOI: 10.1063/1.453467

15. ONODA-YAMAMURO, N. *et al*. Calorimetric and IR spectroscopic

studies of phase transitions in methylammonium trihalogenoplumbates (II). *Journal of Physics and Chemistry of Solids*. 1990, 51(12), 1383–1395. DOI: 10.1016/0022-3697(90)90021-7

16. XU, Q. *et al*. Molecular Motions and Phase Transitions in Solid $CH_3NH_3PbX_3$ (X = C1, Br, I) as Studied by NMR and NQR. *Zeitschrift für Naturforschung A*. 1991, 46(3), 240–246. DOI: 10.1515/zna-1991-0305

17. KAGAN, C.R. *et al*. Organic-Inorganic Hybrid Materials as Semiconducting Channels in Thin-Film Field-Effect Transistors. *Science*. 1999, 286(5441), 945–947. DOI: 10.1126/science.286.5441.945

18. MITZI, D.B. Synthesis, Structure, and Properties of Organic-Inorganic Perovskites and Related Materials. *Progress in Inorganic Chemistry, Volume 48*. [s.l.]: John Wiley & Sons, Inc., 2007. p. 1–121. ISBN 9780470166499. DOI: 10.1002/9780470166499.ch1

19. MITZI, D.B. *et al*. Conducting tin halides with a layered organic-based perovskite structure. *Nature*. 1994, 369(6480), 467–469. DOI: 10.1038/369467a0

20. MITZI, D.B. *et al*. Thin film deposition of organic-inorganic hybrid materials using a single source thermal ablation technique. *Chemistry of Materials*. 1999, 11(3), 542–544. DOI: 10.1021/cm9811139

21. LIANG, K. *et al*. Synthesis and Characterization of Organic-Inorganic Perovskite Thin Films Prepared Using a Versatile Two-Step Dipping Technique. *Chemistry of Materials*. 1998, 10(1), 403–411. DOI: 10.1021/cm970568f

22. CHONDROUDIS, K. and MITZI, D.B. Electroluminescence from an organic-inorganic perovskite incorporating a quaterthiophene dye within lead halide perovskite layers. *Chemistry of Materials*. 1999, 11(11), 3028–3030. DOI: 10.1021/cm990561t

23. MITZI, D.B. *et al*. Structurally tailored organic-inorganic perovskites: Optical properties and solution-processed channel materials for thin-film transistors. *Chemistry of Materials*. 2001, 13(10), 3728–3740. DOI: 10.1021/cm010105g

24. KIM, H.-S. *et al*. Lead Iodide Perovskite Sensitized All-Solid-State Submicron Thin Film Mesoscopic Solar Cell with Efficiency Exceeding 9%. *Scientific Reports*. 2012, 2418–425. DOI: 10.1038/srep00591

25. SALBECK, J. et al. Low molecular organic glasses for blue electroluminescence. *Synthetic Metals*. 1997, 91(1–3), 209–215. 10.1016/S0379-6779(98)80033-7

26. IM, J.H. *et al*. Morphology-photovoltaic property correlation in perovskite solar cells: One-step versus two-step deposition of $CH_3NH_3PbI_3$. *APL Materials*. 2014, 2(8), 081510. DOI: 10.1063/1.4891275

27. BI, C. *et al*. Non-wetting surface-driven high-aspect-ratio crystalline grain growth for efficient hybrid perovskite solar cells. *Nature Communications*. 2015, 6(1), 7747. DOI: 10.1038/ncomms8747

28. JEON, N.J. *et al*. Solvent engineering for high-performance inorganic-organic hybrid perovskite solar cells. *Nature Materials*. 2014, 13(9), 897–903. DOI: 10.1038/nmat4014

29. LIU, M. *et al*. Efficient planar heterojunction perovskite solar cells by

vapour deposition. *Nature*. 2013, 501(7467), 395–398. DOI: 10.1038/nature12509

30. STONE, K.H. *et al*. $PbCl_2$ Derived $MAPbI_3$: Transformation from Crystalline Precursor to Perovskite. *Nature Communications*. 2018, 9, 3458. DOI: 10.1038/s41467-018-05937-4

31. AHN, N. *et al*. Highly Reproducible Perovskite Solar Cells with Average Efficiency of 18.3% and Best Efficiency of 19.7% Fabricated via Lewis Base Adduct of Lead(II) Iodide. *Journal of the American Chemical Society*. 2015, 137(27), 8696–8699. DOI: 10.1021/jacs.5b04930

32. PAEK, S. *et al*. From Nano- to Micrometer Scale: The Role of Antisolvent Treatment on High Performance Perovskite Solar Cells. *Chemistry of Materials*. 2017, 29(8), 3490–3498. DOI: 10.1021/acs.chemmater.6b05353

33. JEON, N.J. *et al*. A fluorene-terminated hole-transporting material for highly efficient and stable perovskite solar cells. *Nature Energy*. 2018, 3(8), 682–689. DOI: 10.1038/s41560-018-0200-6

34. SALIBA, M. *et al*. Cesium-containing triple cation perovskite solar cells: improved stability, reproducibility and high efficiency. *Energy & Environmental Science*. 2016, 9(6), 1989–1997. DOI: 10.1039/C5EE03874J

35. PROCHOWICZ, D. *et al*. Mechanosynthesis of the hybrid perovskite $CH_3NH_3PbI_3$: Characterization and the corresponding solar cell efficiency. *Journal of Materials Chemistry A*. 2015, 3(41), 20772–20777. DOI: 10.1039/C5TA04904K

36. PROCHOWICZ, D. *et al*. Mechanosynthesis of pure phase mixed-cation $MA_xFA_{1-x}PbI_3$ hybrid perovskites: photovoltaic performance and electrochemical properties. *Sustainable Energy Fuels*. 2017, 1(4), 689–693. DOI: 10.1039/C7SE00094D

37. PROCHOWICZ, D. *et al*. One-step mechanochemical incorporation of an insoluble cesium additive for high performance planar heterojunction solar cells. *Nano Energy*. 2018, 49, 523–528. DOI: 10.1016/j.nanoen.2018.05.010

38. FASSL, P. *et al*. Fractional deviations in precursor stoichiometry dictate the properties, performance and stability of perovskite photovoltaic devices. *Energy & Environmental Science*. 2018, 11(12), 3380–3391. DOI: 10.1039/C8EE01136B

39. BURSCHKA, J. *et al*. Sequential deposition as a route to high-performance perovskite-sensitized solar cells. *Nature*. 2013, 499(7458), 316–319. DOI: 10.1038/nature12340

40. SAHLI, F. *et al*. Fully textured monolithic perovskite/silicon tandem solar cells with 25.2% power conversion efficiency. *Nature Materials*. 2018, 17(9), 820–826. DOI: 10.1038/s41563-018-0115-4

41. HSIAO, S.-Y. *et al*. Efficient All-Vacuum Deposited Perovskite Solar Cells by Controlling Reagent Partial Pressure in High Vacuum. *Advanced Materials*. 2016, 28(32), 7013–7019. DOI: 10.1002/adma.201601505

42. ZHAO, D. *et al*. Annealing-free efficient vacuum-deposited planar perovskite solar cells with evaporated fullerenes as electron-selective layers. *Nano Energy*. 2016, 19, 88–97. DOI: 10.1016/j.nanoen.2015.11.008

43. GIL-ESCRIG, L. *et al*. Vacuum Deposited Triple-Cation Mixed-Halide Perovskite Solar Cells. *Advanced Energy Materials*. 2018, 8(14), 1703506. DOI:

10.1002/aenm.201703506

44. PETROV, A.A. *et al*. A new formation strategy of hybrid perovskites via room temperature reactive polyiodide melts. *Materials Horizons*. 2017, 4(4), 625–632. DOI: 10.1039/C7MH00201G

45. TURKEVYCH, I. *et al*. Strategic advantages of reactive polyiodide melts for scalable perovskite photovoltaics. *Nature Nanotechnology*. 2018, 14, 57-63. DOI: 10.1038/s41565-018-0304-y

46. TRESS, W. Organic-Inorganic Halide Perovskite Photovoltaics. *Organic-Inorganic Halide Perovskite Photovoltaics*. 2016. p. 53–77. ISBN 9783319351148

47. PROTESESCU, L. *et al*. Nanocrystals of Cesium Lead Halide Perovskites (CsPbX3, X = Cl, Br, and I): Novel Optoelectronic Materials Showing Bright Emission with Wide Color Gamut. *Nano Letters*. 2015, 15(6), 3692–3696. DOI: 10.1021/nl5048779

48. HONG NOH, J. *et al*. Chemical Management for Colorful, Efficient, and Stable Inorganic-Organic Hybrid Nanostructured Solar Cells. *Nano Letters*. 2013, 13(4), 1764-1769. DOI: 10.1021/nl400349b

49. QIN, T. *et al*. $NH_2CH{=}NH_2PbI_3$: An Alternative Organolead Iodide Perovskite Sensitizer for Mesoscopic Solar Cells. *Chemistry of Materials*. 2014, 26(3), 1485–1491. DOI: 10.1021/cm404006p

50. ZHAO, H. *et al*. Single Crystal Formamidinium Lead Iodide ($FAPbI_3$): Insight into the Structural, Optical, and Electrical Properties. *Advanced Materials*. 2016, 28(11), 2253–2258. DOI: 10.1002/adma.201505002

51. PELLET, N. *et al*. Mixed-Organic-Cation Perovskite Photovoltaics for Enhanced Solar-Light Harvesting. *Angewandte Chemie International Edition*. 2014, 53(12), 3151–3157. DOI: 10.1002/anie.201309361

52. JEON, N.J. *et al*. Compositional engineering of perovskite materials for high-performance solar cells. *Nature*. 2014, 517(7535), 476–480. DOI: 10.1038/nature14133

53. JACOBSSON, T.J. *et al*. Exploration of the compositional space for mixed lead halogen perovskites for high efficiency solar cells. *Energy & Environmental Science*. 2016, 9(5), 1706–1724. DOI: 10.1039/C6EE00030D

54. GRATIA, P. *et al*. The Many Faces of Mixed Ion Perovskites: Unraveling and Understanding the Crystallization Process. *ACS Energy Letters*. 2017, 2(12), 2686–2693. DOI: 10.1021/acsenergylett.7b00981

55. BAG, S., and DURSTOCK, M.F. Large Perovskite Grain Growth in Low-Temperature Solution-Processed Planar p-i-n Solar Cells by Sodium Addition. *ACS Appl. Mater. Interfaces*. 2016, 8(8), 5053–5057. DOI: 10.1021/acsami.5b11494

56. NAM, J.K. *et al*. Potassium Incorporation for Enhanced Performance and Stability of Fully Inorganic Cesium Lead Halide Perovskite Solar Cells. *Nano Lett*. 2017, 17(3), 2028-2033, DOI: 10.1021/acs.nanolett.7b00050

57. SALIBA, M. *et al*. Incorporation of rubidium cations into perovskite solar cells improves photovoltaic performance. *Science*. 2016, 354(6309), 206–209. DOI: 10.1126/science.aah5557

58. KUBICKI, D.J. *et al*. Phase Segregation in Cs-, Rb- and K-Doped Mixed-

Cation $(MA)_x(FA)_{1-x}PbI_3$ Hybrid Perovskites from Solid-State NMR. *Journal of the American Chemical Society*. 2017, 139(40), 14173–14180. DOI: 10.1021/jacs.7b07223

59. ABDI-JALEBI, M. *et al*. Maximizing and stabilizing luminescence from halide perovskites with potassium passivation. *Nature*. 2018, 555(7697), 497–501. DOI: 10.1038/nature25989

60. YADAV, P. *et al*. The Role of Rubidium in Multiple-Cation-Based High-Efficiency Perovskite Solar Cells. *Advanced Materials*. 2017, 29(40), 1701077. DOI: 10.1002/adma.201701077

61. ABDI-JALEBI, M. *et al*. Potassium- and Rubidium-Passivated Alloyed Perovskite Films: Optoelectronic Properties and Moisture Stability. *ACS Energy Letters*. 2018, 3(11), 2671–2678. DOI: 10.1021/acsenergylett.8b01504

62. CAPRIOGLIO, P. *et al*. High Open Circuit Voltages in pin-Type Perovskite Solar Cells through Strontium Addition. *Sustainable Energy & Fuels*. 2019, 3, 550-563. DOI: 10.1039/C8SE00509E

63. HAILEGNAW, B. *et al*. Rain on methylammonium lead iodide based perovskites: Possible environmental effects of perovskite solar cells. *Journal of Physical Chemistry Letters*. 2015, 6(9), 1543–1547. DOI: 10.1021/acs.jpclett.5b00504

64. BABAYIGIT, A. *et al*. Environment versus sustainable energy: The case of lead halide perovskite-based solar cells. *MRS Energy & Sustainability*. 2018, 5E1. DOI: 10.1557/mre.2017.17

65. BINEK, A. *et al*. Recycling Perovskite Solar Cells To Avoid Lead Waste. *ACS Applied Materials & Interfaces*. 2016, 8(20), 12881–12886. DOI: 10.1021/acsami.6b03767

66. KADRO, J.M. *et al*. Proof-of-concept for facile perovskite solar cell recycling. *Energy and Environmental Science*. 2016, 9(10), 3172–3179. DOI: 10.1039/C6EE02013E

67. ZHAO, Z. *et al*. Mixed-Organic-Cation Tin Iodide for Lead-Free Perovskite Solar Cells with an Efficiency of 8.12%. *Advanced Science*. 2017, 4(11), 1700204. DOI: 10.1002/advs.201700204

68. LIAO, W. *et al*. Lead-Free Inverted Planar Formamidinium Tin Triiodide Perovskite Solar Cells Achieving Power Conversion Efficiencies up to 6.22%. *Advanced Materials*. 2016, 28(42), 9333–9340. DOI: 10.1002/adma.201602992

69. LIU, J. *et al*. Lead-Free Solar Cells based on Tin Halide Perovskite Films with High Coverage and Improved Aggregation. *Angewandte Chemie International Edition*. 2018, 57(40), 13221–13225. DOI: 10.1002/ange.201808385

70. ZHANG, H. *et al*. Polystyrene stabilized perovskite component, grain and microstructure for improved efficiency and stability of planar solar cells. *Nano Energy*. 2018, 43, 383–392. DOI: 10.1016/j.nanoen.2017.11.024

71. ARORA, N. *et al*. Perovskite solar cells with CuSCN hole extraction layers yield stabilized efficiencies greater than 20. *Science*. 2017, 358(6364), 768–771. DOI: 10.1126/science.aam5655

72. BELLA, F. *et al*. Improving efficiency and stability of perovskite solar

cells with photocurable fluoropolymers. *Science*. 2016, 354(6309), 203–206. DOI: 10.1126/science.aah4046

73. IDÍGORAS, J. *et al*. Enhancing Moisture and Water Resistance in Perovskite Solar Cells by Encapsulation with Ultrathin Plasma Polymers. *ACS Applied Materials & Interfaces*. 2018, 10(14), 11587–11594. DOI: 10.1021/acsami.7b17824

74. CHEACHAROEN, R. *et al*. Encapsulating perovskite solar cells to withstand damp heat and thermal cycling. *Sustainable Energy & Fuels*. 2018, 2(11), 2398–2406. DOI: 10.1039/C8SE00250A

75. KEGELMANN, L. *et al*. It Takes Two to Tango – Double-Layer Selective Contacts in Perovskite Solar Cells for Improved Device Performance and Reduced Hysteresis. *ACS Applied Materials & Interfaces*. 2017, 9(20), 17245–17255. DOI: 10.1021/acsami.7b00900

76. MAGOMEDOV, A. *et al*. Self-Assembled Hole Transporting Monolayer for Highly Efficient Perovskite Solar Cells. *Advanced Energy Materials*. 2018., 8(32), 1801892.DOI: 10.1002/aenm.201801892

77. LI, L. *et al*. Recent advances of flexible perovskite solar cells. *Journal of Energy Chemistry*. 2018, 27(3), 673–689. DOI: 10.1016/j.jechem.2018.01.003

78. CHEN, H., and YANG, S. Carbon-Based Perovskite Solar Cells without Hole Transport Materials: The Front Runner to the Market? *Advanced Materials*. 2017, 29(24), 1603994. DOI: 10.1002/adma.201603994

79. ANARAKI, E.H. *et al*. Highly efficient and stable planar perovskite solar cells by solution-processed tin oxide. *Energy & Environmental Science*. 2016, 9(10), 3128–3134. DOI: 10.1039/C6EE02390H

80. JENG, J.Y. *et al*. $CH_3NH_3PbI_3$ perovskite/fullerene planar-heterojunction hybrid solar cells. *Advanced Materials*. 2013, 25(27), 3727–3732. DOI: 10.1002/adma.201301327

81. SAKURAI, T. *et al*. Influence of gap states on electrical properties at interface between bathocuproine and various types of metals. *Journal of Applied Physics*. 2010, 107(4), 043707. DOI: 10.1063/1.3309278

82. CHEN, C. *et al*. Effect of BCP buffer layer on eliminating charge accumulation for high performance of inverted perovskite solar cells. *RSC advances*. 2017, 7, 35819-35826. DOI: 10.1039/C7RA06365B

83. WOLFF, C.M. *et al*. Reduced Interface-Mediated Recombination for High Open-Circuit Voltages in $CH_3NH_3PbI_3$ Solar Cells. *Advanced Materials*. 2017, 29(28), 1700159. DOI: 10.1002/adma.201700159

84. JUNG, S.-K. *et al*. Nonfullerene Electron Transporting Material Based on Naphthalene Diimide Small Molecule for Highly Stable Perovskite Solar Cells with Efficiency Exceeding 20%. *Advanced Functional Materials*. 2018, 28(20), 1800346. DOI: 10.1002/adfm.201800346

85. PRAT, D. et al. CHEM21 selection guide of classical- and less classical-solvents. *Green Chemistry*. 2015, 18(1), 288–296. DOI: 10.1039/C5GC01008J

86. LUO, D. *et al*. Enhanced photovoltage for inverted planar heterojunction perovskite solar cells. *Science*. 2018, 360(6396), 1442–1446. DOI:

10.1126/science.aap9282

87. International standard ISO 9845-1, 1992.

88. SHOCKLEY, W., and QUEISSER, H.J. Detailed Balance Limit of Efficiency of *p-n* Junction Solar Cells. *Journal of Applied Physics*. 1961, 32(3), 510–519. DOI: 0.1063/1.1736034

89. RÜHLE, S. Tabulated values of the Shockley-Queisser limit for single junction solar cells. *Solar Energy*. 2016, 130, 139–147. 10.1016/j.solener.2016.02.015

90. National Renewable Energy Laboratory (NREL) Best Research-Cell Efficiency Chart. [seen on 29th January, 2020]. Available at: https://www.nrel.gov/pv/cell-efficiency.html

91. STOLTERFOHT, M. *et al*. Visualization and suppression of interfacial recombination for high-efficiency large-area pin perovskite solar cells. *Nature Energy*. 2018, 3(10), 847–854. 10.1038/s41560-018-0219-8

92. KÖHNEN, E. *et al*. Highly efficient monolithic perovskite silicon tandem solar cells: analyzing the influence of current mismatch on device performance. *Sustainable Energy & Fuels*. 2019, 3, 1995-2005. DOI: 10.1039/C9SE00120D

93. GitHub. Marcus-cmc/Shockley-Queisser-limit. [seen on 29th January, 2020]. Available at: https://github.com/marcus-cmc/Shockley-Queisser-limit

94. GREEN, M.A. *et al*. Solar cell efficiency tables (Version 53). *Progress in Photovoltaics: Research and Applications*. 2019, 27(1), 3–12. DOI: 10.1002/pip.2573

95. SHIN, S.S. *et al*. Colloidally prepared La-doped BaSnO3 electrodes for efficient, photostable perovskite solar cells. *Science*. 2017, 356(6334), 167–171. DOI: 10.1126/science.aam6620

96. LIU, Z. *et al*. Open-Circuit Voltages Exceeding 1.26 V in Planar Methylammonium Lead Iodide Perovskite Solar Cells. *ACS Energy Letters*. 2019, 4(1), 110–117. DOI: 10.1021/acsenergylett.8b01906

97. STOLTERFOHT, M. *et al*. Approaching the fill factor Shockley-Queisser limit in stable, dopant-free triple cation perovskite solar cells. *Energy & Environmental Science*. 2017, 10(6), 1530–1539. DOI: 10.1039/C7EE00899F

98. CORREA-BAENA, J.-P. *et al*. Promises and Challenges of Perovskite Solar Cells in Portable Applications. *Science*. 2017, 358(6364), 739–744. DOI: 10.1126/science.aam6323

99. SARAGI, T.P.I. *et al*. Spiro Compounds for Organic Optoelectronics. *Chemical Reviews*. 2007, 107(4), 1011-1065. DOI: 10.1021/cr0501341

100. GRÄTZEL, M. *et al*. Solid-state dye-sensitized mesoporous TiO_2 solar cells with high photon-to-electron conversion efficiencies. *Nature*. 1998, 395(6702), 583–585. DOI: 10.1038/26936

101. BACH, U. Solid-State Dye-Sensitized Mesoporous TiO_2 Solar Cells. PhD thesis. 2000. DOI: 10.5075/epfl-thesis-2187

102. MALINAUSKAS, T. *et al*. Enhancing Thermal Stability and Lifetime of Solid-State Dye-Sensitized Solar Cells via Molecular Engineering of the Hole-Transporting Material Spiro-OMeTAD. *ACS Applied Materials & Interfaces*. 2015,

7(21), 11107–11116. DOI: 10.1021/am5090385

103. DOMANSKI, K. *et al*. Not All That Glitters Is Gold: Metal-Migration-Induced Degradation in Perovskite Solar Cells. *ACS Nano*. 2016, 10(6), 6306–6314. DOI: /10.1021/acsnano.6b02613

104. CACOVICH, S. *et al*. Gold and iodine diffusion in large area perovskite solar cells under illumination. *Nanoscale*. 2017, 9(14), 4700–4706. DOI: 10.1039/C7NR00784A

105. CLARKSON, R.G. and GOMBERG, M. Spirans with four aromatic radicals on the spiro carbon atom. *Journal of the American Chemical Society*. 1930, 52(7), 2881–2891. DOI: 10.1021/ja01370a048

106. PETRUS, M.L. *et al*. A low cost azomethine-based hole transporting material for perovskite photovoltaics. *Journal of Materials Chemistry A*. 2015, 3(23), 12159–12162. DOI: 10.1039/C5TA03046C

107. OSEDACH, T.P. *et al*. Effect of synthetic accessibility on the commercial viability of organic photovoltaics. *Energy & Environmental Science*. 2013, 6(3), 711. DOI: 10.1039/C3EE24138F

108. MATSUI, T. *et al*. Additive-Free Transparent Triarylamine-Based Polymeric Hole-Transport Materials for Stable Perovskite Solar Cells. *ChemSusChem*. 2016, 9(18), 2567–2571. DOI: 10.1002/cssc.201600762

109. RAKSTYS, K. *et al*. Molecular engineering of face-on oriented dopant-free hole transporting material for perovskite solar cells with 19% PCE. *Journal of Materials Chemistry A*. 2017, 5(17), 7811–7815. DOI: 10.1039/C7TA01718A

110. KIM, G.-W. *et al*. Dopant-free polymeric hole transport materials for highly efficient and stable perovskite solar cells. *Energy Environ. Sci.* 2016, 9(7), 2326–2333. DOI: 10.1039/C6EE00709K

111. JEON, N.J. *et al*. *o*-Methoxy Substituents in Spiro-OMeTAD for Efficient Inorganic-Organic Hybrid Perovskite Solar Cells. *Journal of the American Chemical Society*. 2014, 136(22), 7837–7840. DOI: 10.1021/ja502824c

112. SALIBA, M. *et al*. A molecularly engineered hole-transporting material for efficient perovskite solar cells. *Nature Energy*. 2016, 1(2), 15017. DOI: 10.1038/nenergy.2015.17

113. XIE, L.H. *et al*. Unexpected one-pot method to synthesize spiro[fluorene-9,9′-xanthene] building blocks for blue-light-emitting materials. *Organic Letters*. 2006, 8(13), 2787–2790. DOI: 10.1021/ol060871z

114. MACIEJCZYK, M. *et al*. SFX as a low-cost 'Spiro' hole-transport material for efficient perovskite solar cells. *J. Mater. Chem. A*. 2016, 4(13), 4855–4863. DOI: 10.1039/C6TA00110F

115. XU, B. *et al*. A low-cost spiro[fluorene-9,9′-xanthene]-based hole transport material for highly efficient solid-state dye-sensitized solar cells and perovskite solar cells. *Energy & Environmental Science*. 2016, 9(3), 873–877. DOI: 10.1039/C6EE00056H

116. BI, D. *et al*. Facile synthesized organic hole transporting material for perovskite solar cell with efficiency of 19.8%. *Nano Energy*. 2016, 23, 138-144. DOI: 10.1016/j.nanoen.2016.03.020

117. JEON, N.J. *et al*. Efficient Inorganic–Organic Hybrid Perovskite Solar Cells Based on Pyrene Arylamine Derivatives as Hole-Transporting Materials. *Journal of the American Chemical Society*. 2013, 135(51), 19087–19090. DOI: 10.1021/ja410659k

118. LI, H. *et al*. A simple 3,4-ethylenedioxythiophene based hole-transporting material for perovskite solar cells. *Angewandte Chemie – International Edition*. 2014, 53(16), 4085–4088. DOI: 10.1002/anie.201310877

119. XU, B. *et al*. Carbazole-Based Hole-Transport Materials for Efficient Solid-State Dye-Sensitized Solar Cells and Perovskite Solar Cells. *Advanced Materials*. 2014, 26(38), 6629–6634. DOI: 10.1002/adma.201402415

120. RAKSTYS, K. *et al*. Highly Efficient Perovskite Solar Cells Employing an Easily Attainable Bifluorenylidene-Based Hole-Transporting Material. *Angewandte Chemie – International Edition*. 2016, 55(26), 7464-7468. DOI: 10.1002/anie.201602545

121. NIKIFOROV, M.P. *et al*. Detection and role of trace impurities in high-performance organic solar cells. *Energy & Environmental Science*. 2013, 6(5), 1513. DOI: 10.1039/C3EE40556G

122. DASKEVICIENE, M. *et al*. Carbazole-based enamine: Low-cost and efficient hole transporting material for perovskite solar cells. *Nano Energy*. 2017, 32, 551-557. DOI: 10.1016/j.nanoen.2017.01.015

123. VAITUKAITYTE, D. *et al*. Efficient and Stable Perovskite Solar Cells Using Low-Cost Aniline-Based Enamine Hole-Transporting Materials. *Advanced Materials*. 2018, 30(45), 1803735. DOI: 10.1002/adma.201803735

124. PETRUS, M.L. *et al*. Hydrazone-based hole transporting material prepared via condensation chemistry as alternative for cross-coupling chemistry for perovskite solar cells. *Molecular Systems Design and Engineering*. 2018, 3(5), 734–740. DOI: 10.1039/C8ME00023A

125. PETRUS, M.L. *et al*. New Generation Hole Transporting Materials for Perovskite Solar Cells: Amide-Based Small-Molecules with Nonconjugated Backbones. *Advanced Energy Materials*. 2018, 8(32), 1801605. DOI: 10.1002/aenm.201801605

126. SUN, K. *et al*. Transparent Conductive Oxide-Free Perovskite Solar Cells with PEDOT:PSS as Transparent Electrode. *ACS Applied Materials & Interfaces*. 2015, 7(28), 15314-15320. DOI: 10.1021/acsami.5b03171

127. TVINGSTEDT, K. *et al*. Removing Leakage and Surface Recombination in Planar Perovskite Solar Cells. *ACS Energy Letters*. 2017, 2(2) 424-430, DOI: 10.1021/acsenergylett.6b00719

128. STOLTERFOHT, M. *et al*. The impact of energy alignment and interfacial recombination on the internal and external open-circuit voltage of perovskite solar cells. *Energy & Environmental Science*. 2019, 12, 2778-2788. DOI: 10.1039/C9EE02020A

129. BRUIJNAERS, B.J. *et al*. The effect of oxygen on the efficiency of planar p-i-n metal halide perovskite solar cells with a PEDOT:PSS hole transport layer. *Journal of Materials Chemistry A*. 2018, 6(16), 6882–6890. DOI:

10.1039/C7TA11128B

130. HU, L. *et al*. PEDOT:PSS monolayers to enhance the hole extraction and stability of perovskite solar cells. *Journal of Materials Chemistry A*. 2018, 6, 16583-16589. DOI: 10.1039/C8TA05234D

131. BARARD, S. *et al*. Separate charge transport pathways determined by the time of flight method in bimodal polytriarylamine. *Journal of Applied Physics*. 2009, 105(1), 013701. DOI: 10.1063/1.3054180

132. ALBRECHT, S. *et al*. Monolithic perovskite/silicon-heterojunction tandem solar cells processed at low temperature. *Energy & Environmental Science*. 2016, 981. DOI: 10.1039/C5EE02965A

133. BUSH, K.A. *et al*. 23.6%-efficient monolithic perovskite/silicon tandem solar cells with improved stability. *Nature Energy*. 2017, 2(4), 17009. DOI: 10.1038/nenergy.2017.9

134. JOŠT, M. *et al*. Textured interfaces in monolithic perovskite/silicon tandem solar cells: advanced light management for improved efficiency and energy yield. *Energy & Environmental Science*. 2018, 11(12), 3511–3523. DOI: 10.1039/C8EE02469C

135. SALIBA, M. Perovskite solar cells must come of age. *Science*. 2018, 359(6374), 388–389. DOI: 10.1126/science.aar5684

136. KUNG, P.K. *et al*. A Review of Inorganic Hole Transport Materials for Perovskite Solar Cells. *Advanced Materials Interfaces*. 2018, 5(22), 1800882. DOI: 10.1002/admi.201800882

137. WIJEYASINGHE, N. *et al*. Copper(I) Thiocyanate (CuSCN) Hole-Transport Layers Processed from Aqueous Precursor Solutions and Their Application in Thin-Film Transistors and Highly Efficient Organic and Organometal Halide Perovskite Solar Cells. *Advanced Functional Materials*. 2017, 27(35), 1701818. DOI: 10.1002/adfm.201701818

138. SEO, S. *et al*. An ultra-thin, un-doped NiO hole transporting layer of highly efficient (16.4%) organic-inorganic hybrid perovskite solar cells. *Nanoscale*. 2016, 8(22), 11403–11412. DOI: 10.1039/C6NR01601D

139. PARK, I.J. *et al*. Highly Efficient and Uniform 1 cm^2 Perovskite Solar Cells with an Electrochemically Deposited NiO_x Hole-Extraction Layer. *ChemSusChem*. 2017, 10(12), 2660–2667. DOI: 10.1002/cssc.201700612

140. YIN, X. *et al*. Highly Efficient Flexible Perovskite Solar Cells Using Solution-Derived NiO_x Hole Contacts. *ACS Nano*. 2016, 10(3), 3630–3636. DOI: 10.1021/acsnano.5b08135

141. LI, Z. *et al*. Rational Design of Dipolar Chromophore as an Efficient Dopant-Free Hole-Transporting Material for Perovskite Solar Cells. *Journal of the American Chemical Society*. 2016, 138(36), 11833–11839. DOI: 10.1021/jacs.6b06291

142. CHENG, M. *et al*. Acceptor-Donor-Acceptor type ionic molecule materials for efficient perovskite solar cells and organic solar cells. *Nano Energy*. 2016, 30387–397. DOI: 10.1016/j.nanoen.2016.10.041

143. PAEK, S. *et al*. Dopant-Free Hole-Transporting Materials for Stable and

Efficient Perovskite Solar Cells. *Advanced Materials*. 2017, 29(35), 1606555. DOI: 10.1002/adma.201606555

144. ZHANG, L. *et al*. Intensive Exposure of Functional Rings of a Polymeric Hole-Transporting Material Enables Efficient Perovskite Solar Cells. *Advanced Materials*. 2018, 30(39), 1804028. DOI: 10.1002/adma.201804028

145. MAGOMEDOV, A. *et al*. Diphenylamine-Substituted Carbazole-Based Hole Transporting Materials for Perovskite Solar Cells: Influence of Isomeric Derivatives. *Advanced Functional Materials*. 2018, 28(9), 1704351. DOI: 10.1002/adfm.201704351

146. WOLFF, C.M. *et al*. Reduced Interface-Mediated Recombination for High Open-Circuit Voltages in $CH_3NH_3PbI_3$ Solar Cells. *Advanced Materials*. 2017, 29(28), 1700159. DOI: 10.1002/adfm.201704351

147. BREDAS, J.-L. Mind the gap! *Materials Horizons*. 2014, 1(1), 17–19. DOI: 10.1039/C3MH00098B

148. BELISLE, R.A. *et al*. Minimal Effect of the Hole-Transport Material Ionization Potential on the Open-Circuit Voltage of Perovskite Solar Cells. *ACS Energy Letters*. 2016, 1(3), 556–560. DOI: 10.1021/acsenergylett.6b00270

149. DÄNEKAMP, B. *et al*. Influence of hole transport material ionization energy on performance of perovskite solar cells. *Journal of Materials Chemistry C*. 2019, 7(3), 523–527. DOI: 10.1039/C8TC05372C

150. SCHLOEMER, T.H. *et al*. Doping strategies for small molecule organic hole-transport materials: impacts on perovskite solar cell performance and stability. *Chemical Science*. 2019, 10(7), 1904–1935. DOI: 10.1039/C8SC05284K

151. NGUYEN, W.H. *et al*. Enhancing the Hole-Conductivity of Spiro-OMeTAD without Oxygen or Lithium Salts by Using Spiro$(TFSI)_2$ in Perovskite and Dye-Sensitized Solar Cells. *Journal of the American Chemical Society*. 2014, 136(31), 10996–11001. DOI: 10.1021/ja504539w

152. ABATE, A. *et al*. Lithium salts as "redox active" p-type dopants for organic semiconductors and their impact in solid-state dye-sensitized solar cells. *Physical Chemistry Chemical Physics*. 2013, 15(7), 2572. DOI: 10.1039/C2CP44397J

153. SALIBA, M. *et al*. How to Make over 20% Efficient Perovskite Solar Cells in Regular (n-i-p) and Inverted (p-i-n) Architectures. *Chemistry of Materials*. 2018, 30(13), 4193–4201. DOI: 10.1021/acs.chemmater.8b00136

154. SENOCRATE, A. *et al*. Interaction of oxygen with halide perovskites. *Journal of Materials Chemistry A*. 2018, 6(23), 10847–10855. DOI: 10.1039/C8TA04537B

155. HABISREUTINGER, S.N. *et al*. Carbon Nanotube/Polymer Composites as a Highly Stable Hole Collection Layer in Perovskite Solar Cells. *Nano Letters*. 2014, 14(10), 5561-5568. DOI: 10.1021/nl501982b

156. LI, G. and ZHAO, G. Efficient Acetylation of Alcohols and Phenols Catalyzed by Recyclable Lithium Bis(perfluoroalkylsulfonyl)imide. *Synthetic Communications*. 2013, 43(1), 34–43. DOI: 10.1080/00397911.2011.589563

157. ZHAO, W. and SUN, J. Triflimide ($HNTf_2$) in Organic Synthesis.

Chemical Reviews. 2018, 118(20), 10349-10392. DOI: 10.1021/acs.chemrev.8b00279

158. BURSCHKA, J. *et al*. Tris(2-(1 H -pyrazol-1-yl)pyridine)cobalt(III) as p-type dopant for organic semiconductors and its application in highly efficient solid-state dye-sensitized solar cells. *Journal of the American Chemical Society*. 2011, 133(45), 18042–18045. DOI: 10.1021/ja207367t

159. BURSCHKA, J. *et al*. Co(III) Complexes as p-Dopants in Solid-State Dye-Sensitized Solar Cells. *Chemistry of Materials*. 2013, 25(15), 2986-2990. DOI: 10.1021/cm400796u

160. NOH, J.H. et al. Nanostructured $TiO_2/CH_3NH_3PbI_3$ heterojunction solar cells employing spiro-OMeTAD/Co-complex as hole-transporting material. *Journal of Materials Chemistry A*. 2013, 1(38), 11842-11847. DOI: 10.1039/C3TA12681A

161. LEIJTENS, T. *et al*. Hydrophobic Organic Hole Transporters for Improved Moisture Resistance in Metal Halide Perovskite Solar Cells. *ACS Applied Materials & Interfaces*. 2016, 8(9), 5981-5989. DOI: 10.1021/acsami.5b10093

162. CHRISTIANS, J.A. *et al*. Tailored interfaces of unencapsulated perovskite solar cells for >1,000 hour operational stability. *Nature Energy*. 2018, 3(1), 68–74. DOI: 10.1038/s41560-017-0067-y

163. NAZEERUDDIN, M.K. *et al*. Conversion of light to electricity by cis-X2bis (2, 2′-bipyridyl-4, 4′-dicarboxylate) ruthenium (II) charge-transfer sensitizers (X= Cl-, Br-, I-, CN-, and SCN-). *Journal of the American Chemical Society*. 1993, 115(14), 6382–6390. DOI: 10.1021/ja00067a063

164. NOEL, N.K. *et al*. Enhanced Photoluminescence and Solar Cell Performance *via* Lewis Base Passivation of Organic–Inorganic Lead Halide Perovskites. *ACS Nano*. 2014, 8(10), 9815–9821. DOI: 10.1021/nn5036476

165. HABISREUTINGER, S.N. *et al*. Investigating the Role of 4- *Tert* Butylpyridine in Perovskite Solar Cells. *Advanced Energy Materials*. 2017, 7(1), 1601079. DOI: 10.1002/aenm.201601079

166. WANG, S. *et al*. Role of 4-*tert*-Butylpyridine as a Hole Transport Layer Morphological Controller in Perovskite Solar Cells. *Nano Letters*. 2016, 16(9), 5594–5600. DOI: 10.1021/acs.nanolett.6b02158

167. WANG, S. *et al*. Unveiling the Role of tBP−LiTFSI Complexes in Perovskite Solar Cells. *Journal of the American Chemical Society*. 2018, 140(48), 16720-16730. DOI: 10.1021/jacs.8b09809

168. YUE, Y. *et al*. Enhanced Stability of Perovskite Solar Cells through Corrosion-Free Pyridine Derivatives in Hole-Transporting Materials. *Advanced Materials*. 2016, 28(48), 10738–10743. DOI: 10.1002/adma.201602822

169. LYGAITIS, R. *et al*. Hole-transporting hydrazones. *Chemical Society Reviews*. 2008, 37(4), 770. DOI: 10.1039/B702406C

170. JUBRAN, N. *et al*. Poly(hydrazone)-based charge transport materials. *US20050221212A1*. 2004.

171. KOLB, H.C. *et al*. Click Chemistry: Diverse Chemical Function from a Few Good Reactions. *Angewandte Chemie International Edition*. 2001, 40(11), 2004–2021. DOI: 10.1002/1521-3773(20010601)40:11<2004::AID-

ANIE2004>3.0.CO;2-5

172. URNIKAITE, S. *et al*. Study on the influence of methyl groups and their location on properties of triphenylamino-based charge transporting hydrazones. *Monatshefte für Chemie – Chemical Monthly*. 2009, 140(12), 1453–1458. DOI: 10.1007/s00706-009-0202-y

173. WANG, Y. *et al*. Organic photoconductive materials for advanced xerography. DUCHARME, S. *et al*. (Eds.). *Proceedings of SPIE – The International Society for Optical Engineering*. [s.l.]: International Society for Optics and Photonics, 1999. p. 178–183. DOI: 10.1117/12.363897

174. LEIJTENS, T. *et al*. Hole Transport Materials with Low Glass Transition Temperatures and High Solubility for Application in Solid-State Dye-Sensitized Solar Cells. *ACS Nano*. 2012, 6(2), 1455-1462. DOI: 10.1021/nn204296b

175. MOROFUJI, T. *et al*. Electrochemical C−H Amination: Synthesis of Aromatic Primary. *Journal of the American Chemical Society*. 2013, 135(13), 5000–3. DOI: 10.1021/ja402083e

176. JENA, A.K. *et al*. Severe Morphological Deformation of Spiro-OMeTAD in $(CH_3NH_3)PbI_3$ Solar Cells at High Temperature. *ACS Energy Letters*. 2017, 2(8), 1760–1761. DOI: 10.1021/acsenergylett.7b00582

177. BASTOS, J.P. *et al*. Light-Induced Degradation of Perovskite Solar Cells: The Influence of 4-Tert-Butyl Pyridine and Gold. *Advanced Energy Materials*. 2018, 8(23), 1800554. DOI: 10.1002/aenm.201800554

178. LAMBERTI, F. *et al*. Evidence of Spiro-OMeTAD De-doping by tert-Butylpyridine Additive in Hole-Transporting Layers for Perovskite Solar Cells. *Chem*. 2019, 5(7), 1806-1817. DOI: 10.1016/j.chempr.2019.04.003

7. Curriculum Vitae

Personal information

Name, Surname	Artiom Magomedov
Date of birth	August 12, 1991
Place of birth	Kaunas, Lithuania
Nationality	Lithuanian
email	artiom.magomedov@ktu.lt

Work experience

2016.04 – till now	Kaunas University of Technology, Project junior researcher

Education

2015 – 2019	Kaunas University of Technology PhD studies, Chemistry
2013 – 2015	Kaunas University of Technology Master of chemistry
2014 03 – 2014 09	Technische Universität München (TUM) ERASMUS exchange program Theoretical chemistry
2009 – 2013	Kaunas University of Technology Bachelor of chemistry Group of technology and physical science advanced studies
2006 – 2009	Kaunas A. Puškinas secondary school
2005 – 2009	Kaunas J. Gruodis Conservatory Music theory
1997 – 2006	Kaunas Mikas Petrauskas music school Piano
1997 – 2006	Kaunas L. Karsavinas secondary school, Kaunas A. Timinskis secondary school

Scientific work

2010 – 2019	Research work in prof. dr. Vytautas Getautis scientific group. Synthesis and characterization of stable amorphous organic photosemiconductors for novel applications in electronics (PSC, OLED, DSSC etc.).
Sept. 2017 – Feb. 2018	Guest PhD at Helmholtz-Zentrum Berlin Germany. Research supervisor – dr. Steve Albrecht. Search for alternative hole transporting materials for the

	application in tandem silicon/perovskite solar cells.
2014 03 – 09	Research work in the group of prof. dr. Ville Kaila (TUM) Proton transfer modelling by *ab initio* methods in small molecular systems.
2014 05 – 07	Research work in the group of dr. Wilfried Rozhon (TUM). Synthesis of growth mediators and *in vivo* activity research.
2010 – 2013	6 times participant of the Research council of Lithuania projects *"Students scientific practice", "Students scientific researches"* and *"Students scientific work stimulation"*.

Languages

Russian, Lithuanian – mother tongues. English (C1), Spanish (A2), German (A2).

Awards

April 17, 2019	The Lithuanian Academy of Sciences (LMA) best young researcher and graduate student research work award.
March 21, 2019	"Infobalt" scholarship for the 9th young researchers conference "Interdisciplinary Research in Physical and Technological Sciences" laureate.
September 19, 2018	European Materials Research Society (E-MRS) graduate student award of the 2018 Fall meeting.
May 08, 2015	prof. Juozas Degutis award for the best student work in the field of organic synthesis.

Scholarships and grants

2018	BALTECH Scholarship grant.
2017	DAAD (Deutscher Akademischer Austauschdienst) research grant.
2016–2018	Lithuanian Research Council PhD student scholarship for the academic achievements – 4 times.
2015–2017	KTU most active PhD scholarship – 3 times.
May 23, 2011	KTU honorable dr. Juozas Petras Kazickas scholarship
2011–2014	Rector's promotional scholarship for outstanding academic and study results – 6 times.

8. List of Author's Publications and Conferences

Publications in peer-reviewed journals

1. Al-Ashouri, Amran; Magomedov, Artiom; Roß, Marcel; Jošt, Marko; Talaikis, Martynas; Chistiakova, Ganna; Bertram, Tobias; Márquez, José A.; Köhnen, Eike; Kasparavičius, Ernestas; Levcenco, Sergiu; Gil-Escrig, Lidón; Hages, Charles J.; Schlatmann, Rutger; Rech, Bernd; Malinauskas, Tadas; Unold, Thomas; Kaufmann, Christian A.; Korte, Lars; Niaura, Gediminas; Getautis, Vytautas; Albrecht, Steve. Conformal monolayer contacts with lossless interfaces for perovskite single junction and monolithic tandem solar cells // Energy & environmental science. Cambridge: Royal Society of Chemistry. ISSN 1754-5692. 2019, vol. 12, iss. 11, p. 3356–3369. DOI: 10.1039/c9ee02268f. [Scopus; Science Citation Index Expanded (Web of Science)] [IF: 33.250; AIF: 4,955; IF/AIF: 6.710 (2018, InCites JCR SCIE)]
2. Braukyla, Titas; Xia, Rui; Malinauskas, Tadas; Daskeviciene, Maryte; Magomedov, Artiom; Kamarauskas, Egidijus; Jankauskas, Vygintas; Fei, Zhaofu; Roldan-Carmona, Cristina; Momblona, Cristina; Nazeeruddin, Mohammad Khaja; Dyson, Paul J.; Getautis, Vytautas. Application of a tetra-TPD-type hole-transporting material fused by a Troger's base core in perovskite solar cells // Solar RRL. Weinheim: Wiley-VCH. ISSN 2367-198X. 2019, vol. 00, p. 1–6. DOI: 10.1002/solr.201900224. [Science Citation Index Expanded (Web of Science)]
3. Daskeviciene, Maryte; Paek, Sanghyun; Magomedov, Artiom; Cho, Kyoung Taek; Saliba, Michael; Kizeleviciute, Ausra; Malinauskas, Tadas; Gruodis, Alytis; Jankauskas, Vygintas; Kamarauskas, Egidijus; Nazeeruddin, Mohammad Khaja; Getautis, Vytautas. Molecular engineering of enamine-based small organic compounds as hole-transporting materials for perovskite solar cells // Journal of materials chemistry C. London: Royal Society of Chemistry. ISSN 2050-7534. eISSN 2050-7526. 2019, vol. 7, iss. 9, p. 2717–2724. DOI: 10.1039/c8tc06297h. [Scopus; Science Citation Index Expanded (Web of Science)] [IF: 6.641; AIF: 4.591; IF/AIF: 1.446 (2018, InCites JCR SCIE)]
4. Magomedov, Artiom; Al-Ashouri, Amran; Kasparavičius, Ernestas; Strazdaitė, Simona; Niaura, Gediminas; Jošt, Marko; Malinauskas, Tadas; Albrecht, Steve; Getautis, Vytautas. Self-assembled hole transporting monolayer for highly efficient perovskite solar cells // Advanced energy materials. Weinheim: Wiley. ISSN 1614-6832. eISSN 1614-6840. 2018, vol. 8, iss. 32, art. no. 1801892, p. 1–5. DOI: 10.1002/aenm.201801892. [Scopus; Science Citation Index Expanded (Web of Science)] [IF: 24.884; AIF: 5.204; IF/AIF: 4.781 (2018, InCites JCR SCIE)]
5. Vaitukaityte, Deimante; Wang, Zhiping; Malinauskas, Tadas; Magomedov, Artiom; Bubniene, Giedre; Jankauskas, Vygintas; Getautis, Vytautas;

Snaith, Henry J. Efficient and stable perovskite solar cells using low-cost aniline-based enamine hole-transporting materials // Advanced materials. Weinheim: Wiley. ISSN 0935-9648. eISSN 1521-4095. 2018, vol. 30, iss. 45, art. no. 1803735, p. 1–7. DOI: 10.1002/adma.201803735. [PubMed; Scopus; Science Citation Index Expanded (Web of Science)] [IF: 25.809; AIF: 5.478; IF/AIF: 4.711 (2018, InCites JCR SCIE)]

6. Magomedov, Artiom; Kasparavičius, Ernestas; Rakstys, Kasparas; Paek, Sanghyun; Gasilova, Natalia; Genevičius, Kristijonas; Juška, Gytis;; Malinauskas, Tadas; Nazeeruddin, Mohammad Khaja; Getautis, Vytautas. Pyridination of hole transporting material in perovskite solar cells questions the long-term stability // Journal of materials chemistry C. Cambridge: Royal Society of Chemistry. ISSN 2050-7534. eISSN 2050-7526. 2018, vol. 6, iss. 33, p. 8874–8878. DOI: 10.1039/c8tc02242a. [Scopus; Science Citation Index Expanded (Web of Science)] [IF: 6.641; AIF: 4.591; IF/AIF: 1.446 (2018, InCites JCR SCIE)]
7. Kasparavicius, Ernestas; Magomedov, Artiom; Malinauskas, Tadas; Getautis, Vytautas. Long-term stability of the oxidized hole transporting materials used in perovskite solar cells // Chemistry – A European journal. Weinheim: Wiley-VCH. ISSN 0947-6539. 2018, vol. 24, iss. 39, p. 9910–9918. DOI: 10.1002/chem.201801441. [PubMed; Scopus; Science Citation Index Expanded (Web of Science)] [IF: 5.160; AIF: 5.880; IF/AIF: 0.877 (2018, InCites JCR SCIE)]
8. Magomedov, Artiom; Paek, S.; Gratia, P.; Kasparavičius, Ernestas; Daškevičienė, Marytė; Kamarauskas, Egidijus; Gruodis, Alytis; Jankauskas, Vygintas; Kantminienė, Kristina; Cho, K.T.; Rakštys, Kasparas; Malinauskas, Tadas; Getautis, Vytautas; Nazeeruddin, M.K. Diphenylamine-substituted carbazole-based hole transporting materials for perovskite solar cells: influence of isomeric derivatives // Advanced Functional Materials. Weinheim: Wiley-VCH. ISSN 1616-301X. eISSN 1616-3028. 2018, Vol. 28, iss. 9, art. 1704351, p. 1–13. DOI: 10.1002/adfm.201704351. [Scopus; Science Citation Index Expanded (Web of Science)] [IF: 15.621; AIF: 5.478; IF/AIF: 2.851 (2018, InCites JCR SCIE)]
9. Daškevičiūtė, Šarūnė; Sakai, Nobuya; Franckevičius, Marius; Daškevičienė, Marytė; Magomedov, Artiom; Jankauskas, Vygintas; Snaith, Henry J.; Getautis, Vytautas. Nonspiro, fluorene-based, amorphous hole transporting materials for efficient and stable perovskite solar cells // Advanced science. Weinheim: Wiley-VCH. eISSN 2198-3844. 2018, vol. 5, iss. 4, art. no. 1700811, p. 1–7. DOI: 10.1002/advs.201700811. [DOAJ; Scopus; MEDLINE; Science Citation Index Expanded (Web of Science)] [IF: 15.804; AIF: 5.875; IF/AIF: 2.690 (2018, InCites JCR SCIE)]
10. Magomedov, Artiom; Sakai, Nobuya; Kamarauskas, Egidijus; Jokubauskaitė, Gabrielė; Franckevičius, Marius; Jankauskas, Vygintas; Snaith, Henry J.; Getautis, Vytautas. Amorphous hole-transporting material

based on 2,2'-bis-substituted 1,1'-biphenyl scaffold for application in perovskite solar cells // Chemistry – An Asian journal. Weinheim: Wiley-VCH. ISSN 1861-4728. eISSN 1861-471X. 2017, Vol. 12, iss. 9, p. 958–962. DOI: 10.1002/asia.201700173. [Scopus; MEDLINE; Science Citation Index Expanded (Web of Science)] [IF: 3.692; AIF: 5.561; IF/AIF: 0.663 (2017, InCites JCR SCIE)]

11. Urnikaitė, Simona; Braukyla, Titas; Magomedov, Artiom; Kamarauskas, Egidijus; Malinauskas, Tadas; Getautis, Vytautas. A structural study of Troger's base scaffold-based dyes for DSSC applications // Dyes and pigments. Oxford: Elsevier. ISSN 0143-7208. eISSN 1873-3743. 2017, vol. 143, p. 48–61. DOI: 10.1016/j.dyepig.2017.04.012. [Academic Search Research & Development; Academic Search Complete; Scopus; Science Citation Index Expanded (Web of Science)] [IF: 3.767; AIF: 2.926; IF/AIF: 1.287 (2017, InCites JCR SCIE)]
12. Daškevičienė, Marytė; Paek, Sanghyun; Wang, Zhiping; Malinauskas, Tadas; Jokubauskaitė, Gabrielė; Rakštys, Kasparas; Cho, Kyung Taek; Magomedov, Artiom; Jankauskas, Vygintas; Ahmad, Shahzada; Snaith, Henry J; Getautis, Vytautas; Nazeeruddin, Mohammad Khaja. Carbazole-based enamine: low-cost and efficient hole transporting material for perovskite solar cells // Nano energy. Amsterdam: Elsevier. ISSN 2211-2855. eISSN 2211-3282. 2017, vol. 32, p. 551–557. DOI: 10.1016/j.nanoen.2017.01.015. [Scopus; Science Citation Index Expanded (Web of Science)] [IF: 13.120; AIF: 5.030; IF/AIF: 2.608 (2017, InCites JCR SCIE)]
13. Magomedov, Artiom; Urnikaitė, Simona; Paliulis, Osvaldas; Jankauskas, Vygintas; Getautis, Vytautas. "Click-chemistry" inspired synthesis of hydrazone-based molecular glasses // RSC advances. Cambridge : Royal Society of Chemistry. ISSN 2046-2069. 2016, vol. 6, iss. 11, p. 8701-8704. DOI: 10.1039/C5RA24211H. [Scopus; Current Contents / Physical, Chemical & Earth Sciences; Science Citation Index Expanded (Web of Science)] [IF: 3,108; AIF: 5,649; IF/AIF: 0,550 (2016, InCites JCR SCIE)]
14. Gratia, Paul; Magomedov, Artiom; Malinauskas, Tadas; Daskeviciene, Maryte; Abate, Antonio; Ahmad, Shahzada; Grätzel, Michael; Getautis, Vytautas; Nazeeruddin, Mohammad Khaja. A methoxydiphenylaminesubstituted carbazole twin derivative: an efficient hole-transporting material for Perovskite solar cells // Angewandte chemie international edition. Weinheim: Wiley-VCH. ISSN 1433-7851. eISSN 1521-3773. 2015, vol. 54, iss. 39, p. 11409–11413. DOI: 10.1002/anie.201504666. [Scopus; Science Citation Index Expanded (Web of Science)] [IF: 11.709; AIF: 5.586; IF/AIF: 2.096 (2015, InCites JCR SCIE)]
15. Gamiz-Hernandez, Ana P.; Magomedov, Artiom; Hummer, Gerhard; Kaila, Ville R.I. Linear energy relationships in ground state proton transfer and excited state proton-coupled electron transfer // Journal of physical

chemistry B. Washington: ACS publications. ISSN 1520-6106. 2015, vol. 119, iss. 6, spec. iss. SL, p. 2611–2619. DOI: 10.1021/jp508790n. [Science Citation Index Expanded (Web of Science)] [IF: 3.187; AIF: 4.638; IF/AIF: 0.687 (2015, InCites JCR SCIE)]

Patents

1. EP 16707981.3; US 15/554,373; JP2017546731; WO2016139570 A1. Gratia, P.; Nazeeruddin, M.K.; Grätzel, M.; Getautis, V.; Magomedov, Artiom; Malinauskas, T.; Daškevičienė, M. WO2016139570 A1. Small molecule hole transporting material for optoelectronic and photoelectrochemical devices / Applicants: Ecole Polytechnique Fed de Lausanne (EPFL); Kaunas Univ of Tech (KTU). September 09, 2016.
2. EP18000405.3; DE102018115379 (B3). Artiom Magomedov, Amran Al-Ashouri, Ernestas Kasparavicius, Steve Albrecht, Vytautas Getautis, Marko Jost, Tadas Malinauskas, Lukas Kegelmann, Eike Köhnen. Hole Transporting Self-Assembled Monolayer for Perovskite Solar Cells / Applicants: Helmholtz-Berlin (HZB); Kaunas Univ of Tech (KTU). April 25, 2018.

List of conferences

2019 05 27 – 31	"*European Materials Research Society 2019 Spring Meeting"*, Nice, France Oral presentation "*Dopant-free hole transporting monolayers for inverted perovskite solar cells*"
2019 05 12 – 15	"*11th International Conference on Hybrid and Organic Photovoltaics*", Rome, Italy Poster presentation "*Hole-Selective Monolayers: Synthesis, Deposition, and Application in Efficient Perovskite Solar Cells*"
2019 03 19 – 22	"*Open readings 2019*", Vilnius, Lithuania Oral presentation "*Monolayer as a hole-selective contact for efficient perovskite solar cells*"
2019 03 12	"*Fizinių ir technologijos mokslų tarpdalykiniai tyrimai*", Vilnius, Lithuania Oral presentation "*Nauja selektyvaus sluoksnio formavimo technologija, skirta perovskitiniams saulės elementams*"
2018 09 30 – 10 02	"*4th International Conference on Perovskite Solar Cells and Optoelectronics*", Lausanne, Switzerland Poster presentation *"Novel Self-Assembled Hole Transporting Monolayer for Highly Efficient Inverted Perovskite Solar Cells"*
2018 09 17 – 20	*"European Materials Research Society 2018 Fall Meeting"*,

	Warsaw, Poland Oral presentation *"Carbazole-based hole transporting materials for perovskite solar cells: synthesis, stability, and further development"*
2018 07 01 – 04	"*Balticum Organicum Syntheticum 2018*", Tallinn, Estonia Poster presentation "*Pyridination of hole transporting material in perovskite solar cells"*
2018 05 28 – 31	"*10th International Conference on Hybrid and Organic Photovoltaics*", Benidorm, Spain Poster presentation "*Pyridination of Hole Transporting Materials in Perovskite Solar Cells*"
2017 09 18 – 20	"*3rd International Conference on Perovskite Solar Cells and Optoelectronics*", Oxford, United Kingdom Poster presentation "*Isomeric derivatives of diphenylamine-substituted carbazole-based hole transporting materials"*
2017 08 29 – 09 02	"*14th European Conference on Molecular Electronics*", Dresden, Germany Poster presentation "*Amorphous hole transporting material based on 2,2'- bissubstituted 1,1'- biphenyl scaffold for application in perovskite solar cells*"
2017 04 28	"*Chemistry & Chemical Technology 2017*", Kaunas, Lithuania Oral presentation "*Neutral color electrochromic device utilizing triphenylamine functionalised redox active materials"*
2017 03 14	"*Open readings 2017*", Vilnius, Lithuania Oral presentation "*Novel branched hole transporting materials for perovskite solar cells: synthesis and performance*"
2016 08 27	*"Advanced materials and technologies 2016"*, Palanga, Lithuania Poster presentation "*Influence of the Alkyl Linker Length on the Properties of the Carbazole-based Hole Transporting Materials"*
2016 07 03	"*Balticum Organicum Syntheticum 2016*", Riga, Latvia Poster presentation ""*Click-chemistry" inspired synthesis of hydrazone-based molecular glasses and polymers"*
2016 06 12	"*Advanced Perovskite, Hybrid and Thin-film Photovoltaics*", Krutyn, Poland Oral presentation "*Synthesis of Carbazolyl-Based Charge Transporting Materials for Perovskite Solar Cells*"
2016 04 28	"*Chemistry & Chemical Technology 2016*", Vilnius, Lithuania Poster presentation "*Cheap and Efficient Carbazole-Based Hole Transporting Materials for Perovskite Solar Cells*"
2015 09 27	"*1st International Conference on Perovskite Solar Cells and Optoelectronics*", Lausanne, Switzerland Poster presentation "*Simple and inexpensive synthesis of*

	carbazole based branched hole transporting materials for perovskite solar cells"
2015 08 27	*"Advanced materials and technologies 2015"*, Palanga, Lithuania Poster presentation *"Change Transfer Process in the Oxidized Carbazole Based Branched Hole Transporting Material"*
2015 05 08	"*Chemija ir cheminė technologija 2015*", Kaunas, Lithuania Oral presentation "*Simple, inexpensive and efficient hole transporting materials for perovskite solar cells"*
2014 08 27	*"Advanced materials and technologies 2014"*, Palanga, Lithuania Poster presentation *"Novel Hydrazone-Based Photoconductive Materials"*
2013 08 27	*"Advanced materials and technologies 2013"*, Palanga, Lithuania Poster presentation *"Photoconductive materials possessing two, three or four hydrazone-based chromophores"*

SL344. 2020-02-10, 11,5 leidyb. apsk. l. Tiražas 12 egz.
Išleido Kauno technologijos universitetas, K. Donelaičio g. 73, 44249 Kaunas
Spausdino leidyklos „Technologija“ spaustuvė, Studentų g. 54, 51424 Kaunas